NTNU

Norwegian University of
Science and Technology

Chemical Looping Combustion Cold Flow Model commissioning and performance evaluation

Sindre Tjøstheim

Master of Science in Energy and Environment
Submission date: June 2010
Supervisor: Olav Bolland, EPT
Co-supervisor: Aldo Bischi, EPT

Norwegian University of Science and Technology
Department of Energy and Process Engineering

Problem Description

Background and objective.
SINTEF Energy Research and the Norwegian University of Science and Technology (NTNU) designed a 150kWth Chemical Looping Combustion (CLC) reactor system which deals with many of the industrial and scale-up issues of this technology. It consists of a Double Loop Circulating Fluidized Bed (DLCFB) reactor system made of two reactors: an Air Reactor (AR) and a Fuel Reactor (FR), both working in the fast fluidization regime and interconnected by divided loop-seals. A one to one scale Cold Flow Model (CFM) has been built in order to test the CLC reactor system hydrodynamics and to support the design of the 150 kWth unit.

An experimental campaign will be performed in January and February in order to prove that the set-up is working according to design and to find the more suitable operational window. These analyses will be carried out making use of the following measurement devices: pressure transducers distributed all over the reactor system and disc-valves located in the down-comers after the cyclones to estimate the solid flow entrained by the reactors.

Afterwards, simulations of the risers will be executed. The simulation tool will be ERGUN. An investigation and evaluation of the applicability of ERGUN for simulating the experiments in the CFM is to be done. The outcome of the simulations will be compared with the experimental results at the same conditions.

The following questions should be considered in the project work:

1) The student is required to take actively part to the CFM commissioning contributing to the research team experimental activities and results interpretation within the experimental campaign.

2) Once a good understanding of the reactor system performance is achieved, simulations of the experiments executed in the lab should be done with the software ERGUN. The results and applicability of ERGUN shall be discussed.

Assignment given: 26. January 2010
Supervisor: Olav Bolland, EPT

Preface

This master thesis was done as the finalization of a Master in technology in Energy & environment at the Norwegian University of Science and Technology, NTNU. The master thesis was produced at the Department of Energy and Process Engineering and is a continuation of a project thesis last semester. The project thesis comprised a literature study, commissioning of the rig and a small experimental campaign. After the project thesis was completed the rig was developed further and a flux measurement system was installed.

The work was challenging since Chemical Looping Combustion is a new technology and NTNU/SINTEF also have limited experience on Circulating Fluidized Beds, CFBs. No course in this field of engineering is available at NTNU. Since CLC is a new concept the design of the hot rig has been done from scratch. The 150 kW_{th} will be among the largest of its kind in the world. To verify the design of the rig, a full scale cold flow model has been built. The cold flow model is the basis for this master thesis.

I would like to express my gratitude to supervisor Olav Bolland and especially co-supervisor Aldo Bischi. Their help and guidance has been greatly appreciated. The CLC scientist group led by Øyvind Langørgen and lab personnel Ola Gudmund Storrø, Paul Svendsen and Halvor Flatberg should not be forgotten. Without them the experimental campaign would be impossible to complete.

Thanks to friend and media-student Christian Vassbakk for designing the image at the front page.

June 22, 2010, Trondheim

Abstract

SINTEF and NTNU are planning to build a 150 kW_{th} Chemical Looping Combustion (CLC) reactor system. This is new technology and the CLC reactor system is going to be one of the largest of its kind in the world. The technology is promising for CO_2 capture in terms of energy efficiency and economics. To verify the design a Cold Flow Model, CFM, has been built. In the CFM no reactions take place, but it simulates the hydrodynamics of the 150 kW_{th} CLC reactor system. The reactor system consists of two reactors exchanging solids in a loop. The two reactors are one air reactor, AR, and one fuel reactor, FR. Air is injected at different locations in the CFM to fluidize the solids and achieve the proper mass flows. The Cold Flow Model has been commissioned and an experimental campaign was executed.

A series of experiments running each reactor singularly were performed. The rig seems to be functioning satisfactory and a minimum of plugging in the pipes were observed. The Cold Flow model has two cyclones that showed collection efficiencies at approximately 99 %. This is important to avoid emissions of solids from the future CLC reactor system, both for economic and environmental reasons.

An investigation and mapping of the operating area of the reactors singularly and coupled was the target of the experiments. Correlations between operating velocity, total solid inventory, air distribution and flux were found.

Appropriate flow regimes, meant to give good gas solid contact efficiency, and mass flow's entrainments were achieved. The targets of a solid circulation rate of 2 kg/s in the AR and 1 kg/s in the FR were also achieved. Air is injected in the bottom of the reactors to fluidize the particles. This air is distributed through primary and secondary nozzles. The highest primary air percentage tested in the FR, 75%, gave the highest flux. In the AR 100% was tested, but 70% gave the highest flux. The last result is in contradiction with other experimental work in the area which says that 100% primary air should give the highest flux.

After the mapping of the operating area of the single reactors it was possible to try to run the two reactors coupled. The divided loop seal was tested but led to a pressure short circuit and a large amount of the total solid inventory was lost out of the cyclones in a short time. The operation of a divided loop seal is probably possible, but seems difficult. The internal part of the loop seals were sealed to make the operation easier. The loop seals could then be operated as traditional loop seals.

A challenge was the mass balance between the fuel reactor and air reactor. The mass flows of particles from both reactors must be equal to have a mass balance. Otherwise all the particles eventually ends up in one reactor. Results from the single reactor experiments were used to

know approximately which operating conditions gave a mass balance between the reactors. The Cold Flow Model seemed to a certain degree be self regulating for achieving a mass balance if initial operating conditions were reasonable.

Two experiments with coupled reactors and mass exchange only through the loop seals were done. A global solid circulation rate of 0.7 kg/s and 1 kg/s was achieved. Both AR and FR had the proper flow regimes. Proper flow regimes in the reactors are turbulent or fast fluidization.

A third experiment utilized a *lifter* to enhance the solid transport between the reactors. A lifter is a additional transporter of solids from one reactor to another. The lifter worked successfully. The experiment had a global solid circulation rate of 1.4 kg/s. The mass flows were 1.4 kg/s from the AR loop seal and 1 kg/s from the FR loop seal. The remaining part 0.4 kg/s from the FR to the AR was transported with the lifter. Both reactors had proper flow regimes.

A fourth experiment trying to achieve a global solid circulation rate of 2 kg/s failed. The bottleneck seems to be the AR loop seal. Solids accumulated and the loop seal was not able to handle this rate of solid flow. A new operation philosophy and design of the loop seal has been proposed. The new design of the loop seal and operation philosophy reduces the air flow needed in the loop seal, but it may not necessarily solve the solid circulation limit in the AR loop seal. Further investigation is needed. Manipulating the pressure in the AR may contribute to enhance the rate of solid flow through the loop seal.

The successful experiments were presented at the 1st International Conference on Chemical Looping, IFP-Lyon, France, 17 - 19 March 2010.

After the experimental campaign was finished the experiments were simulated with the fluidization software ERGUN developed by Compiegne University of Technology. ERGUN applies different mathematical models. For the simulations performed Horio's and Berruti's model were applied. The evaluation of the ERGUN simulations by means of the experiments shows that Horio's and Berruti's model should not be used for a detailed investigation of the flow structure in the CFM's risers. However, despite its strongly empirical nature, a preliminary investigation of the riser's behavior with Berruti's model may be useful. Berruti's model is a reasonable tool for modeling the upper part of the pressure profile in the AR and FR at the operating conditions tested. The operating conditions tested in the AR are total solid inventories of 35 and 45 kg, and superficial gas velocities from 0.9-1.9 m/s.

The operating conditions tested in the FR are total solid inventories of 35 and 50 kg, and superficial gas velocities from 1.5-2.0 m/s. Berruti's model is not capable of accounting for the dense bed in the lower part of the reactor as Horio's model does. However, Horio's model mismatched the experimental results too much. Horio's model seems to be a provide a better

match at larger total solid inventory and smaller operating velocities, hence flow regimes not relevant for the CLC reactor system.

Sammendrag

SINTEF og NTNU planlegger å bygge et 150 kW_{th} to-stegs forbrenningsanlegg. Dette er ny teknologi og anlegget blir det største I sitt slag I verden. Teknologien er lovende fordi den kan fange CO_2 på en relativt billig og energieffektiv måte. For å verifisere prosjekteringen og designet av forbrenningsanlegget har det blitt bygget en "kald" modell. I denne modellen er det ingen reaksjoner, men hydrodynamikken I det fremtidige anlegget kan undersøkes. Forbrenningsanlegget består av to reaktorer som utveksler partikler. Luft brukes for å fluidisere partiklene og oppnå de ønskede massestrømmene i de forskjellige seksjonene i den kalde modellen. Den kalde modellen har blitt klargjort og et eksperimentelt program har blitt gjennomført.

En serie med forsøk er utført på hver reaktor for seg. Modellen ser ut til å fungere og minimal blokkering i systemet av partiklene ble observert. Modellen har to sykloner som samlet sett hadde en virkningsgrad på 99 %. Dette er viktig for å unngå utslipp av partikler fra det fremtidige forbrenningsanlegget, både av hensyn til miljø og økonomiske grunner.

Målet for eksperimentene var å undersøke og kartlegge det aktuelle operasjonsområdet. En sammenheng mellom hastighet, partikkelmasse i systemet, fordeling av lufttilførsel og fluks/massestrøm i reaktorene ble funnet. Det ble oppnådd egnede strømningsregimer, dvs. god gass partikkel kontakt, og massestrømmer. Målet for massestrømmene var 2kg/s i luftreaktoren og 1 kg/s i brenselreaktoren. Luft sendes inn i bunnen av reaktorene for å fluidisere partiklene. Denne luften distribueres av primær og sekundær dyser. Den høyeste prosentvise primær lufttilførsel undersøkt i brenselreaktoren, 75 %, gav den høyeste fluksen i reaktoren. I luftreaktoren ble det undersøkt å kjøre 100 % primær lufttilførsel, men 70 % gav den høyeste fluksen. Dette siste resultatet er motstridende med litteraturen som er undersøkt. Den antyder at 100 % primær lufttilførsel burde gi den høyeste fluksen i reaktoren.

Etter å ha kartlagt operasjonsområdet til hver reaktor for seg ble det mulig å kjøre begge reaktorene koplet sammen. Hver reaktor har et *loop seal*. Et *loop seal* transporterer i prinsippet partikler, men ikke gass, tilbake til reaktoren. Delte *loop seal* transporterer partikler både tilbake til reaktor og til den andre reaktoren. De delte *loop seal* til reaktorene ble testet, men førte til en trykk-kortslutning, og det aller meste av partiklene forsvant ut av syklonene. Et delt *loop seal* kan nok fungere, men i et begrenset operasjonsområde. Den indre delen av *loop seal* ble forseglet for å gjøre videre forsøk enklere. Videre forsøk ble da gjort med enkle *loop seal* som kun transporterer partikler til den andre reaktoren.

En utfordring ved å kjøre begge reaktorene var at det måtte være massebalanse mellom dem. Massestrømmen av partikler ut fra reaktorene må være like store for at det skal være balanse

og forhindre at alle partiklene ender opp i kun den ene reaktoren. Resultater fra forsøkene med hver reaktor for seg ble brukt å fastslå sånn noenlunde hvilke operasjonsbetingelser som måtte til i hver reaktor for at det skulle være massebalanse. Modellen ser ut til å ha en viss selvregulerende effekt for å oppnå massebalanse hvis reaktorene kjøres fornuftig i forhold til forventede massestrømmer ut av hver reaktor.

To eksperimenter med samkjøring av begge reaktorene og masseutveksling kun gjennom *loop seal* ble utført. Det ble oppnådd en masseutveksling på henholdsvis 0.7 kg/s og 1 kg/s. Begge reaktorene oppnådde egnede strømningsregimer.

Et tredje eksperiment brukte en *lifter* for å øke partikkelutvekslingen mellom reaktorene. Den fungerte bra. Eksperimentet oppnådde en partikkelutveksling totalt på 1.4 kg/s. Massestrømmene var 1.4 kg/s fra luftreaktorens *loop seal* og 1 kg/s fra brenselreaktorens *loop seal*. De gjenværende 0.4 kg/s fra brenselreaktoren ble transportert med *lifter*. Begge reaktorene oppnådde egnede strømningsregimer også i dette forsøket.

Et fjerde eksperiment hvor hensikten var å oppnå målet om en masseutveksling på 2 kg/s var mislykket. Flaskehalsen i systemet ser ut til å være *loop seal* i luftreaktoren. Partiklene akkumulerer i *loop seal* og det klarer ikke å behandle en så stor massestrøm av partikler. En ny operasjonsfilosofi og design er foreslått. Denne reduserer luftmengden som brukes i *loop seal*, men løser nødvendigvis ikke kapasitetsproblemet i *loop seal*. Ytterligere undersøking av dette er nødvendig. Manipulering av trykket i luftreaktoren kan muligens øke massestrømmen av partikler gjennom *loop seal*.

De vellykkede forsøkene i det eksperimentelle programmet ble presentert på den første internasjonale konferansen om to-stegs forbrenning, IFP-Lyon i Frankrike, 17 – 19 Mars 2010.

Etter at det eksperimentelle programmet var avsluttet ble eksperimentene simulert med fluidiseringsprogrammet ERGUN. Evalueringen av ERGUN simuleringene og eksperimentene i laben viser at Horio og Berruti's modell ikke burde brukes for en detaljert undersøkelse av strømningsbildet i reaktorene i den kalde modellen. Imidlertid, med en viss reservasjon, kan Berruti's modell i ERGUN være rimelig. Berruti's modell er et nyttig verktøy for modellering av den øvre delen av trykkprofilen i reaktorene for de operasjonsbetingelsene som ble undersøkt. De operasjonsbetingelsene som ble undersøkt i luftreaktoren er en total partikkelmasse i systemet på henholdsvis 35 kg og 45 kg, og superficielle gasshastigheter fra 0.9 m/s til 1.9 m/s. Operasjonsbetingelsene som ble undersøkt i brenselreaktoren er en total partikkelmasse i systemet på henholdsvis 35 kg og 50 kg, og superficielle gasshastigheter fra 1.5 m/s til 2.0 m/s. Berruti's modell er ikke i stand til å ta med i beregning "senga" av partikler i bunnen av reaktoren slik som Horio's modell gjør. Imidlertid så var det for stor avstand mellom de eksperimentelle resultatene og simuleringene med Horio's modell. Horio's modell ser ut til å

passe bedre for simuleringer med større partikkelmasse i reaktorene og lavere hastigheter. Det er strømningsregimer som ikke er aktuelle for modellen.

Nomenclature

AR	*Air Reactor*
AR LS	*Air Reactor Loop Seal*
CCS	*Carbon Capture & Storage*
CFB	*Circulating Fluidized Bed*
CFM	*Cold Flow Model*
CLC	*Chemical Looping Combustion*
CLR	Chemical Looping Reformer
DCFB	Dual Circulating Fluidized Bed
FR	*Fuel Reactor*
FR LS	*Fuel Reactor Loop Seal*
GHG	*Greenhouse Gas*
HSE	*Health, Safety and Environment*
IPCC	*Intergovernmental Panel on Climate Change*
LHV	*Lower Heating Value*
LS	*Loop Seal*
NTNU	*Norwegian University of Science and Technology*
OC	*Oxygen Carrier*
PT	*Pressure Transducer*
SINTEF	*The Foundation for Scientific and Industrial Research at the Norwegian Institute of Technology*
STDEV	*Standard deviation*

TDH *transport disengaging height*

A1	*Single reactor experiment performed with the AR and a total solid inventory of 35 kg*
A2	*Single reactor experiment performed with the AR and a total solid inventory of 45 kg*
Archimedes number	*Dimensionless number used to determine the motion of fluids due to density differences*
Active inventory	*In this report defined as the actual solid inventory in the riser during operation. It is estimated by equation 24*
Bulk particle density	*Density of a bulk amount of particles. This will be different than the density of a single particle due to the voidage between the particles*
C1	*Coupled reactor experiment performed with mass exchange through loop seals only*
C2	*Coupled reactor experiment performed with mass exchange through loop seals only*
C3	*Coupled reactor experiment performed with mass exchange through loop seals and lifter*
Downcomer	*The pipe from the cyclone to the loop seal. The purpose of the downcomer is to transport the solids from a region of lower pressure to a region of higher pressure*
F1	*Single reactor experiment performed with the FR and a total solid inventory of 35 kg*
F2	*Single reactor experiment performed with the FR and a total solid inventory of 50 kg*
ERGUN	*Software for modeling and simulation of fluidization*
LabView	*Software for graphical programming for measurement and automation*
Lifter	*Unit to used enhance solid exchange between two reactors*
Loop seal	*Common configuration for providing the return of solids without reverse flow of gases*

Particle density	*The density of a single particle [kg/m^3]*
Purging air	*Supplementary air injection points in a loop seal, sometimes referred to as "grease air"*
Riser	*Tall reactor vessel or column and is the principal reaction zone.*
Reynolds number	*Dimensionless number that gives a measure of the ratio of inertial forces to viscous forces and consequently quantifies the relative importance of these two types of forces for given flow conditions*
Superficial gas velocity	*Gas flow rate per unit cross section area [m^3/m^2]*
Standpipe	*See downcomer*
Total flow	*Total air flow injected to in the bottom of the riser to fluidize the particles. The flow is distributed by primary and secondary nozzles*
Total solid inventory	*Total amount of solids in the reactor system , including riser, cyclone, downcomer and loop seal [kg]*

a	acceleration	[m/s^2]
A	cross sectional area of the bed and relevant riser, which are equal	[m^2]
A_{FR}	cross sectional area of the Fuel Reactor	[m^2]
A_{AR}	cross sectional area of the Air Reactor	[m^2]
C_D	Drag coefficient	[-]
d_{scr}	particle size gained from screen analysis	[m]
d_p	particle size	[m]
d'_p	dimensionless particle size	[-]
d_{sph}	equivalent spherical diameter	[m]
F	mass fraction of particles less than 45 μm	[-]
g	gravity acceleration	[m/s^2]
G_s	flux, solid circulation rate	[kg/m^2s]
h_R	height of the relevant riser	[m]
Δh	Measured height of particles in the downcomer	[m]
L	height of the bed	[m]
LHV	Lower Heating Value	[MJ/kg]
m	bed inventory	[kg]
$\dot{m}$	mass flow	[kg/s]
m_p	mass of particle	[kg]
m_{AR}	amount of solids in Air Reactor	[kg]
m_{FR}	amount of solids in Fuel Reactor	[kg]
$\dot{m}_{fuel}$	mass flow of fuel	[kg_{fuel}/s]

$\dot{m}_{OC}$	mass flow of oxygen carrier	[kg_{OC}/s]
$M_{OC,ox}$	Molar mass of the oxygen carrier	[g/mol]
$M_{OC,ox}$	Molar mass of fully oxidized oxygen carrier	[g/mol]
$M_{OC,red}$	Molar mass of fully reduced oxygen carrier	[g/mol]
$\dot{M}_C$	mass flow of solids separated in the cyclone	[kg_{solids}/s]
$\dot{M}_{gas}$	mass flow of gas entering the cyclone	[kg_{gas}/s]
$\dot{M}_i$	mass flow of solids entering the cyclone	[kg_{solids}/s]
$\dot{M}_{solids}$	mass flow of solids entering the cyclone	[kg_{solids}/s]
O_{min}	Oxygen demand for fully oxidation of fuel	[kg_{O2}/kg_{fuel}]
P_{AR}	Pressure before distributor/nozzle in bottom of the air reactor	[Pa]
$P_{bottom,AR}$	Pressure at the bottom of the Air Reactor	[Pa]
$P_{bottom,FR}$	Pressure at the bottom of the Fuel Reactor	[Pa]
P_{fuel}	Fuel power	[W]
P_{FR}	Pressure before distributor in bottom of the fuel reactor	[Pa]
$P_{LSAR/LSFR}$	Pressure in the plenum of the loop-seal	[Pa]
$\mathrm{P_{top,AR}}$	Pressure at the top of the Air Reactor	[Pa]
$\mathrm{P_{top,FR}}$	Pressure at the top of the Fuel Reactor	[Pa]
ΔP	pressure drop	[Pa]
$\Delta P_{AR,\ dist}$	Pressure drop across distributor between the loop seal and air reactor	[Pa]
ΔP_{AR}	Pressure drop from reactor bottom to the height of the bed where recycle solids enter the air reactor	[Pa]

$\Delta P_{FR,\ dist}$	Pressure drop across distributor of the loop seal and fuel reactor	[Pa]
ΔP_{FR}	Pressure drop from reactor bottom to the height of the bed where recycle solids enter the fuel reactor	[Pa]
$\Delta P_{LSAR/LSFR,\ dist}$	Pressure drop across the distributer of the loop-seal	[Pa]
$\Delta P_{LSAR/LSFR}$	Pressure drop across fluidized bed in loop-seal recycle chamber	[Pa]
q	gas flow through the mass flow controllers given in Nl/min from LabView	[Nl/min]
r	radius of the downcomer	[m]
R_0	oxygen ratio, oxygen transport capacity of OC	[kg_{O2}/kg_{OC}]
Re	Reynolds number	[-]
Re_{mf}	Reynolds number at minimum fluidization	[-]
Re_{se}	Reynolds number at the critical transition between turbulent and fast fluidization	[-]
t_{res}	residence time	[s]
Δt	Length of time interval the valve was closed	[s]
$T(x)$	grade efficiency	[-]
U	superficial gas velocity	[m/s]
u'	dimensionless gas velocity	[-]
U_{mb}	minimum bubbling velocity	[m/s]
U_{mf}	minimum fluidization velocity	[m/s]
U_s	velocity of a particle	[m/s]
U_{se}	Critical transition velocity between turbulent and fast fluidization	[m/s]
Ut	terminal gas velocity	[m/s]
$V_{particle}$	volume of particle	[m^3]

V_g	velocity of gas	[m/s]
V_r	relative gas-solids velocity	[m/s]
V_s	velocity of solids	[m/s]
W_R	amount of solids indirectly estimated by ERGUN	[kg]
X	Conversion of oxygen carrier	[-]
$X_{FR,in}$	conversion of the OC entering the FR	[-]
$X_{FR,out}$	conversion of the OC leaving the FR	[-]
$X_{AR,out}$	conversion of the OC leaving the AR	[-]
ΔX	conversion difference between the fuel reactor inlet and outlet	[-]

ϵ	voidage, fraction of the bed not filled with particles	[m^3_{void}/m^3_{total}]
μ	dynamic viscosity	[kg/ms]
μ_e	Loading	[kg_{solids}/kg_{gas}]
ρ	bulk density of particles used in the CFM	[kg/m^3]
ρ_p	density a particle	[kg/m^3]
Φ	collection efficiency in cyclone	[-]
Φ_s	sphericity	[-]

Table of Contents

1. Introduction

Global warming is considered one of the main challenges the world faces today. The general consensus of international climate researchers and the Intergovernmental Panel on Climate Change, IPCC, is that anthropogenic emissions of Green House Gases, GHGs, are the main cause for the global warming of the earth. This is clearly stated in (IPCC 2007):

> *"This rapid warming is consistent with the scientific understanding of how the climate should respond to a rapid increase in greenhouse gases like that which has occurred over the past century, and the warming is inconsistent with the scientific understanding of how the climate should respond to natural external factors such as variability in solar output and volcanic activity".*

Hence it seems very likely that most of the global warming observed the past century is man-made. GHGs are produced by nature also, but anthropogenic GHG emissions add on top of this destroying the previously existing balance.

Water vapor is the most important GHG. However the amount of water vapor in the atmosphere is controlled by the temperature in the atmosphere. CO_2 is the second most important one, hence reducing CO_2 emissions is crucial for limiting global warming. Reducing emissions can be done in numerous ways; reduce energy consumption, increase energy efficiency, more renewable energy, reduce deforestation, more nuclear energy etc. Although renewable energy has a lot of potential, it is however today not capable of delivering the vast amounts of energy the world uses. The energy demand in the world is expected to increase and in figure 1.1 projections of the future energy use and mix is given.

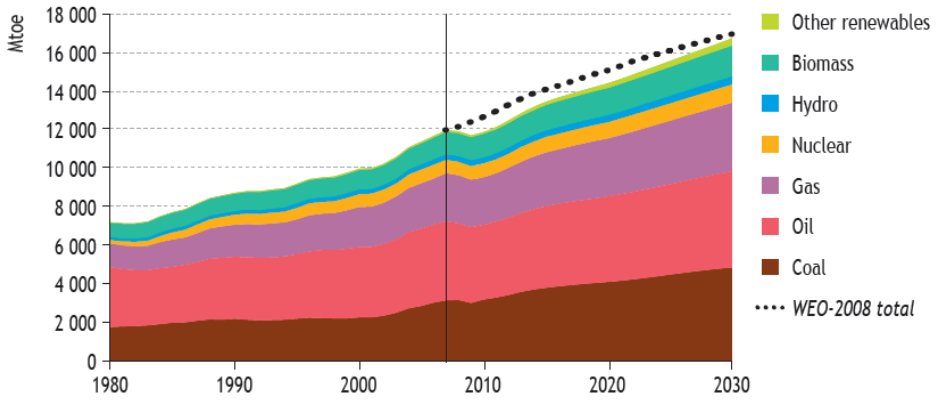

Figure 1.1 - *World primary energy demand and projection by fuel* (IEA 2009)

Figure 1.1 provides a baseline picture of how global energy markets may evolve if the underlying trends in energy demand and supply are not changed. Climate change could

however become the main driver of policy in the upcoming decades. There is not a single solution to reduce global warming, but a mix of different actions must be done. If the greenhouse gas emissions are not cut, the remaining alternatives are to adapt to the climate changes or attempt geoengineering. Both alternatives are considered as a last resort. If the world is not capable of reducing the use of fossil fuels down to a sustainable rate an alternative can be to keep harvesting the energy in fossil fuels but capture the CO_2.

The idea is to capture the CO_2 in the flue gas from large point sources such as power plants and industry, and then store it underground. This is known as Carbon Capture and Storage, CCS. Large point sources as power plants accounts for approximately 2/3 of the anthropogenic CO_2 emissions (Bolland 2009). Introducing CCS as a possible solution means that capture technologies and new thermal power plants concepts need to be developed. One of the biggest challenges in CCS is the large energy consumption of the different technologies. A lot of research is therefore done to find concepts with low energy demand and hence low operating cost. NTNU and SINTEF are for the time being investigating the capture technology Chemical Looping Combustion, CLC. This technology is very promising in terms of maintaining high overall efficiency for the power plant. When it comes to estimated capture costs these are down to about 10€/ton CO_2 and a CLC combined cycle is expected to have net efficiencies up to 51.2% (ENCAPCO2 2009).

SINTEF and NTNU are currently in the design phase of a $150kW_{th}$ CLC reactor. A 1:1 scaled Cold Flow Model, CFM, has been erected in NTNUs laboratory facilities in Trondheim in order to study and verify the hydrodynamics and design solutions of the hot rig.

This master thesis is focused on the CFM built in the lab. The master thesis comprise two parts: an experimental campaign performed on the CFM and simulations of the experiments in a commercial modeling software. An overview of the time spent on the different phases of the project is given in a Gantt diagram in appendix II. The Gantt diagram made shows the actual time spent and not the planned time as in regular Gantt diagram. It illustrates the amount of lab work during this master thesis.

The experimental campaign on the CFM aimed to map the operating area of the system and to verify the design of the hot rig, the 150kW CLC reactor. A lot of time and effort was spent in the lab commissioning the rig, planning test matrixes, doing the experiments and at last interpreting the experimental results. Doing the experiments were very time consuming. The author joined all the experiments done due to a lack of qualified lab personnel. The results from the experimental campaign were presented at the 1st International Conference on Chemical Looping, IFP-Lyon, France, 17 - 19 March 2010.

The second part of the master thesis included simulations in the software program ERGUN, developed by Compiegne University of Technology. An investigation of the applicability of

ERGUN to simulate the hydrodynamic behavior of the CFM was done. The experiments performed in the lab were simulated and the results were compared.

An extensive theory part has been included in the report since:

- No courses are available at NTNU in this field of engineering. Although it is used in several industrial processes in Norway.
- The new and innovative design of the CLC reactor also calls for a solid theoretical foundation to be able to evaluate and understand it.

2. Theory

2.1 Chemical Looping Combustion

2.1.1 Introduction to the concept

CLC is a two step combustion process in which fuel and air are not mixed during combustion. CLC was first introduced with the intention to increase the reversibility of the combustion processes, hence increasing thermal efficiency. In the later years there has been more focus on this technology due to the almost pure CO_2 exit stream of the fuel reactor if the water is removed, simply by condensation. Since this technology first was introduced to increase thermal efficiency and as a side effect separate CO_2 and H_2O from the rest of the flue gas, it goes without saying that this technology is a high potential CO_2 capture technology. CLC can be considered as an oxyfuel-process. Oxy-fuel is the process of burning a fuel using pure oxygen instead of air as the primary oxidant.

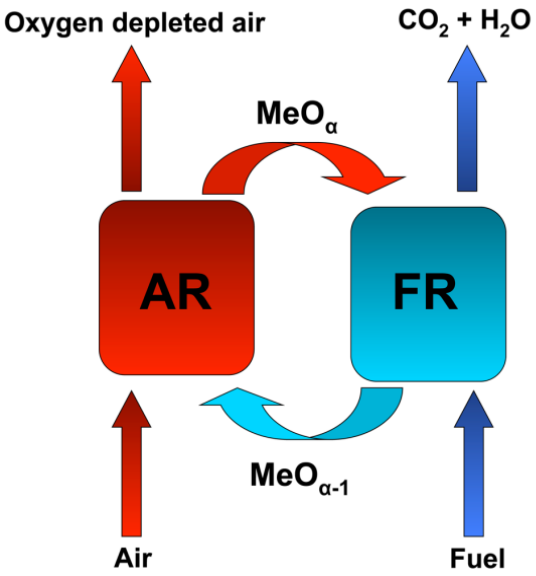

Figure 2.1 - *Illustration of the CLC concept*

Figure 2.1 shows the principle of the CLC concept. It uses a metallic powder as oxygen carrier in order to transport the oxygen from one reactor to the other. The oxygen carrier is oxidized in the air reactor before being transported to the fuel reactor where it reacts with the fuel and is reduced. The oxidation reaction is an exothermic reaction. The reduction of the oxygen on the other hand can be either exothermic or endothermic depending on the properties of the metal oxide. The reduced oxygen carrier then flows back to the air reactor. Loop-seals stop

interchange of gas between the two reactors, and ideally only solids circulate between the two reactors.

The gaseous fuel reacts according to the following global reactions in the fuel reactor:

$$C_xH_y + \left(2x + \frac{y}{2}\right) MeO_\alpha \leftrightarrow xCO_2 + \frac{y}{2}H_2O + \left(2x + \frac{y}{2}\right) MeO_{\alpha-1} \quad (1)$$

$$CO + MeO_\alpha \leftrightarrow CO_2 + MeO_{\alpha-1} \quad (2)$$

$$H_2 + MeO_\alpha \leftrightarrow H_2O + MeO_{\alpha-1} \quad (3)$$

In the air reactor, the reduced oxygen carrier is re-oxidized according to:

$$MeO_{\alpha-1} + \frac{1}{2}O_2 \leftrightarrow MeO_\alpha \quad (4)$$

2.1.2 Using fluidized bed technology to achieve CLC

The CLC-technology can utilize the principal of fluidized beds. Fluidized beds are based on the principles of fluidization: By passing a fluid through granular solids at adequately high velocities, the solids will be suspended and get fluid-like characteristics. A circulating fluidized bed, CFB, is characterized by a continuous recirculation of particles across the reactor system. The particle separation and return systems are integral and essential components of the overall reactor configuration. Note that since most CFBs operate in a “fast fluidization” hydrodynamic regime, in which there is no distinct or recognizable upper bed surface, there will not be a true “bed” in normal sense.

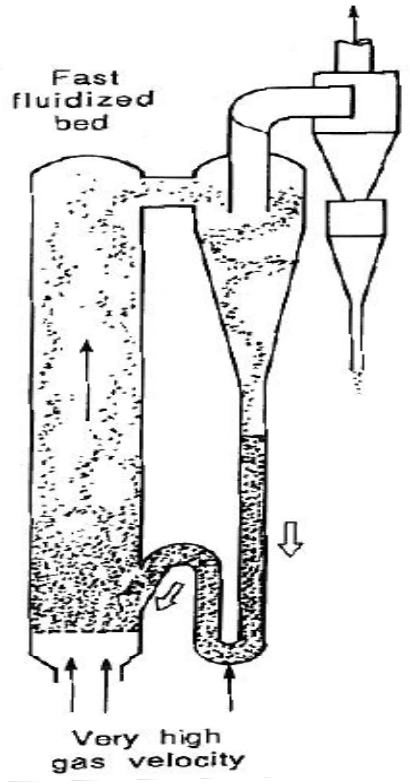

Figure 2.1 - *A circulating fluidized bed reactor operated in fast fluidization mode (Daizo Kunii 1991)*

There are alternatives to using fluidized beds and in recent time it has been conducted research on several different reactor design concepts (Hossain and de Lasa 2008). Most focus has however been directed towards a reactor design interconnecting two circulating fluidized bed reactors to form a two step reaction system known as Dual Circulating Fluidized Bed , DCFB. This means that two CFBs are connected and that the particles are transferred between the two reactors. Figure 2.3 shows an example of a CLC power cycle.

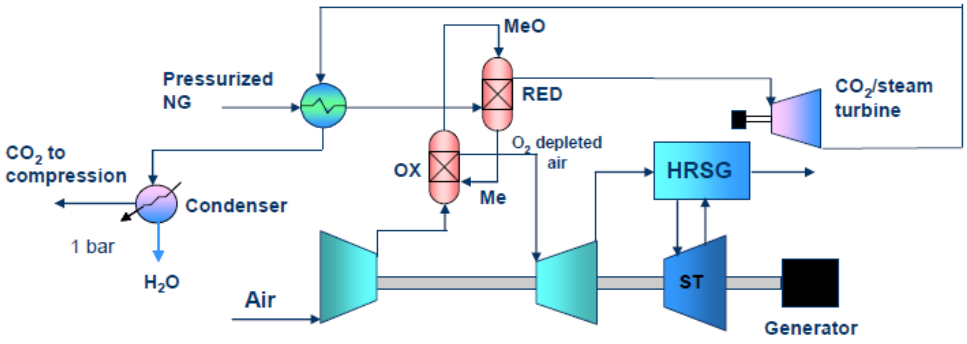

Figure 2.3 - *An example of a CLC power cycle (M. Bysveen 2009)*

2.2 Particle fundamentals

2.2.1 Characterization of particles

Particles can have different size, shape and density. In order to characterize the particles in a CFB, an equivalent spherical diameter d_{sph} and sphericity ϕ_s is used. The equivalent spherical diameter is the diameter of a sphere which has the same volume as the particle. d_{sph} and ϕ_s is defined in the two equations below.

$$d_{sph} = \left(\frac{6 \times V_{particle}}{\pi}\right)^{1/3} \tag{5}$$

The sphericity is given by:

$$\Phi_s = \left(\frac{surface\ of\ a\ sphere}{surface\ of\ particle}\right)_{same\ volume} \tag{6}$$

The two parameters are combined to give a particle size d_p. In this way we represent a bed of nonspherical particles by a bed of spheres of diameter d_p such that the two beds have the same total surface area and same fractional voidage.

$$d_p = \Phi_s \times d_{sph} \tag{7}$$

For intermediate particle sizes the size is evaluated by screen analysis, which gives d_{scr}. Most fluidized bed operations treat particles whose sizes are measured with screen analysis. According to (Daizo Kunii 1991) there is no general relationship between d_{scr} and d_p, and the best approximation for d_p when it comes to pressure drop considerations is given in the following equation.

$$d_p \cong \begin{cases} \Phi_s \times d_{scr} & (a) \\ d_{scr} & (b) \\ {\Phi_s}^2 \times d_{scr} & (c) \end{cases} \tag{8}$$

(a) for irregular particles with no seeming longer or shorter dimension

(b) for irregular particles with somewhat longer dimension, but with length ratio no higher than 2:1

(c) for irregular particles with shorter dimension, but with length ratio no lower than 1:2

The particle size decides the particle properties. Therefore a change in particle size changes the properties of the particles. According to (Krammer 2008a) decreasing the particle size results in the following changes:

- The light scattering increases. This property is widely used for particle size characterization.
- The particle strength increases and particle grinding becomes increasingly more energy consuming.
- The ratio of particle surface to particle volume becomes larger. Consequently an interfacial phenomenon such as agglomeration becomes increasingly important.

The properties of a system consisting of numerous particles also become changed when decreasing the particle size:

- Particle separation becomes increasingly more difficult.
- Specific area, which is defined as the surface area to the particle divided by the volume, increases. Hence solubility and reactivity which is a function of the surface area increases.

In a system of particles there will be a certain distribution of the particle size. This is described in a particle size distribution diagram. Particle size distribution is often abbreviated PSD. The PSD diagram can show both cumulative and specific distribution. The PSD of the particles used in the Cold Flow model is shown in figure 2.4. This diagram is volume based. Other diagrams can be mass based or frequency (number) based. The mean size particle, d_{50}, can be read from the diagram. The d_{50} is 34.5 μm. This means that half of the particles is larger than this and the other half is smaller.

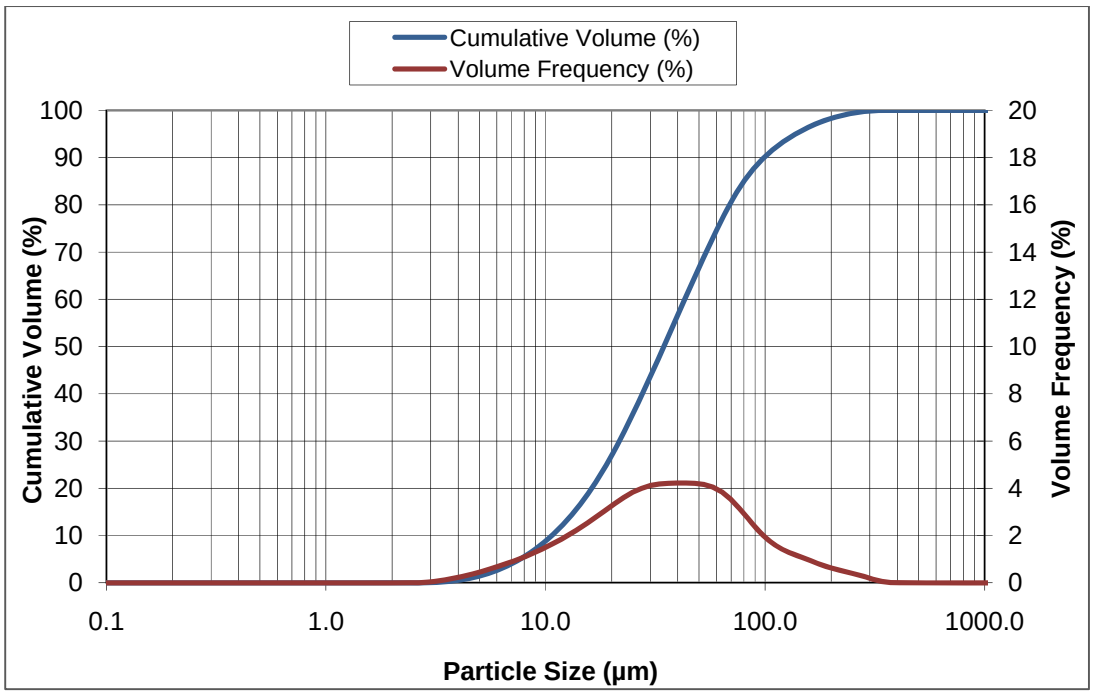

Figure 2.4 - *PSD diagram for the particles used in the Cold Flow Model*

2.2.2 Geldart classification

By carefully observing the fluidization of all sorts and sizes of solids, four clearly recognizable kinds of particle behavior are identified (Basu 2006). They are classified in four groups, A, B, C and D. This is shown in figure 2.5. The mean particle size used in the experiments done in this report is plotted in the diagram. The particle's classification is plotted against the density difference between the solid and the fluidizing gas and the particle size.

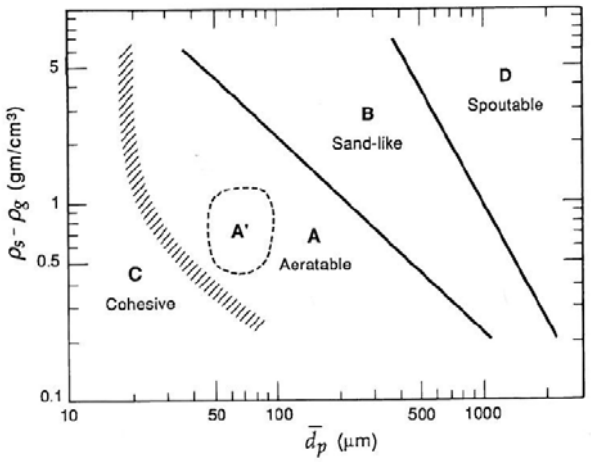

Figure 2.5 – *Geldart classification of particles for air at ambient conditions* (Daizo Kunii 1991)

Classification of the particles is important to be able to predict the behavior of the fluidized system since the different groups may behave entirely different under similar operating conditions. From smallest to largest particle, they are as follows:

Group C: Cohesive, very fine powders. The interparticle forces are comparable to the gravitational forces on these particles. Hence these particles are difficult to fluidize.

Group A: Aeratable, materials having a small mean particle size and/or low particle density (<~1.4 g/cm^3). This class of particles is easy to fluidize and is used in many CFB systems. They have a smooth fluidization at low gas velocities and controlled bubbling with small bubbles at higher gas velocities.

Group B: Sandlike, most particles of size 40 μm < d_p < 500 μm and density 1.4 < ρ < 4g/cm^3. They fluidize well with vigorous bubbling action and bubbles grow large. And according to (Basu 2006) the majority of fluidized bed boilers use this group of particles.

Group D: Spoutable, large and/or dense particles. Deep beds of these particles are difficult to fluidize.

Geldart's classification is clear and easy to use. It is an important tool to predict behavior of a fluidized system. This is illustrated in figure 2.6.

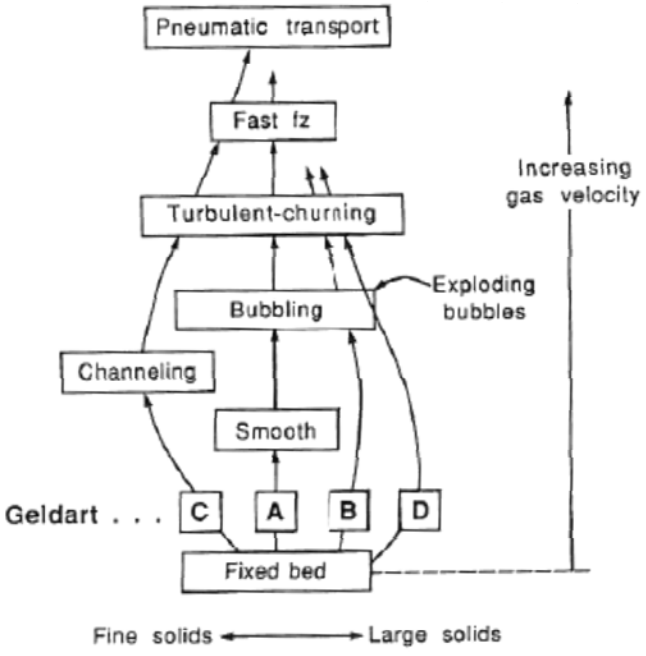

Figure 2.6 – *Behavior of a fluidized bed system is dependent on the properties of the particles* (Daizo Kunii 1991)

2.3 Hydrodynamics

Hydrodynamics is of high importance when looking at performance characteristics of a CFB. The hydrodynamic condition affects parameters of the reactor like heat absorption, temperature distribution, combustion conditions, bed inventory, and erosion. If operating conditions for some reason differ from the designed fluidization regime, one can expect changes in these parameters and a significant drop of overall performance. Thus, getting a good understanding of the gas-solids motion in the reactor of a fluidized bed system is essential. Fluidization is defined as the operation through which fine solids are transformed into a fluid-like state through contact with a gas or liquid (Basu 2006).

To give a short description of how fluidization occurs one can picture gas moving at a fixed velocity upward through a bed of solids lying on the bottom of a reactor. As the gas velocity increases, it will eventually reach a critical value, U_{mf}, known as the minimum fluidization velocity. Below the fluidization velocity the term fixed bed is used, while fluidized bed is used for velocities above.

In practice fluidization occurs as the pressure drop due to the fluid drag rises to a critical level where the weight of a particle is less than the buoyancy, and as a result the fixed bed transforms into a state known as incipiently fluidization. In this state the solids start behaving as a liquid. The pressure drop across the bed is equal to the weight of the bed, and the drag force of the fluidized particles can therefore be determined by the following equation:

$$F_b = \Delta P \times A = A \times L(1-\epsilon)\left(\rho_p - \rho_g\right)g \tag{9}$$

where A is the area of the bed, L is the height of the bed, ϵ is the voidage in the bed, while ρ_p and ρ_g are the densities of the particles and the gas respectively.

A more applicable way of using the formula is by giving it as the pressure drop per unit height:

$$\frac{\Delta P}{L} = (1-\epsilon)\left(\rho_p - \rho_g\right)g \tag{10}$$

Or as the differential equation:

$$\frac{dP(L)}{dL} = (1-\epsilon(L))\left(\rho_p - \rho_g\right)g \tag{11}$$

Superficial gas velocity U is defined as the gas flow rate per unit of cross section of the bed. As U is now defined an equation for the Reynolds number at minimum fluidization, Re_{mf}, can now be developed:

$$Re_{mf} = \frac{U_{mf} \times d_p \times \rho_g}{\mu} \quad (12)$$

where d_p is the surface volume mean diameter of particles as explained in 2.2.1, μ is the dynamic viscosity.

As the velocity increases, changes in the particle motions occur. At low velocities the particles may lay still, but as the velocity reaches an adequately high velocity the particles are transported out of the bed-vessel. As the gas velocity increases the solids move from one regime to another. In theory of CFB design and operation, three flow regimes are most often represented with respect to fluidization; bubbling, turbulent and fast fluidization. In this section characteristics of four fluidization regimes (figure 2.9) are presented and their applicability in the CLC concept discussed. Figure 2.7 illustrates the four flow regimes.

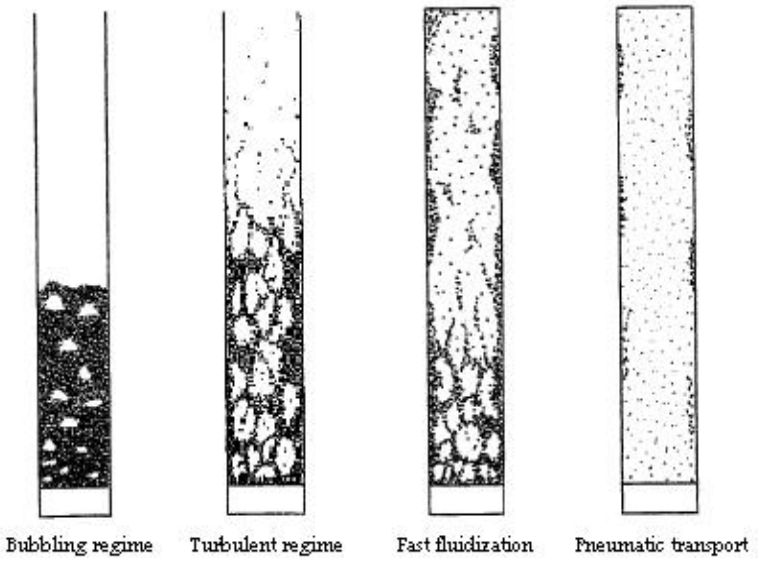

Figure 2.7 - *Flow regimes (J.R Grace 1997)*

There are two important factors for oxidation and reduction of the oxygen carrier. The flow regime describes the gas solid contact efficiency. The other factor is the residence time of the solids in the reactor. A conservative estimation of the residence time of the solids is given in equation 13:

$$t_{res} = \frac{m}{\dot{m}} \quad (13)$$

where t_{res} is the residence time [s], m the bed inventory [kg] and $\dot{m}$ the mass flow [kg/s].

2.3.1 Bubbly fluidization

Bubbling fluidization is recognized by rising voids (bubbles) formed near the bottom of the bed. At the top the bubbles break up periodically. The increasing bubble size is mostly due to coalescence, and increases with higher gas velocity. The superficial gas velocity in this case, U_{mb}, is known as the minimum bubbling velocity. U_{mb} is for Group A particles given by:

$$U_{mb} = 2.07e^{(0.716F)}d_p\left[\frac{\rho_g^{0.06}}{\mu^{0.347}}\right] \quad (14)$$

where F is the mass fraction of particles less than 45 μm.

Beyond a certain height in the riser, only a negligible amount of particles disengage from the gas to return to dense bed. This height is known as *transport disengaging height*, TDH. Figure 2.8 shows the different regions in a bubbling fluidized bed.

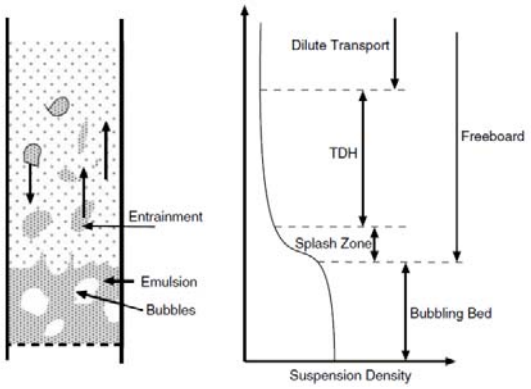

Figure 2.8 – A bubbling bed and its characteristic regions (Basu 2006)

Bubbling fluidized beds is not applicable to the CLC reactor due to constraints related to the gas-solids contact requirements. The problem with a bubbling bed system lies in unconverted fuel bypassing the bubble phase. Since CLC is a combustion process, a high fuel conversion ratio is required. Gas slip can be minimized by lowering the fluidization numbers and increasing the bed height. This results however in a large cross sectional area of the bed and large inventories (P. Kolbitsch 2009). Hence the reactor would not be economically feasible.

2.3.2 Turbulent fluidization

Turbulent fluidization is the transition from the bubbly regime and does not take place at a specific velocity. The transition starts at the top of the solids bed moving downwards and can be identified as small voids and particle clusters form eddies hurling around in the bed. As a

result of this chaotic behavior, the top surface is difficult to distinguish. The gas-solids contact is higher than in the case of bubbly fluidization. For beds containing fine particles, as is the case for CLC reactors, the turbulent fluidization occurs at a velocity sufficiently above their terminal velocity whereas coarser particles may enter turbulent fluidization at a velocity below their terminal velocity (Basu 2006). The terminal velocity, U_t, is the equilibrium velocity of a particle with respect to the forces exerted on the particle. In other words the terminal velocity is obtained when the acceleration force is equal to zero as shown in figure 2.9 and equation 14.

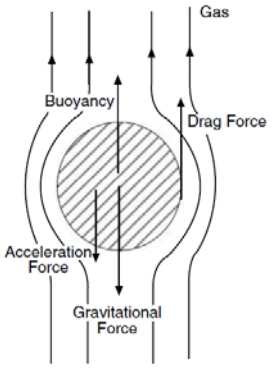

Figure 2.9 - *Force balance on a spherical particle moving upward (Basu 2006)*

The force balance presented in figure 2.9 gives the following steady-state equation for one single particle:

Acceleration force = Gravitation force - Buoyancy force - Drag force = 0

$$m_p a(U_t) = m_p g - \left(m_p \frac{\rho_g}{\rho_p} + C_D \frac{\pi (U - U_s)^2 \rho_g}{8} d_p^2 \right) = 0 \qquad (15)$$

where m_p is the mass of the particle, a acceleration, C_D is the drag coefficient, U is the free stream velocity and U_s is the velocity of the particle.

According to (Basu 2006) one can acquire the Reynolds number based on the terminal velocity by substituting the appropriate drag coefficient values in equation 15. This relation only applies to spherical particles. To simplify the Archimedes number is introduced:

$$Ar \equiv \frac{g d_p^3 \rho_g (\rho_p - \rho_g)}{\mu^2} \qquad (16)$$

Rearranging equation 15 and introducing the Archimedes number in the equation:

$$Ar = \frac{3}{4} \times C_D \left[\frac{d_p(U - U_s)\rho_g}{\mu}\right]^2 \quad (17)$$

Equation 15 reduces to the following forms for different values of the drag coefficient:

Stokes law, Re < 0.4 :

$$Re = \frac{d_p \times U_t \times \rho_g}{\mu} = \frac{Ar}{18} \quad (18)$$

Intermediate law, 0.4 < Re < 500 :

$$Re = \frac{d_p \times U_t \times \rho_g}{\mu} = \frac{Ar^{0.666}}{7.5} \quad (19)$$

Newton's law, Re > 500 :

$$Re = \frac{d_p \times U_t \times \rho_g}{\mu} = \frac{Ar^{0.5}}{0.33} \quad (20)$$

In terms of operating a CLC reactor in the turbulent fluidization regime compared to bubbling fluidization a benefit one obtains is gas-solids contact over the whole height of the reactor. This potentially allows operation with lower solids inventories which is especially relevant at increased plant capacities (P. Kolbitsch 2009).

2.3.3 Fast fluidization

The *fast fluidization* regime is the transition lying between turbulent fluidization and pneumatic transport. A clear picture of the transition to and from fast fluidization is currently not properly established, although a description has been composed. The critical transition velocity between turbulent and fast fluidization is denoted as U_{se} and the corresponding Reynolds number can be found from the following equation (H. T. Bi 1995) :

$$Re_{se} = 1.53 \times \mathrm{Ar}^{0.5} \qquad (2 < Ar < 4 \times 10^6) \quad (21)$$

The characteristics of fast fluidization are: High slip velocity between the gas and solids, formation and disintegration of particle clusters, and good mixing of particles and gas. Clusters are described in section 2.3.7. Fast fluidization has no distinguishable upper bed surface and the particles are transported out of the bed at the top. Therefore more particles must be added at the bottom of the bed in order to maintain continuous solids circulation. As discussed in section 2.3.8, clusters of particles move downward along the wall while gas moves upwards, entraining dispersed particles also moving upward. The gas-solids contact is higher compared to turbulent fluidization.

(Basu 2006) gives a detailed and descriptive interpretation of the transition taking place in reaching the fast fluidization regime. In the following this interpretation is presented.

In a riser the gas flows upward at a fixed solids circulation rate, G_s. The reactor in this case is assumed to operate in pneumatic transport. As the superficial gas velocity decreases the pressure drop as a function of the height will decrease due to reduced fluid friction on the wall. This is illustrated by the line descending from point C to point D in figure 2.10. As the velocity keeps decreasing the density of particles will increase, and as a result the gas-solid drag will dominate the pressure drop across the riser. As a consequence a pressure drop will occur due to both the wall-gas friction already mentioned as well as the gas-solid drag. Operating the reactor at steady-state conditions the gas-solid drag will be equivalent to the weight of the solids. As the superficial velocity keeps descending, the pressure drop increases. This can be seen as the line connecting point D and E in the figure. The low point of the curve, point D, represents the final transition to the complete fast fluidization regime.

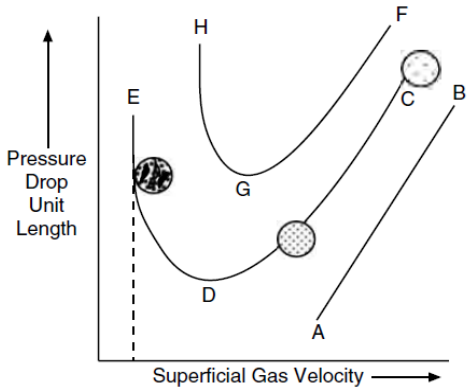

Figure 2.10 - *Regimes of gas-solids flow through a vertical riser (Basu 2006)*

If the velocity decreases further in the riser the solids hold-up increases and eventually becomes saturated with solids. At this point the solids start accumulating and clogging the riser, causing a rapid pressure increase. This state is known as choking and can be seen as point E in the figure. In large diameter-reactors such as the CLC-reactor the choking results in a transformation to a nonslugging dense-phase, such as turbulent fluidization. The state below

the vertical dotted line in figure 2.10 is known as the captive state and may include the turbulent and bubbling state, depending on the reactor design and operating conditions.

A useful way to qualitatively determine the transition from captive state to fast fluidization is presented in figure 2.11. In the flow regime map the solids circulation rate is plotted as a function of the superficial gas velocity. As the figure shows a minimum gas velocity must be achieved in order to bring the solids in the riser from the turbulent regime to the fast fluidization flow regime .This velocity , point A in the figure, is known as the transport velocity, U_{tr}. The transport velocity is defined as the critical velocity above which there is a sudden drop in particle residence time. Also, depending on the solid circulation rate, there is a maximum velocity boundary from which the bed passes into pneumatic transport, illustrated in the figure by the line connecting point A and C.

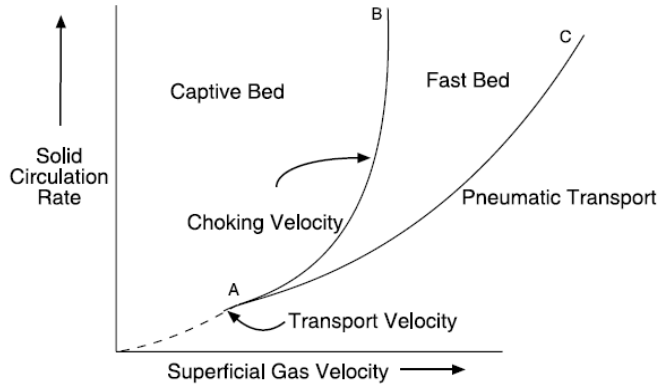

Figure 2.11 - *Fast fluidization constraints (Basu 2006)*

The transition to fast fluidization is dependent on various parameters, such as particle diameter, particle density, gas viscosity, gas density and the cross-sectional area of the riser. The flow regime diagram presented in figure 2.12 gives a qualitative representation of transition values of the mentioned parameters as a function of the superficial gas velocity. The most important point to extract from the diagram is the fact that the operating range of a fast fluidization reactor declines as the particles become coarser.

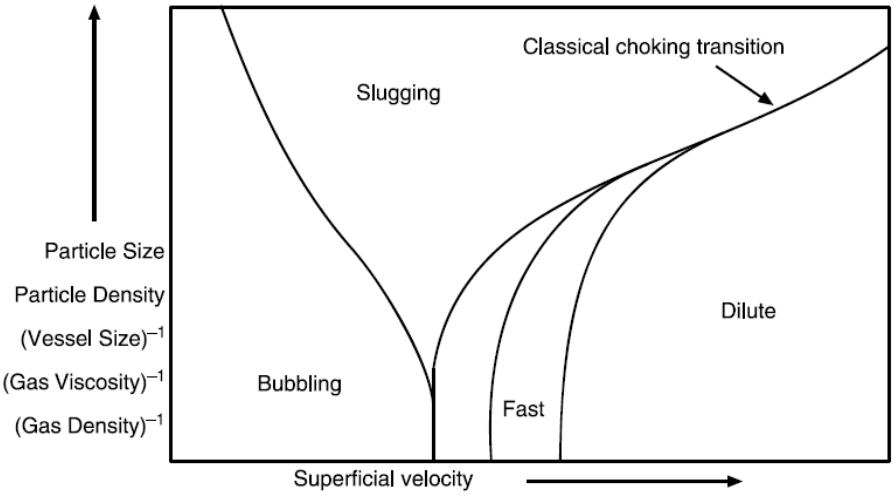

Figure 2.12 - *The transition from one regime to another depends on design parameters (Basu 2006)*

For a reactor system running two combined CFB reactors as is the case of a CLC reactor, it is advantageous to operate the beds in the fast fluidization regime. The reason for this is the fact that the gas-solids contact increases along the reactor height and the required amount of solids inventories decreases. With higher gas-solids contact one may also obtain a higher oxygen and fuel conversion. This depends on if the increased gas solid contact compensates for the reduced residence time for the particles in the reactors.

2.3.4 Pneumatic transport

Pneumatic transport also known as dilute-phase transport occurs when the gas velocity exceeds the boundary velocity of fast fluidization. It is characterized by the absence of axial variation of solids concentration through the reactor. The exception is at the bottom acceleration section of the reactor. Some clusters of particles may be observed close to the wall.

Operating in this regime is not commonly practiced, due to very low residence time. Descending residence time results in lower fuel conversion, and as a consequence, lowering the overall efficiency.

2.3.5 Flow regime maps

When determining the appropriate regime to operate the bed in it becomes necessary to evaluate the dimensionless numbers for particle size and gas velocity respectively. The equations for these two parameters are defined below.

$$d_p' = d_p \left[\frac{\rho_g(\rho_s - \rho_g)g}{\mu^2}\right]^{1/3} = Ar^{1/3} \qquad (22)$$

$$u' = u\left[\frac{\rho_g^2}{\mu(\rho_s - \rho_g)g}\right]^{1/3} = \frac{Re}{Ar^{1/3}} \quad (23)$$

To give a good visual idea of which hydrodynamic flow regime the air and fuel reactor should operate in, a flow regime map is very useful. Below the general flow regime map for gas-solids fluidization is presented. The superficial gas velocity, U^*, plotted against the dimensionless particle size, d_p^*, gives a good representation of the most important regimes related to CLC reactors. An example of this kind of regime map is presented in figure 2.13. U_c and U_{se} is the superficial velocity at the border between bubbling and turbulent regime and between turbulent and fast fluidization, respectively. Both the axis of abscissas and ordinate follow the log-normal function.

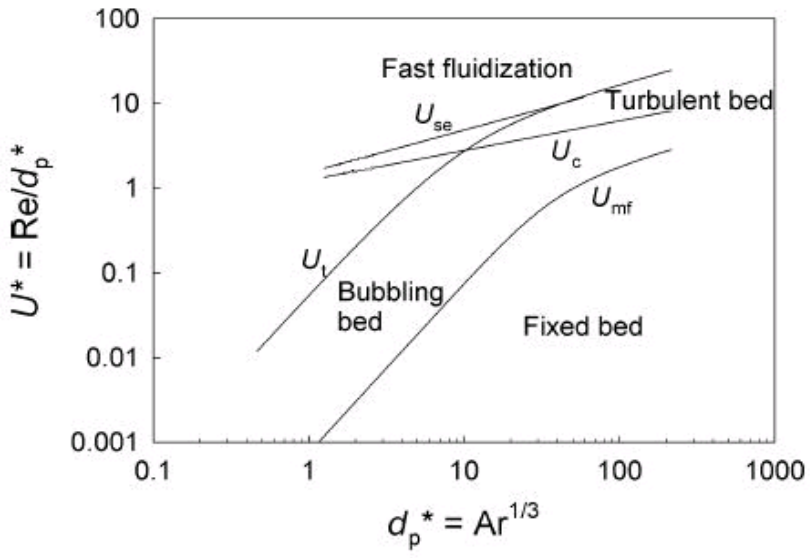

Figure 2.13 - *Flow regime map for gas-solids fluidization (P. Kolbitsch 2009)*

2.3.6 Pressure profile in fast bed reactors

The particle distribution and fluidization regime is closely related to the pressure profile along the reactor height. A close to exponential declining pressure profile from the bottom to the top of the reactors riser gives the distribution of particles wanted in a CLC reactor. This corresponds to turbulent or fast fluidization, commonly referred to as the regimes found in fast beds.

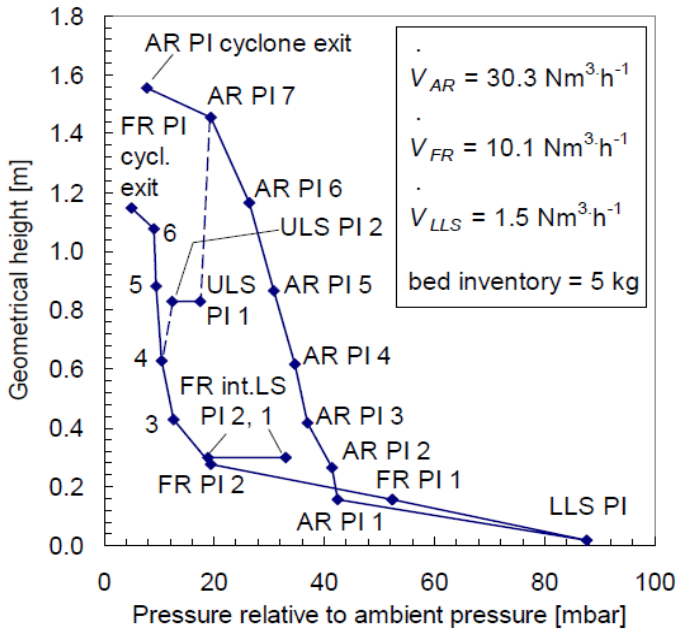

Figure 2.14 - *A typical pressure profile in a Chemical Looping reactor system, CFM from Vienna University (Tobias Pröll 2009)*

The high pressure at the bottom of the reactors indicates a dense region of particles. Along the reactor height the pressure drops. This is a partially a result of lower particle concentrations, but mainly due to a smaller gas-solid head. When the reactor design parameters are set, the pressure profile will vary depending on the solids inventory, mean particle size and volume flow of gas. From the pressure profile one also gets an indication of the solids level in the riser. This is the point where the pressure drop gradient decreases significantly. In figure 2.14 these points are recognized as AR PI 1 and FR PI 2 at 0.15m and 0.30m, respectively. The total amount of solids in the riser can be estimated from equation 24 and is defined as "active inventory" in this report. The equation can also be used to calculate the amount of solids located at different heights in the riser.

$$m_{AR/FR} \approx \frac{(P_{top,AR/FR} - P_{bottom,AR/FR})A_{AR/FR}}{g} \qquad (24)$$

where $P_{top,AR/FR}$ and $P_{bottom,AR/FR}$ is the pressure at the top and bottom of the respective reactors, $A_{AR/FR}$ is the cross sectional areas of the respective reactors and $m_{AR/FR}$ is the amount of solids in the respective reactor.

It should be noted that the equation only gives an estimation of amount of solids in the riser. It does not take into account that some of the pressure drop energy is used to accelerate the

solids, friction losses. However, the pressure drop due to solids acceleration and friction are not considered significant at low circulation rates according to (Bi and Zhu 1993).

As seen in figure 2.14 there is a pressure drop through the cyclone. This can be observed as the final pressure drop at the top of the pressure profile curves. The pressure loss in the cyclone is proportional with the gas flow.

2.3.7 Cluster phenomenon

Clusters are an agglomeration of solids. As shown in figure 2.15 a wake is produced behind the particles. Clusters are made at conditions where the solids concentration is high and the particles enter each others wakes. When a particle enters another particle's wake it will fall down on this particle due to the reduced drag. The effective surface area of the pair just formed is lower, so the fluid drag will be lower than their combined weight, causing to fall further and collide with other particles. The result of this is that an increasing number of particles combine together to form agglomerates known as clusters. It should be emphasized that clusters are not permanent, but are continuously torn apart by the up-flowing gas.

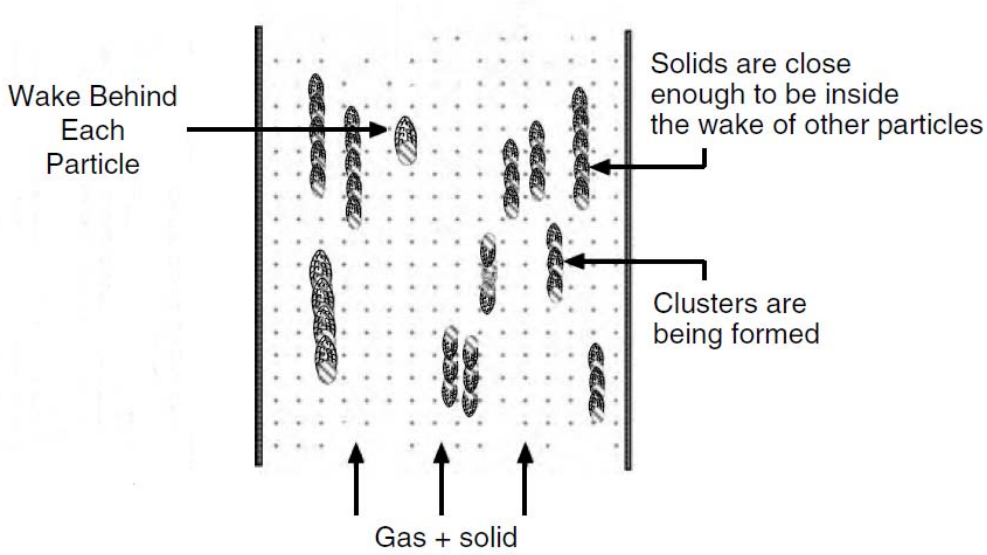

Figure 2.15 – *Illustration of the cluster phenomenon* (Basu 2006)

2.3.7 Lateral distribution of solids in a fast bed

According to (Basu 2006) the typical riser of a CFB boiler can be split into two vertical regions: core and annulus. The velocity in the core is higher than the superficial gas velocity through the riser, while the velotcity of the gas in the annulus is low or even negative. The solids move upwards through the core with occasional presence of clusters. Clusters drift sideways due to

hydrodynamic interactions they are exposed for and are then exposed for gas velocities that are too low or even negative to carry the clusters upwards. The result is that the clusters falls down in the low-velocity region near the riser wall. This leads to a internal circulation of solids in the bed, in addition to the external circulation where the solids are captured in the cyclone and returned to the bed. (Basu 2006) states that the internal circulation rate can be many times the external circulation rate. The temperature uniformity of the bed in CFB boilers is a direct consequence of this internal solid circulation. Figure 2.16 shows the core annulus model of the flow structure of a fast bed riser.

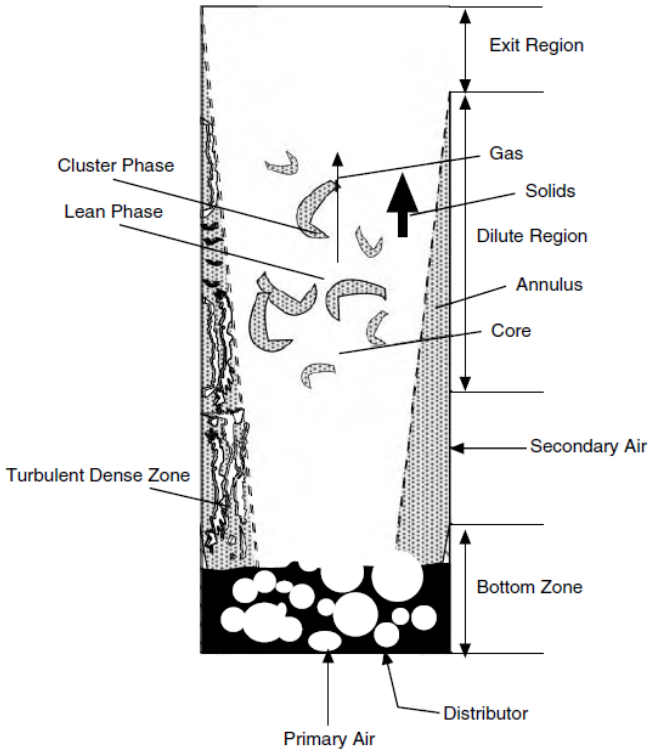

Figure 2.16 - *Core annulus model of the flow structure in a fast bed riser* (Basu 2006)

2.4 150 kWth DCFB CLC reactor – SINTEF/NTNU, Hot rig

SINTEF and NTNU have worked out the design of a new and innovative CLC reactor system. The reactor has yet to be built, but it is estimated that the rig should be completed and ready for operation some time in 2010. The 150 kW_{th} DLCFB CLC reactor – SINTEF/NTNU will from now on be referred to as the hot rig. The hot rig can also operate as a CLR, Chemical Looping Reformer. The design focuses on being strongly industrial oriented, making it easier to perform a scale up from lab-scale to industrial size, and eventually commercialization. The rig

has a very compact design both of industrial reasons as well as simplifying the process of disclosing the rig inside a pressurized vessel for integration in a gas turbine power cycle.

The reactor design uses two divided loop-seals interconnecting the two reactors. Further the air, steam and fuel injection nozzles are designed in accordance to conventional industrial CFB units. When it comes to the cooling panels used for the reactor, these are a type of industrial protruding cooling panels integrated into the reactor body. Also, the scientists involved are striving to make the rig flexible in terms of operating it with multiple types of oxygen carriers and fuels. The key factor in order to realize this is the divided loop-seal which allows recirculation of particles, hence increasing the particle residence time. This enables the use of oxygen carriers with poor fuel conversion rates.

When designing the cyclone separator of the rig, special focus was addressed to the fact that it should be able to operate as a heavy load cyclone aiming at reducing particle losses to the flue gas exit stream to a minimum. Special characteristics of the cyclone separator, which improve the cyclone efficiency, are related to the design of the inlet ducts vertical angel and cross section. The inlet duct angel is downward declining, while the cross sectional area has a sharp reduction improving the cyclone efficiency this is further explained in section 2.4.4.

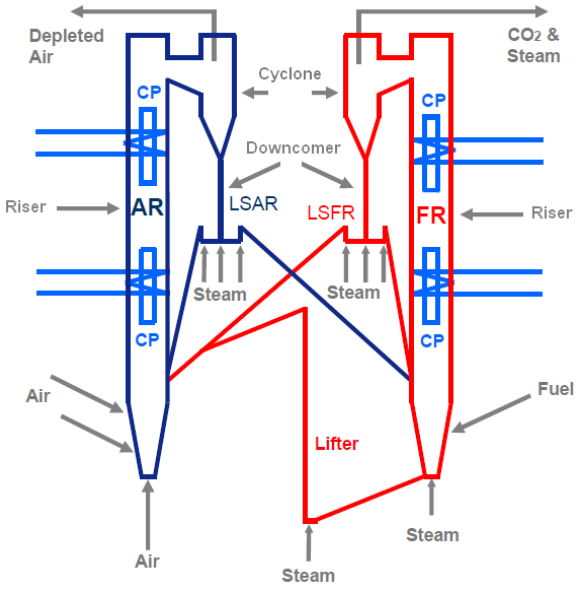

Figure 2.17 - *Process flow diagram (M. Bysveen 2009)*

The Cold Flow Model has been built to verify the design of the hot rig. Even though the experiments will be performed on the CFM, a good understanding of the mode of operation of

the hot rig is important to be able to verify the hot rig design. The hot rig and its components are therefore explained. Figure 2.17 shows the flow diagram of the entire process.

The architecture of a CLC reactor differs somewhat from the original CFB design. As mentioned introductorily the CLC reactor system consists of two interconnected circulating fluidized beds which circulate a metal oxide between them. In this design two divided loop-seals are introduced. The purpose of this design aspect is to both enable recirculation of particles to the same reactor and transport to the other. The benefit one achieves with this kind of configuration is better control of mass flows and particle residence time; the latter increasing oxidation in the air reactor and fuel conversion in the fuel reactor. The particles known as oxygen carriers are transported upward through the reactor bodies. This circular tube is known as the riser. To avoid air and fuel from being transported to the opposite reactor, the oxygen carrier particles are separated in a cyclone separator and transported through the downcomer section before and sent through the divided loop-seal. The divided loop seals prevent gas mixing between AR and FR. Steam is applied at various points in the reactor in order to control circulation rates. The essential components of the hot rig are further explained in the following sections, 2.41 – 2.4.7.

2.4.1 Oxygen carrier

The oxygen carrier is, as mentioned in the previous section, used to transport oxygen from the air reactor to the fuel reactor. When choosing an oxygen carrier it is important that the material has a high level of reactivity both in terms of oxidation and reduction. The ability of combusting completely with the fuel is also of significant importance. Other important characteristics of the oxygen carrier are; stability under repeated oxidation/redaction at high temperature, fluidization ability, agglomeration resistance, mechanical resistance when exposed to friction stress associated with high circulation of particles, low local environmental impact and economically feasible (Hossain and de Lasa 2008). There exist a variety of metal oxides suitable for use in a CLC reactor. The ones given most attention are Ni-, Cu- and Fe-based metal oxides. OCs should be available in large quantities and be a less harmful as possible.

An important point to investigate when choosing an oxygen carrier is that the oxygen transport capacity is high enough. This in order to obtain necessary solids circulation rates in the reactors. The solids circulation rate can be determined by finding the oxygen ratio, R_o:

$$R_0 = \frac{M_{OC,ox} - M_{OC,red}}{M_{OC,ox}} \tag{25}$$

where $M_{OC,ox}$and $M_{OC,red}$ are the molar masses of the oxygen carrier fully oxidized and fully reduced

The higher R_0 is, the less solids circulation is required. This can be explained by the fact that the total amount of oxygen transported is the oxygen released in the fuel reactor. When dividing this number by the total amount of oxygen transported into the reactor the oxygen ratio is found.

The conversion of the oxygen carrier, X, is defined as:

$$X = \frac{M_{OC} - M_{OC,red}}{M_{OC,ox} - M_{OC,red}} \tag{26}$$

Where $M_{OC}$is the actual molar mass of the oxygen carrier

When approximating steady-state operating conditions, the conversion difference between the fuel reactor inlet and outlet, ΔX, is given by:

$$\Delta X = X_{FR,in} - X_{FR,out} = X_{AR,out} - X_{FR,out} \tag{27}$$

where $X_{FR,in}$is the conversion of the OC entering the FR, $X_{FR,out}$ leaving the FR and $X_{AR,out}$ leaving the AR

The degree of oxidation describes the exploitation of the oxygen carried by the OC within the reactors. This parameter is especially crucial for the reduction reaction in the FR which is slower than the oxidation reaction in the AR. Using this parameter one can decide the necessary solids circulation rate from the equations for fuel flow and oxygen carrier flow:

$$\dot{m}_{fuel} = \frac{P_{fuel}}{LHV} \tag{28}$$

where P_{fuel}thermal effect of the reactor system and LHV is the lower heating value of the fuel

$$\dot{m}_{OC} = \frac{O_{min}\dot{m}_{fuel}}{R_0 \Delta X} \tag{29}$$

where O_{min} is the oxygen demand for full oxidation of the fuel

From equation 29 one can see that high conversion difference, gives low required solids circulation rate.

The solids circulation rate is defined as:

(30)

where A_{AR} is the cross-section area of the air reactor.

Degradation of the oxygen carrier is a major challenge within Chemical Looping Combustion. (Rubel, Liu et al. 2009) performed a study of oxygen carriers and its properties during an extended period of time. Degradation leads to decreased performance and further research should be done on optimal OCs and operating conditions.

2.4.2 Air reactor riser

The main function of the air reactor riser is to oxidize the oxygen carrier. Cold or preheated air enters the lower section of the air reactor fluidizing the solids bed. One way of securing proper fluidization is by staging the air injection points. By staging the air injection the particles in the upper part of the bed are better distributed. The bottom nozzle is in figure 2.18 is the primary nozzle. The nozzles located above the primary nozzle are the secondary nozzles #1 and #2.

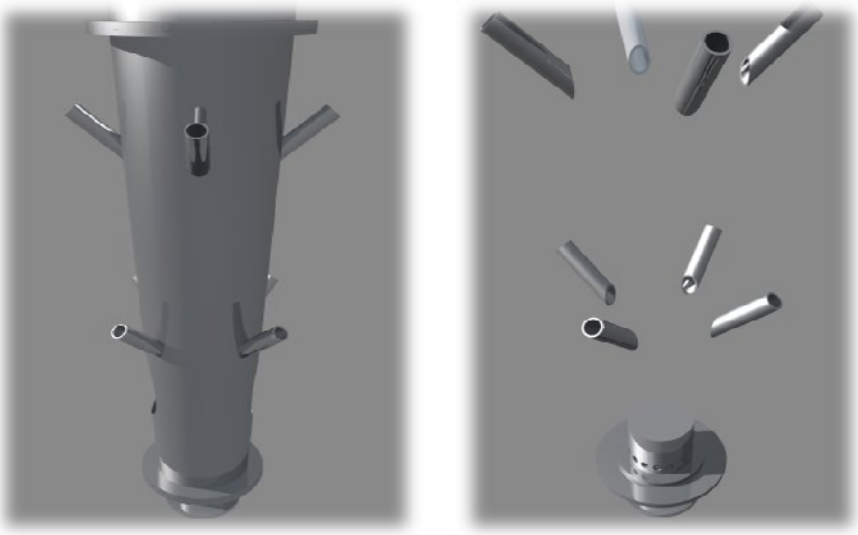

Figure 2.18 - *Primary and secondary air injection nozzles*

The reaction taking place in the air reactor is strictly exothermic and a large amount of heat is released. The temperature of the air reactor, also referred to as the oxidation temperature is typically in the magnitude of 1200K. Due to this high temperature, the reactor must be equipped with proper insulation and cooling panels. Also selecting an appropriate type of material for the reactor is a point to note during the design phase of the CLC reactor.

The oxygen in the air flow reacts with the oxygen carrier by oxidation. The oxidized carrier is then transported to the fuel reactor. The depleted air is vented out at the exit section located at the top of the reactor.

For a CLC reactor system, the air reactor is operated as a turbulent or a fast fluidized bed. What characterizes the different fluidization regimes is discussed in sections 2.3.2 and 2.3.3. These two types of flow regimes are very similar and the vital factor in terms of what is the preferred regime to operate in is determined by the highest oxygen conversion, X.

When setting the design parameters for the air reactor, it may prove useful to first decide what regime is most suitable to operate in. For fast fluidization the low-limit velocity and Reynolds number are denoted U_{se} and Re_{se}. U_{se} and Re_{se} is defined as the transition- velocity and Reynolds number from the turbulent regime to the fast fluidization regime. The maximum design gas velocity should be set to 2 U_{se} to ensure proper solid circulation at different operating conditions (P. Kolbitsch 2009). Further the reactor height is decided with respect to the necessary residence time of the solids and gas. Once this is done the equations presented in section 2.4.1 are used to determine the solids circulation rate.

2.4.3 Fuel reactor riser

The fuel reactor riser in a CLC reactor system reduces the oxidized oxygen carrier entering from the air reactor. The oxidized oxygen carrier enters the bottom part of the fuel reactor and is fluidized with staged gaseous fuel and steam. The fuel and steam flows fluidize the solids in the fuel reactor, most commonly in the fast fluidization regime. The fuel reactor is operated as a fast bed because the fast fluidization regime provides the best particle distribution along the reactor height and best gas solid contact efficiency.

Steam is utilized in order to secure sufficient gas velocities, thus appropriate fluidization and gas solid contact efficiency. Air would not be a good idea to ensure fluidization in the fuel reactor. This is because the air would react with the fuel. Steam is a neutral fluidization medium in the fuel reactor compared to air in this way. The critical point in terms of obtaining satisfying reactions between the oxygen-rich carrier and the fuel is to ensure sufficient solids-gas contact throughout the entire reactor body. High particle entrainment is therefore important, as it gives a good particle distribution. A high level of entrainment is obtained by regulating the solids circulation rate as a function of the fuel flow, operating at velocities higher than U_{se}. The corresponding Reynolds number, Re_{se}, can then be calculated.

The design of the fuel reactor focuses on the gas-solids contact and solids inventory of the reactor. Optimizing the operating conditions in the fuel reactor is essential as it seems that the crucial reaction steps in a Chemical Looping Combustion reactor from a kinetic point of view are located in the fuel reactor.

2.4.4 Cyclone separator

At the upper end of both the air and fuel reactor the particles need to be separated from the exit air and fuel streams, respectively. There are numerous methods of particle separation from gas streams. Since every separator uses different principles they each have different properties regarding collection efficiency and process suitability. Separators have a practical size range which means that reasonable collection efficiencies are achieved in that range. This is shown in figure 2.19.

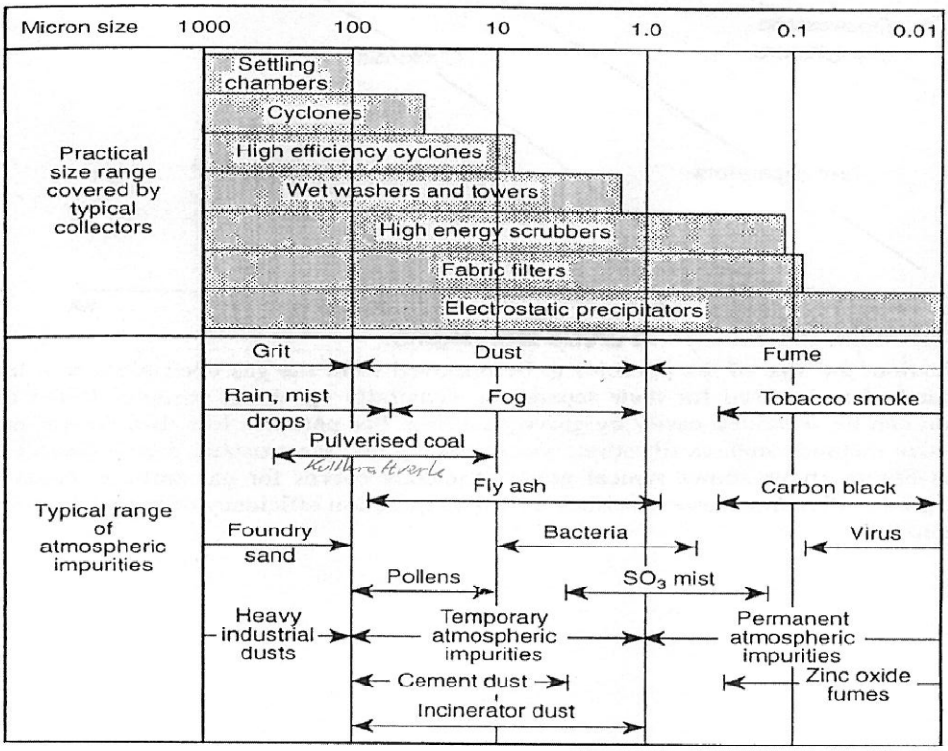

Figure 2.19 - *Practical size range covered by typical collectors (Krammer 2008b)*

The component used for the solids-gas separation in a CLC reactor is called a cyclone separator. The cyclone exposes the mixed stream to a radial centrifugal force which in turn drives the solid particles to the cyclone wall, where they slide down to the loop-seal. It is also exposed to drag and buoyancy forces. While the centrifugal force works radially outwards these two forces work radially inwards.

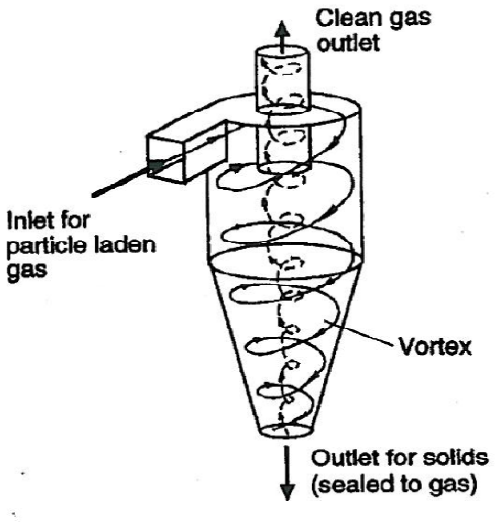

Figure 2.20 - *Gas-solids separation in a cyclone (Krammer 2008b)*

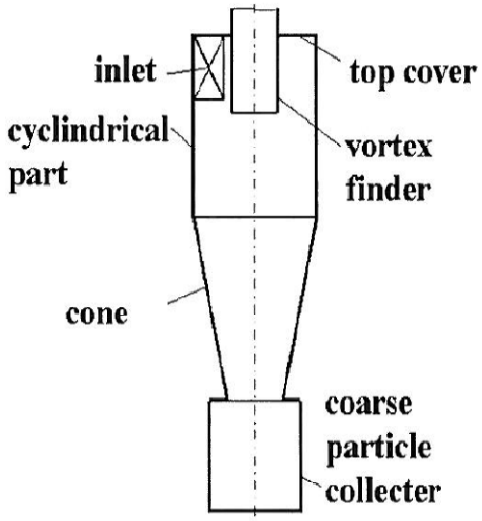

Figure 2.21 - *Typical cyclone configuration (Krammer 2008b)*

According to (Krammer 2008b) there are three major values of interest when designing a cyclone. These are the total pressure loss, critical particle size and separation efficiency. Ideally the critically particle diameter means that larger particles can only be found in the coarse fraction, the separated particles, and smaller particles in the fine fraction which exits through the vortex finder. Both ideal and real separation is illustrated in the grade efficiency curve in figure 2.20. A collection efficiency, Φ, can be defined as the ratio of mass flow of the separated particles, $\dot{M}_C$, and the total mass flow of the solids entering the cyclone $\dot{M}_i$:

$$\Phi = \frac{\dot{M}_C}{\dot{M}_i} \tag{31}$$

However, the effectiveness of dust separation is strongly dependent on particle size. A term known as the grade efficiency is therefore defined. The grade efficiency, T(x), is simply the collection efficiency as a function of the particle size x. It shows how well the cyclone separates particles at certain particle sizes. T(x) is in general independent of the PSD and is constant for a certain set of operation parameters e.g. viscosity, solid concentration, total mass stream, (Krammer 2008b). T(x) is characteristic for the separation unit:

$$\mathrm{T(x)} = \frac{\dot{M}_C(x)}{\dot{M}_i(x)} \tag{32}$$

The grade efficiency covers the range from zero (no particles collected) to one (all particles collected). The steeper the grade efficiency curve is, the better the separation.

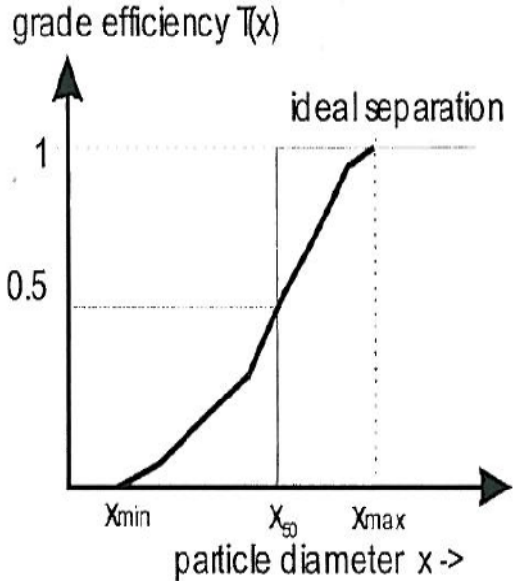

Figure 2.22 - *Example of a grade efficiency curve (Krammer 2008a)*

The collection efficiency can be used to tell how efficient the cyclone is, but it will not be a number comparable with cyclones at other operating conditions. This is why the grade efficiency is a useful parameter.

It should also be mentioned that the loading is an important parameter. The loading is the mass flow, $\dot{M}_{solids}$, of solids divided by the gas mass flow, $\dot{M}_{gas}$, entering the inlet of the cylinder:

$$\mu_e = \frac{\dot{M}_{solids}}{\dot{M}_{gas}} \tag{33}$$

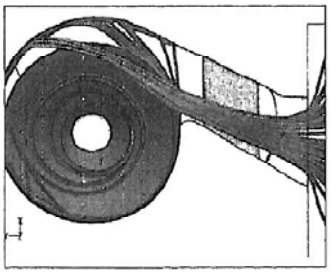

Figure 2.23 - *Before reconstruction (Krohmer 2006)*

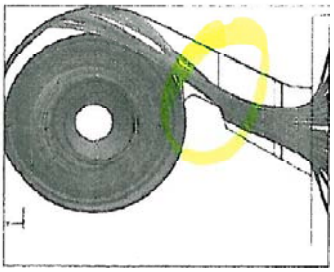

Figure 2.24 - After reconstruction (Krohmer 2006)

The rig uses a so called heavy load cyclone. This is cyclones designed for a high load of solids in the gas stream. It is vital to have a good collection efficiency since this reduces necessary OC refilling and is essential if the system is to be integrated in a gas turbine cycle. A great deal of research has been done in order to improve cyclone design in CFBs, and furthermore increase the collection efficiency. In recent years research on the inlet duct of the cyclone has been performed. A result of this study shows that by decreasing the inlet surface area of the inlet duct one can improve several parameters such as the collection efficiency and long term stable pressure profile (Krohmer 2006).

2.4.5 Downcomer

The downcomer is basically a vertical piece of pipe, connecting the cyclone and the loop seal. The purpose of a downcomer is to transport solids from a region of lower pressure to a region of higher pressure.

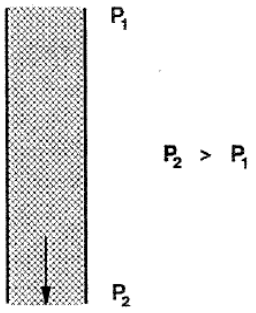

Figure 2.25 - *Downcomer (J.R Grace 1997)*

This can be accomplished by the gravitational force against an adverse pressure gradient if the gas flows upward relative to the downward flowing solids (J.R Grace 1997).When solids travel down in the downcomer, they drag some air with them. Thus the direction of the gas flow relative to the wall can be either upward or downward. The relative gas-solids velocity should

however be directed upward, as seen in figure 2.26 and 2.27. The gas flowing upwards relative to the solids generates a frictional pressure drop.

The relative gas-solids velocity is defined as:

$$V_r = |V_s - V_g| \tag{34}$$

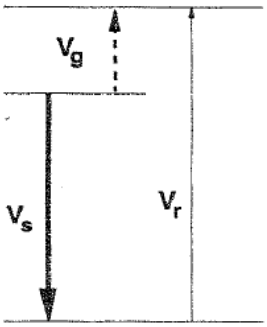

$$V_r = V_s - V_g$$

$$V_r = V_s - (-V_g)$$

$$V_r = V_s + V_g$$

Figure 2.26 - *Gas flowing upward relative to pipe wall (J.R Grace 1997)*

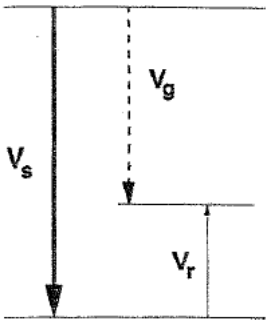

$$V_r = |V_s - V_g|$$

Figure 2.27 - *Gas flowing downward relative to pipe wall (J.R Grace 1997)*

2.4.6 Loop-seal

A loop-seal is a non-mechanical valve that facilitates the flow of solids between the downcomer and the riser, without any external mechanical force (Basu 2006). The CLC reactor is equipped with a divided loop-seal. The loop-seal consists of three sections; one supply chamber connected to the downcomer, and two recycling chambers transporting the oxygen carrier to the air and fuel reactor, respectively. A traditional loop seal has only one recycle chamber. Three steam injection nozzles are introduced at the bottom of each section and can be regulated in order to secure fluidization and for controlling the distribution of the solid flow between the two exit flows. According to (Basu 2006) solids circulation through the loop-seal increases with:

- Increasing fluidizing velocity through recirculation sections
- Higher solids inventory in the reactor system
- Larger downcomer dimensions
- Finer particle size
- Higher gas velocity in riser
- Higher system pressure.
- Increasing purging air on the vertical wall of the supply chamber. Purging air is explained later in this section.

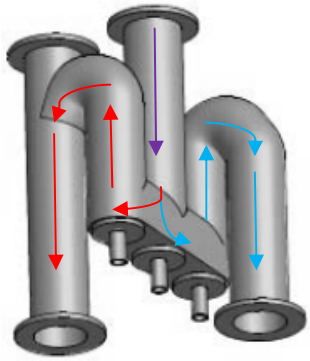

Figure 2.28 - *Divided loop-seal design*

The loop-seal is designed in way that provides a loop seal exit pressure greater than the pressure at the lowest elevation of the reactors. This pressure difference is essential to have a

pressure seal in the loop seal. A simple pressure balance for the two reactor loop-seals can be set up in order to illustrate the function of this unit.

Pressure balance for air reactor loop seal:

$$P_{FR} - \Delta P_{FR,dist} - \Delta P_{FR} < P_{LSAR} - \Delta P_{LSAR,dist} - \Delta P_{LSAR} > P_{AR} - \Delta P_{AR,dist} - \Delta P_{AR} \quad (35)$$

Pressure balance for fuel reactor loop seal:

$$P_{FR} - \Delta P_{FR,dist} - \Delta P_{FR} < P_{LSFR} - \Delta P_{LSFR,dist} - \Delta P_{LSFR} > P_{AR} - \Delta P_{AR,dist} - \Delta P_{AR} \quad (36)$$

P_{AR}:	Pressure before distributor in bottom of the air reactor
$\Delta P_{AR,\ dist}$:	Pressure drop across distributor between the loop seal and air reactor
ΔP_{AR}:	Pressure drop from reactor bottom to the height of the bed where recycle solids enter the air reactor
P_{FR}:	Pressure before distributor in bottom of the fuel reactor
$\Delta P_{FR,\ dist}$:	Pressure drop across distributor of the loop seal and fuel reactor
ΔP_{FR}:	Pressure drop from reactor bottom to the height of the bed where recycle solids enter the fuel reactor
$P_{LSAR/LSFR}$:	Pressure in the plenum of the loop-seal
$\Delta P_{LSAR/LSFR,\ dist}$:	Pressure drop across the distributer of the loop-seal
$\Delta P_{LSAR/LSFR}$:	Pressure drop across fluidized bed in loop-seal recycle chamber

The driving forces for the solid transport in the loop seal are the pressure difference between the loop seal and the return leg and the recirculation air.

In the CFM air is used as the fluidizing medium. However in the hot rig steam will used as a fluidizing medium. Steam injections in the loop seal should be limited. Excessive use of steam increases operating costs and may also break down the pressure seal around the loop seal. According to (Basu 2006) air/steam to the supply chamber should not exceed the minimum fluidization velocity for the average particle size of the circulating solids. The recycle chamber should be kept fluidized at a velocity greater than 1.25 times the minimum fluidization velocity of the larger particles in the loop seal.

Purging air is small amounts of additional air added at strategic locations in the loop seal. This is shown in figure 2.29. This reduces friction between the wall and the particles. It also reduces the interparticle frictional forces since air percolating through the particles acts like a lubricant. Interparticle friction is a function of particle shape and size. Hence purging air helps the solids move better through the loop seal.

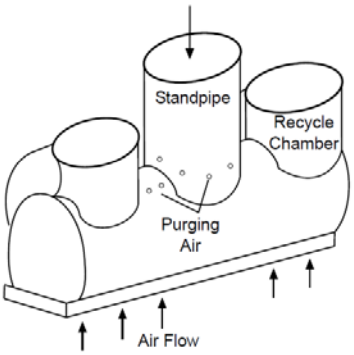

Figure 2.29 – *Loop seal with "grease air", also called purging air* (Basu 2006)

Purging air was not used during the experimental campaign, but was later installed and showed promising results during testing.

2.4.7 Lifter

A lifter is assembled between the two reactors in order to increase the maximum physically possible solid circulation rate from the fuel reactor back to the air reactor and to give the rig a higher degree of operational flexibility. The driving forces are two steam injection nozzles, one located at the bottom part of the lifter and the second one located a higher elevation on the lifter. To a certain degree the pressure difference between the bottom part of the FR and AR is also a driving force. The pressure is in general higher in the FR than in the AR and aids the solid transport. Figure 3.1 shows the lifter going from the bottom of the fuel reactor to the air reactor.

2.5 150 kWth DCFB CLC reactor – SINTEF/NTNU, Cold Flow Model

A 1:1 scaled cold flow model of the hot rig has been built. The CFM circulates non-reacting particles and air, simulating the oxygen carrier and gas flows in a hot rig. No reactions take place in the cold flow model, and all steam injections are simulated with air injections.

The CFM is used to verify the design of the hot rig and gain operating experience. This includes testing unit designs and how to operate them: the new divided loop seal technology, lifter, cyclone separator and the AR- and FR riser. Therefore the main objective of the CFM is to achieve the solids circulation rate between AR and FR and have the appropriate gas solid

contact efficiency, hence the proper flow regime and solid distribution in the risers. The process of determining these parameters is done by finding the optimal volume flows at the different staged air injection points in the risers, lifter and loop seals. A tool for describing the solids distribution and flow regime in the risers are pressure profiles as a function of the height. Learning how to operate and regulate the solids circulation rates internally and between the reactors is an important lesson from the CFM, since there must be a mass balance between AR and FR when running both reactors.

Design and operation of the CFM is complex, however the hot rig offers many additional challenges. Therefore thorough testing with the CFM is essential to gain operating experience and find faults and possible improvements of the system so that adjustments can be done before building the hot rig.

3. Experimental setup

The rig has been mounted inside a steal bearing structure. This structure is meant to stabilize and reduce vibrations during operation both in horizontal and vertical direction. In order to perform necessary pressure measurements along the reactor bodies, tubes are connected between nipples on the reactors and pressure transducers. The air flow entering the rig is controlled by fourteen mass flow controllers; six for each reactor, and two for the lifter. In the riser of the two reactors air injection is controlled at three stages through a primary, secondary #1 and secondary #2. The secondary #2 nozzle in the FR is not used in any of the experiments. The location of these three injection stages are for the both reactors 0m, 0.4m and 0.8m. In addition the loop-seals have three air flow nozzle which are adjusted according to the desired amount of solids flux back to the reactor of origin, or opposite reactor. Downstream the cyclone separators a filter box is installed. The filter box will stop the rest of the particles from escaping. The collected particles can be extracted from the filter box and weighted. This provides the opportunity to test the cyclone efficiencies at different operating conditions. Figure 3.1 shows the principle of the rig, air injection points, exhaust flows and flux measurement valves. Figure 3.2 shows the location of the pressure transducers on the rig.

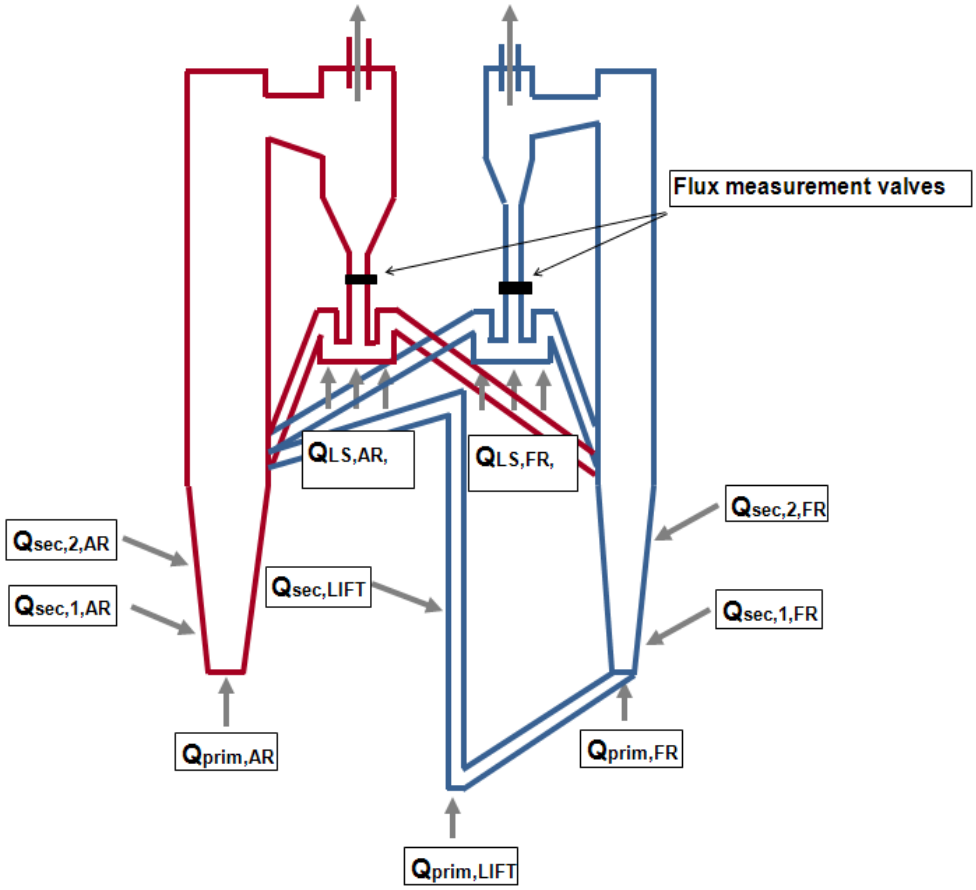

Figure 3.1 - *Air injection points and flux measurement valves at the CFM*

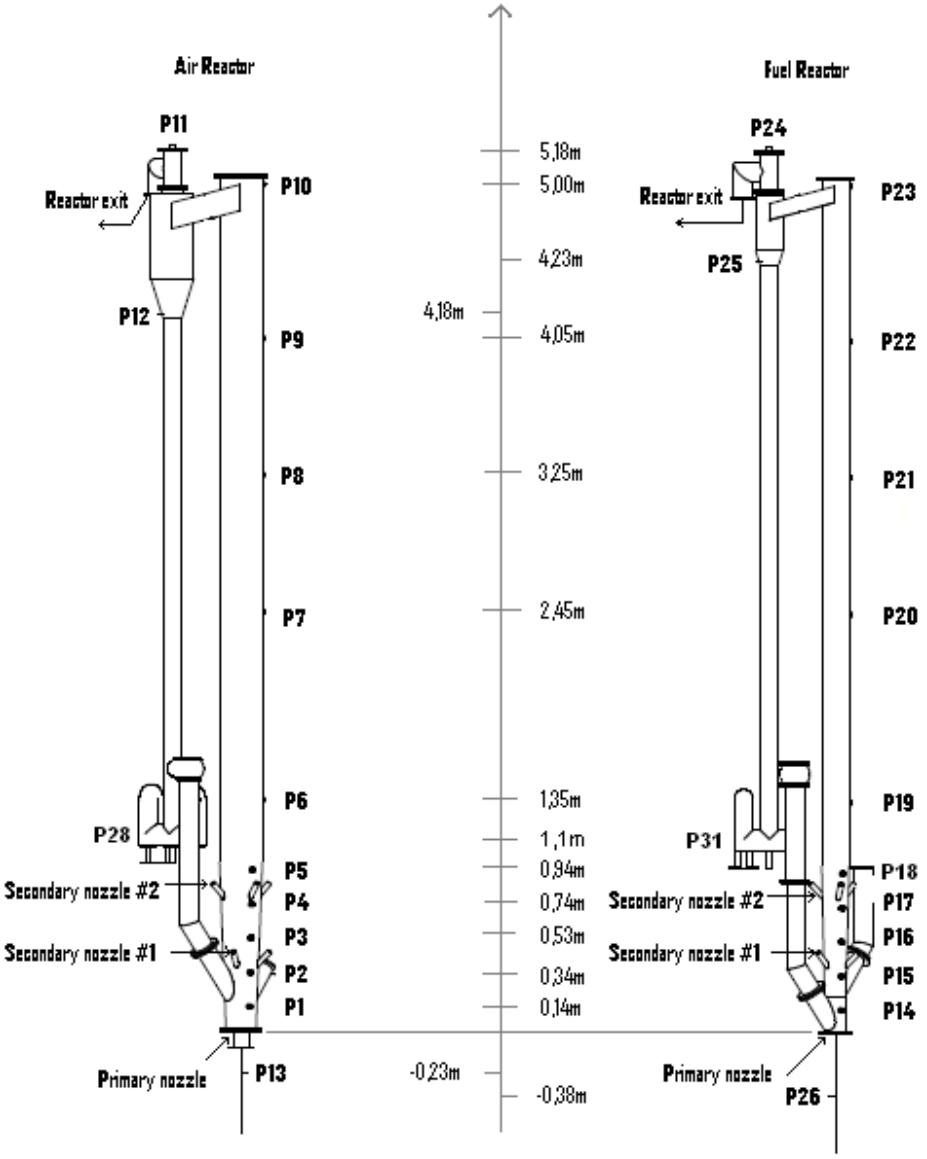

Figure 3.2 - *Reactor system with pressure transducer elevation points*

The results from the pressure transducers P13 & P26 shown in figure 3.2 are not used in this report. They measure the pressure before the nozzles into the reactors. They are useful to check if a proper pressure drop is achieved in the nozzle. This is essential if the nozzle is to function according to design and distribute the flow as designed.

4 Measurement equipment and software

4.1 Pressure Transducers - Fuji FCX-AII

The Cold Flow Model has been equipped with 31 differential pressure transducers that are connected with plastic tubes at various points along the two reactors. The pressure transducers are of the type FCX-AII and measure the relative pressure difference when a reference pressure is set. In the case of the 150kW CFM the pressure transducers are set to the pressure at the top point of each reactor, P10 and P23. The pressure measurement at the top of the reactors is referenced to atmospheric pressure. All pressure measurements given in this report are recalculated to be relative to the atmosphere.

Figure 4.1 - *FCX-AII, Differential Pressure Transducer* (AT&P Journal 2010)

The pressure transducer transmits a 4 to 20mA DC digital signal that is acquired and processed by a LabView acquisition system described in section 4.4. Each transducer has been calibrated individually at two points, low and high pressure, to generate a linear conversion curve. This curve is used to convert the digital current signal into proportional pressure readings.

Furthermore, the tubes connected between the pressure transducers, PTs, and the reactors are coupled via a magnet valve which is triggered manually in LabView and applies the tubes with a countercurrent air flow. This “blow out”-system is used in order to avoid solids from entering the PT tubes, causing errors in the pressure measurements.

4.2 Mass flow controller - Brooks® Mass Flow Meter Model 5863

In order to control the amount of air flowing into the reactors providing circulation and fluidization of the solid inventory, 15 mass flow controllers have been installed at different points along the lower part of the reactor bodies. The mass flow controllers are operated by a LabView program designed for operating the rig. LabView is described in section 4.4. By adjusting the volume flow rate in LabView one can determine the optimal mass flow rates for each of the mass flow controllers, thus obtaining specified operating conditions.

Figure 4.2 - *Brooks® Mass Flow Meter Model 5863* (Brooks Instruments 2008)

4.3 Weight - Mettler Toledo XS 32000L

To weight used was a Mettler Toledo XS 32000L. This is a high accuracy weight and more data are given in appendix VIII. The weight was used to weigh the particles that were to be added in the reactors, loop seals, but also the particles lost through the cyclone to the filter box.

4.4 Data-acquisition and operating system – LabView

For data-acquisition and rig operation, a control system has been designed in LabView. For operating the CFM the program is used to control and monitor the air flow through the injection nozzles and also for monitoring the pressures at different elevation points of the two reactors.

Behind the shell of the LabView program signal processing is an important feature. Both incoming and outgoing signals are being processed in order to provide the desired signal. An example are the pressure transducers that operate based on a digital current signal, but are desired to display the pressure in mbar. A conversion from mA to mbar is required, and this conversion is done by signal processing in LabView.

Another important feature of the data-acquisition system is the possibility of logging and storing important parameters. Pressure measurements and volume flows used for data analysis are stored in a text file. The logging frequency can be adjusted according to the preferred number of samplings.

A figure of the control system layout can be found in Appendix I.

4.5 Flux measurement

To measure the flux in the reactor, valves were installed in the downcomers. The valve was then closed automatically for a predetermined amount of time. The height of the accumulated particles above the valve could then be measured visually. Mass flow or flux could then be calculated with equation 37 or 38 respectively.

$$Mass\ flow = \frac{\pi r^2 \times \rho \times \Delta h}{\Delta t} \qquad [kg/s] \tag{37}$$

$$Flux \quad = \frac{\rho \times \Delta h}{\Delta t} \qquad [kg/m^2 s] \tag{38}$$

r: radius of the downcomer [m]

ρ: bulk density, 3900 [kg/m^3]

Δh: Measured height of particles in the downcomer [m]

Δt: Length of time interval the valve was closed [s]

The bulk density of the particles was found by measuring a sample of particles in the lab. Since the flap valves is not able to make a 100% air tight seal the respective loop seal were shut down during measurements of the flux. This minimized any fluidization of the accumulated particles potentially giving another density.

5 Experimental methodology

The first step was to fill the reactor system with an amount of particles in accordance to the data given in the test matrix. The riser were filled with a certain amount of particles. Then the loop seal to be used in the experiment were filled to a predefined level shown in figure 5.1.

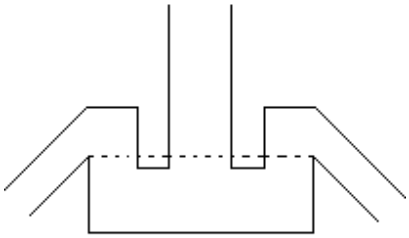

Figure 5.1 – *Predefined level of solids in loop seal*

The term *total solid inventory* was defined to be the total amount of particles active in the reactor system during an experiment. For example inventories of riser and loop seal for a single reactor experiment. For coupled reactor experiment both risers and loop seals are included. If the lifter is active the amount of solids in this is also added.

The inventory data was recorded in a log before the experiments were started in order to have an overview of how much solids was put into the system. However, solids redistribute in the system during operation. This is the reason why the term total solid inventory is used in this report and not the initial inventories at the different locations in the reactor system. The initial inventories change during operation and may not be representative and are only given in appendix IV. The amount of solids in the riser during operation can however be estimated by equation 24 and is defined as *active inventory* in this report.

Particles could also disappear to the filter box. The filter box was designed to make it easy to weigh the particles escaping out of the cyclone to the filter box. This was included in the total solid inventory log and/or refilled.

During operation of the single reactors the lifter were blocked and the reactors isolated. This means that the external part of the loop seals and the lifter were blocked physically. This was not done for experiment F1, showed in figure 7.1. It did not however seem to be a problem for this experiment as the particles in the loop seal was enough to block. The lifter was blocked in the same way by filling it with particles. The problem was discovered in the next experiment with a mass inventory of 30kg. That experiment failed because of loosing mass to the other reactor and is therefore not mentioned in figure 7.1. To solve this problem the reactors were isolated as described above.

When running both reactors coupled the internal part of the loop seals were blocked to avoid a pressure short circuit through the loop seals. This is explained in section 7.8.6. The lifter was naturally not physically blocked.

Before start up all the pressure transducers where cleared by a "blow-out"-system. The "blow-out"-system blows particles suspended in the pressure tubes back into the reactor by applying a counter-current air flow hence unclogging the tubes. This system was also used during experiments.

When starting up the reactor the primary and secondary air flows were gradually increased to a level given in the test matrix. After these parameters had been set correctly the air injection points into the bottom of the loop-seal were adjusted. This was a tentative process which was completed when steady-state with respect to circulation was obtained.

In the experiments performed, the dependent variables are the volume flows injected into the two reactors, the solids inventory, and air injections in loop seals and lifter. Based on these values pressure and flux measurements are recorded. The set of combinations of various volume flows give a test matrix as shown in chapter 7.2.

The reactor requires some time to reach steady-state conditions. To make sure the reactor was in steady-state, a steady-state criterion was established. The criterion was related the behavior of the top pressures in the two reactors, P10 and P23, as well as the solids level in the loop-seals. The steady-state criterion states that the pressure levels of P10 and P23 should be stable and the solids level in the loop-seals should be constant. The steady state issue was also double checked after the experiments and is treated further in chapter 7.5.

For coupled reactor experiments online values of the active inventory in the AR and the FR was monitored, in addition to P10/ P23 and the loop seals, to evaluate when steady state was achieved.

When the steady-state criterion was obtained, data logging could be initiated. As mentioned in chapter 4.3, the logged data was the pressure measurements as well as all the volume flow rates. The data was stored in a text file and imported into a spread-sheet used for data analysis. The logging frequency was set to 1 logging per second. The results are based on the averaged values of these loggings.

The general procedure for the experiments is given in table 5.1.

Procedure for experiments
1. Start up of rig to operating conditions set in test matrix.
2. Achieve steady-state
3. Start logging
4. Run for 5 min.
5. Flux measurement and blowing of the tubes from the pressure transducers.
6. Run for 5 min
7. Flux measurement and blowing of the tubes from the pressure transducers.
8. Run for 5 min
9. Flux measurement and blowing of the tubes from the pressure transducers.
10. Experiment finished.

Table 5.1: Procedure for experiments

6. HSE for operating the Cold Flow Model

6.1 Dust explosion hazard

In (T. Abbasi 2006) dust explosions are described in the following way: A dust explosion is initiated by the rapid combustion of flammable particulates suspended in air. Any solid material that can burn in air will do so with a violence and speed that increases with the degree of sub-division (particle size reduction) of the material.

In processes operating with fine particles, a safety risk one may encounter is dust explosions. Therefore an important HSE-aspect that must be investigated thoroughly before operating dust-processing equipment is the dust explosion hazard or potential. This is highly relevant for operating the Cold Flow Model. In studies by (Eckhoff 1994) and (T. Abbasi 2006) these issues are discussed and described in detail.

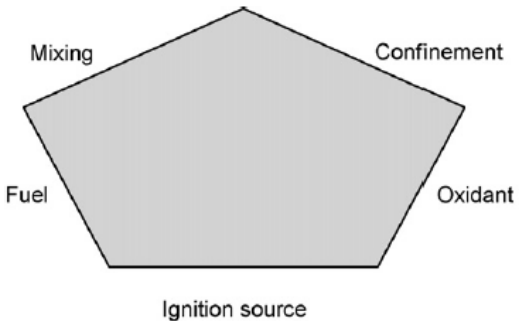

Figure 6.1 - *Dust explosion pentagon (T. Abbasi 2006)*

There are a number of factors that might trigger an explosion. In figure 6.1, five factors that need to occur simultaneously in order to provoke an explosion are presented. For a fire to occur, three factors are necessary; fuel, oxidant and ignition. For a dust explosion on the other hand, two more factors are required: mixing of the dust and the air, and confinement of the dust cloud.

Perhaps the most important parameter to investigate is the presence of fine dust, labeled 'fuel' in the pentagon. Unless the concentration of fine dust is high enough dust in air will not ignite. This is analogues to upper and lower flammability limits in combustion of homogeneous gaseous mixtures in air.

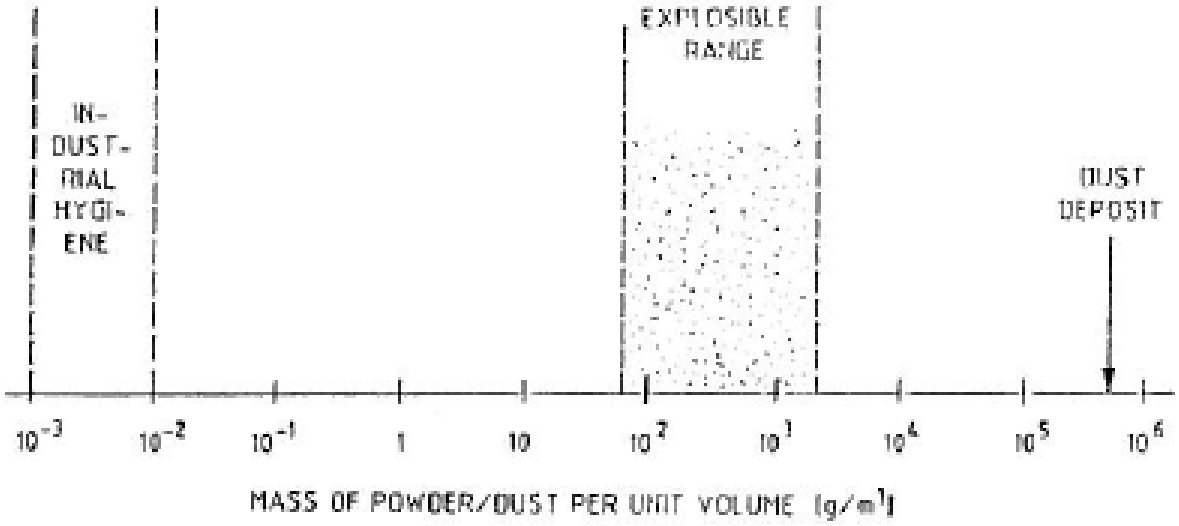

Figure 6.2 - *Explosive range of dust concentration at ambient temperature and pressure* (T. Abbasi 2006)

In figure 6.2 the explosion range of a natural organic material is presented. For most metal dust particles the lower concentration limit can be found around 100-500 g/m^3. This variation is mainly dependent on parameters such as chemical composition and particle size. The upper limit usually is two orders of magnitude higher than the lower limit (Eckhoff 1994).

We divide the types of explosions into two classes; primary explosions and secondary explosions. Primary explosions are initiated by an ignition source located on the inside of the vessel. Typical sources of ignition are open flames, smoldering or burning dust layers, hot surfaces, metal sparks and electrostatic discharges. Secondary explosion occur as a consequence of the primary explosion. In secondary explosion dust clouds are generated by entrainment of dust layers by the blast wave released by the primary explosion. The consequences and damage from a secondary explosion is more severe than the primary explosion; one might say the primary explosion is what ignites the secondary. According to (Eckhoff 1994) the dust layer thickness limit allowing ignition is surprisingly small.

To prevent dust explosions it is essential to remove one or more of the five factors presented in figure 2.30. This can be achieved by modifying process equipment, preventing suspensions of flammable dusts, removing ignition sources and inerting. For Chemical Looping Combustion the dust explosion issue is mainly related to the Cold Flow Model, as well as the air reactor of the hot rig. For the hot rig, removing ignition sources and inerting are obviously not realistic solutions as one of the main targets is to transport an oxidant to the fuel reactor. For the CFM

this might prove valuable, but due to the large mass flow rate availability of sufficient amounts of inerts is a problem. Preventing suspensions of flammable dusts by introducing particle size control is an effective way of preventing dust explosions. This can be achieved by using procedure that secures statistical independency of particle size when filling the reactor, securing an even distribution of particle sizes.

6.2 Ambient air quality during operation

Inhalation of fine particles like the particles used in the CFM is not healthy. Measurements of the concentration of particles in the air during different operations related to the CFM were therefore executed. The results showed acceptable levels during ordinary operation of the rig. During filling of particles in the reactors and emptying the filter box the concentration of particles were too high. Additional protective equipment then have to be used as explained in section 6.3. Exhaust fan were also installed to use during filling and emptying.

6.3 Personal protective equipment

In fulfilling HSE requirements related operation, and manual adjustment work on the rig, certain protective equipment is imperative. After examination of the rig, it has been decided what equipment is necessary. When operating the rig the crew must wear a hard hat, protective footwear and goggles. During work on the rig, the same equipment is required. Additional equipment is required when filling particles in the reactor and emptying the filter box. A protective mask classified P3 must be worn to avoid inhaling particles. Also wearing glows is recommended.

6.4 Water seal safety system

A water seal has been implemented on the reactor system for precautionary reasons. In a situation of a sudden and uncontrolled pressure increase (e.g. due to plugging) in the vessel, the water seal will blow out before the pressure level reaches a critical level. If the pressure reaches a to high level it might lead to damage of the reactor system, or in the worst case pose a safety threat to personnel operating the reactor. The benefit of having a mechanical safety valve of this kind is that one can follow the overpressure in the reactor at all times. The water seal is designed after the U-tube pressure manometer, hence allowing personnel to monitor the overpressure closely while operating the rig. Complications related to electrical failure and malfunction is also avoided, since the valve works completely mechanical.

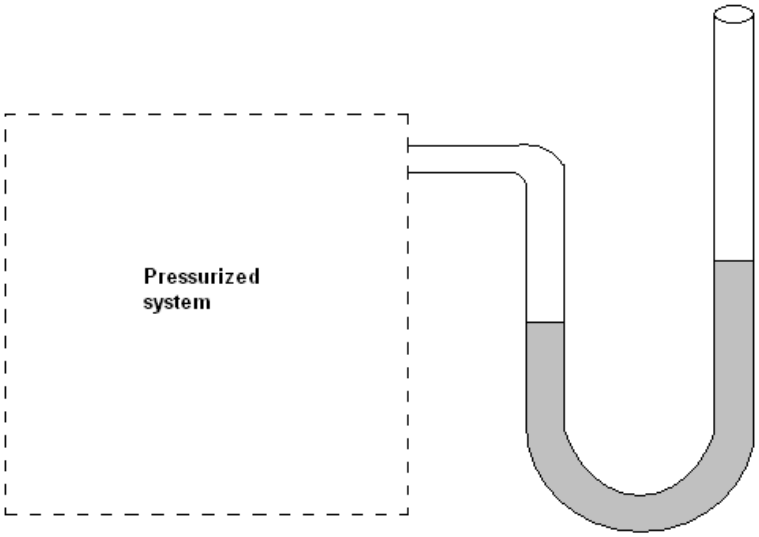

Figure 6.3- *Illustration showing the principal of using a water seal as a safety valve on a general pressurized system.*

7. Experimental campaign

7.1 Objectives for the campaign

- Ensure that the setup is working according to design.
- Map the behavior of the system and find operational window.
- The hot rig has been designed to achieve certain solids fluxes. It is therefore essential to investigate the fluxes at different operating conditions and mass inventories in the CFM. Both separately and coupled. The goals set for the fluxes in the reactors are 61 kg/m^{2}s and 48 kg/m^{2}s in FR and AR, respectively. In mass flows this is equivalent to 1kg/s in the FR and 2 kg/s in the AR.
- Achieve the planned fluidization regime: fast fluidization. It should increase the gas-solids contact in the 150kW$_{th}$ reactors.
- Test the lifter design and capacity. The goal is to achieve a mass flow of 1kg/s.
- Achieve a global mass circulation of 2 kg/s between the two reactors. Specifically 2kg/s through AR LS, 1kg/s through FR LS and additional 1kg/s from the lifter.

7.2 Overview of experiments performed

This chapter gives an overview of the experiments performed during the experimental campaign. They are presented graphically to make their understanding easier. The y-axis in figure 7.1-7.3 represents the total solid inventory as defined in chapter 5. The x-axis is merely showing the experiments. The figures 7.1 and 7.2 are to be read in the following way: if we use experiment F1 as an example we have 35 kg as the total solid inventory. The reactor is operated at three different total flows, 1500, 1750 and 2000Nl/min. Total flow is in this report as the total flow of the primary and secondary nozzles in the riser. At each total flow three different percentage distributions between primary and secondary air injections were tested. This means that in experiment F1 nine different operating modes were investigated. The test matrixes were designed on based on velocities needed to achieve proper flow regimes.

As seen in figure 7.2, experiment A1 was executed with total flows of 2000, 3000 and 4500 Nl/min. However, experiment A2 was done with total flows of 3000, 3750 and 4500 Nl/min. The reason for this difference is that the test matrix was adjusted since 2000 Nl/min gave velocities too far from design velocities of the hot rig.

The experiments for both reactors coupled are presented in figure 7.3. In these experiments it is essential to have a mass balance between the two reactors. The operating conditions needed for this was derived from the experiments done on the single reactors.

Extended operating conditions for the experiments can be found in appendix IV.

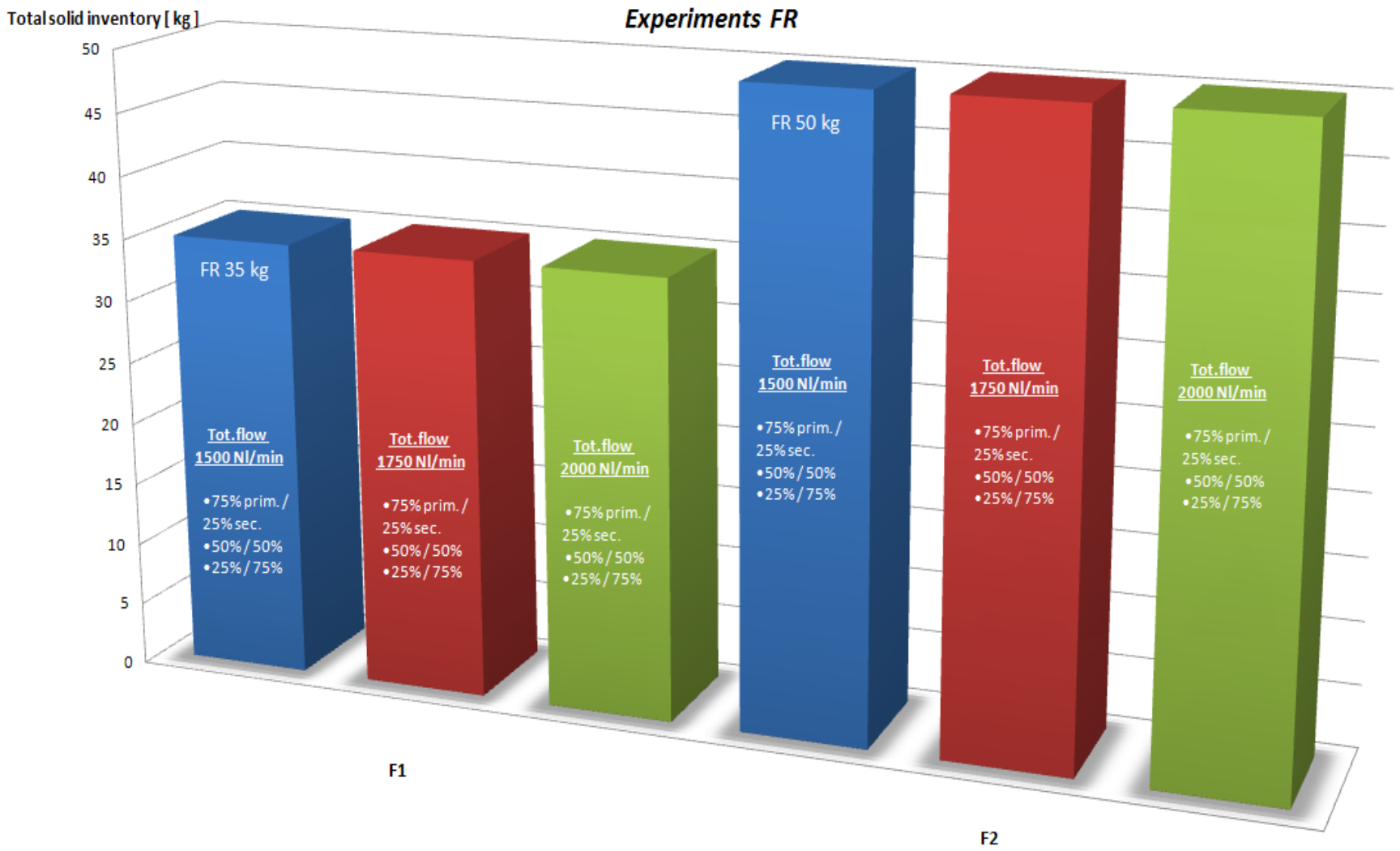

Figure 7.1 – *Single reactor experiments performed on the FR, F1 and F2*

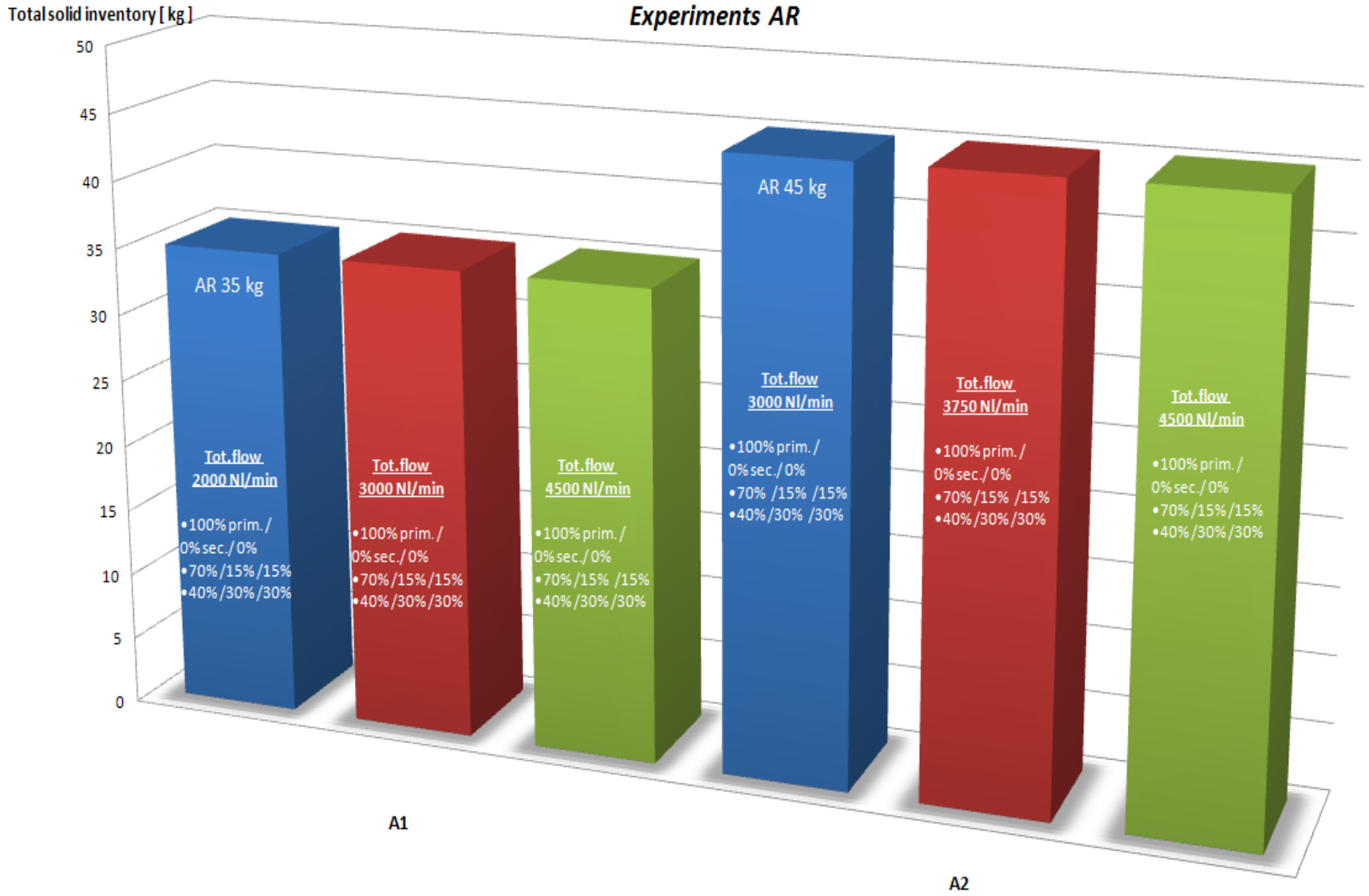

Figure 7.2 – *Single reactor experiments performed on the AR, A1 and A2*

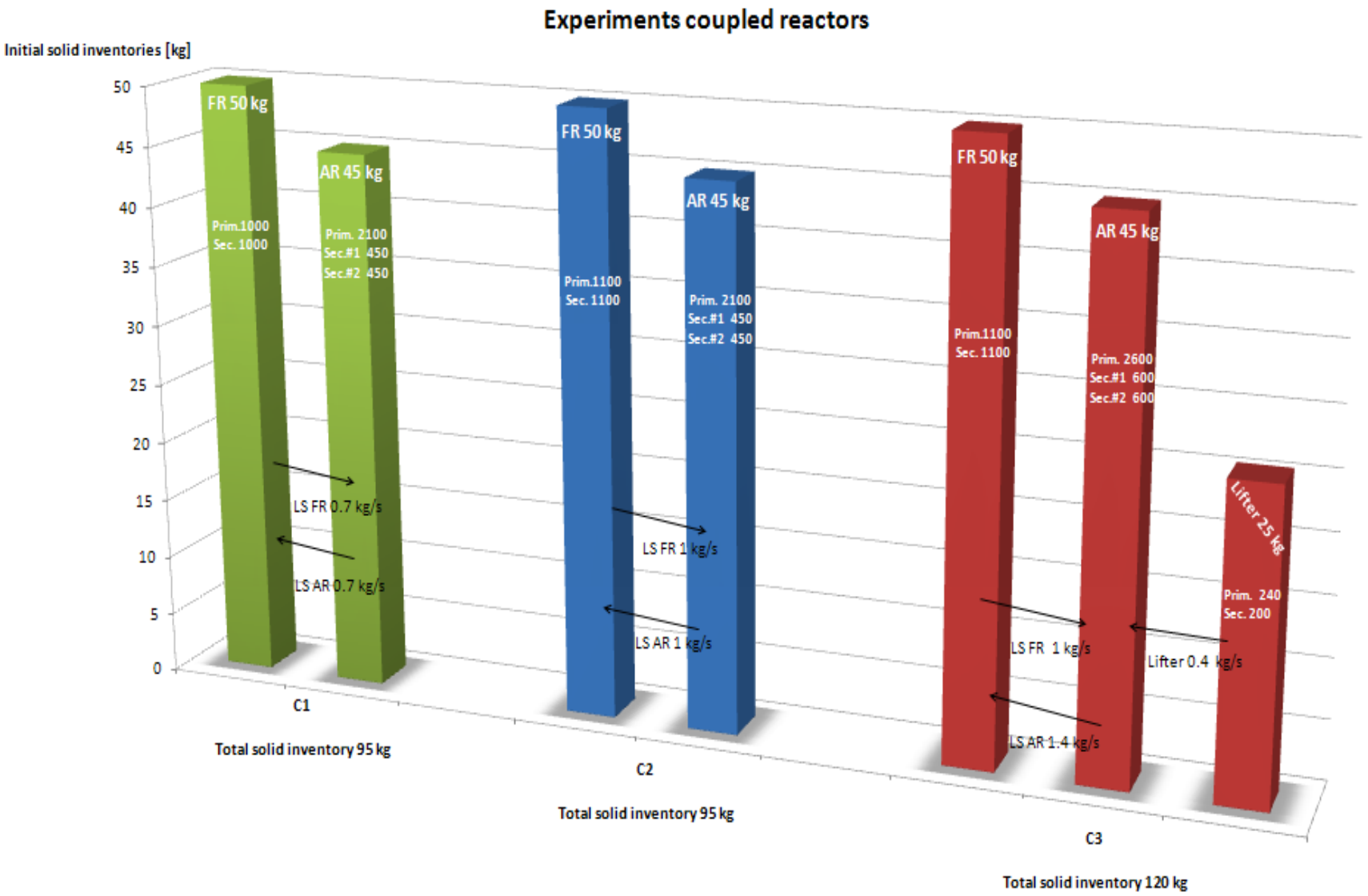

Figure 7.3 - *Experiments performed with both reactors coupled, C1, C2 and C3*

7.3 Experimental results and discussion

Two important parameters that are investigated in the Cold Flow Model are solids circulation and pressure profiles. Pressure profiles give an indication of the solids distribution and flow regimes in the reactors. Hence this is what the experiments are focused on. The reactors are flexible and are meant to be flexible and operate in a turbulent or fast fluidization regime according to which gives the best results conversion efficiency in the hot rig.

To give a better understanding of the pressure profiles figure 7.4 shows the coherence between a general pressure profile and locations in the physical reactor. The marked line on the y-axis at 0.3 m indicates the height of the return leg in the riser. The height of where the return leg enters in the riser is the same for both AR and FR, 0.3m. This is important since it is essential that the pressure in the loop seal is larger than the pressure where the return leg enters the riser.

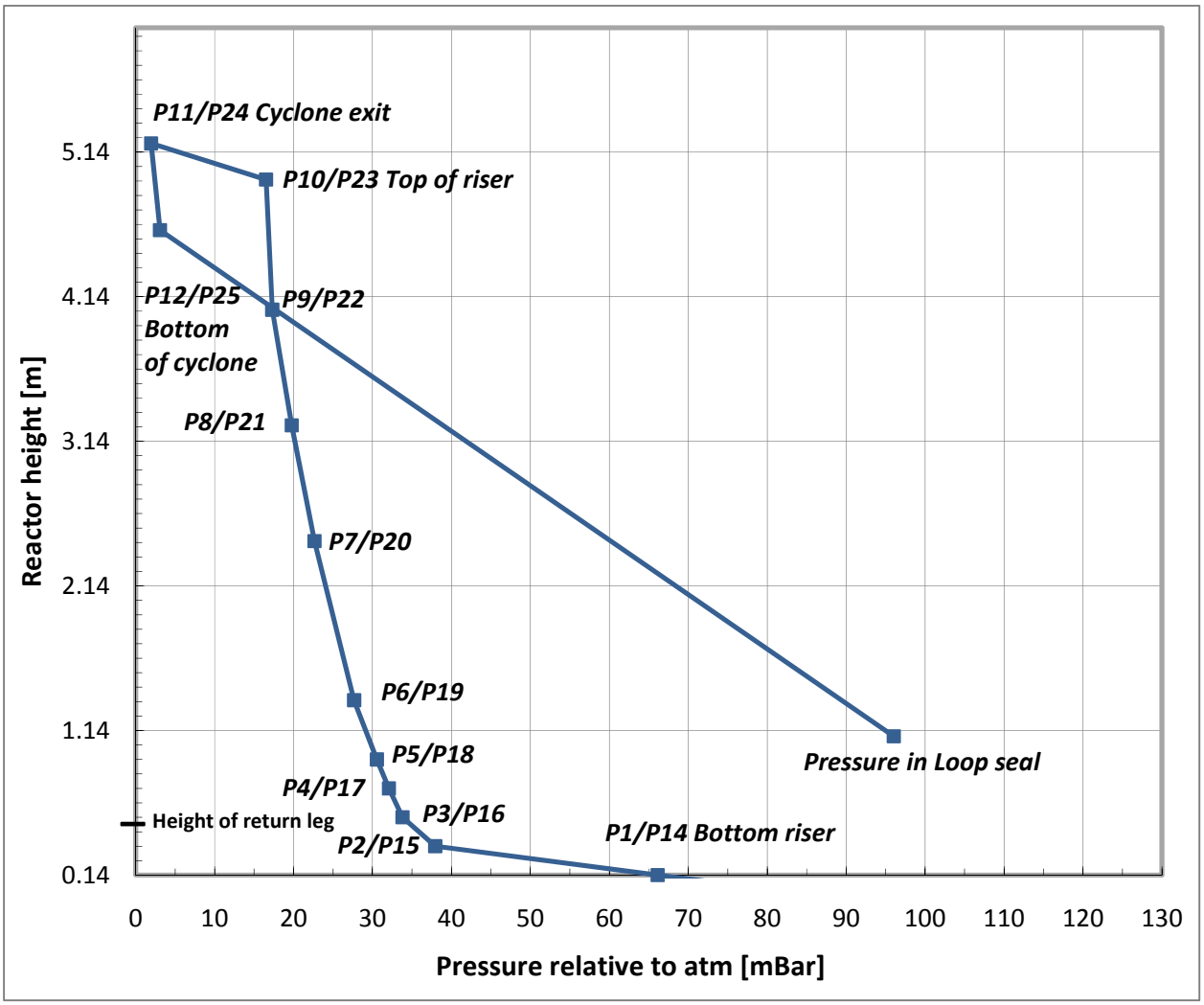

Figure 7.4 - *Random pressure profile showing the position of the pressure transducers in AR and FR*

The pressure profiles given in this report start at 0.14 m, since this is the height of the first pressure transducer in the reactors. The pressure in the loop seal is the pressure measured before the distributing nozzle, P28 or P31 depending on reactor, minus the pressure drop in the nozzle. The pressure drop in the nozzles is estimated from a nozzle characteristic investigated earlier where the pressure drop is given as a function of the flow.

7.3.1 Pressure profiles for single reactor experiments

Experiments F1, F2, A1 and A2 are the experiments done operating the AR and FR singularly. The cyclone exit pressure has been set to approximately zero in the experiments by adjusting an exhaust fan located downstream the filter box. The shape of the pressure profiles gives a good indication regarding the solid distribution in the reactor. The congruence of the pressure profiles show that they operate in similar flow regimes. The expected flow regimes have been achieved. The experiments are in a turbulent or fast fluidization flow regime. This can be seen from the pressure profiles. A bubbling bed would have a more exponential pressure profile than the ones in figures 7.5-7.8 and the pneumatic transport flow regime would have a much steeper one.

In general higher total flows, which means higher operating velocities, leads to a higher pressure in the system and increased pressure losses in the entire system. This related to a higher solid circulation rate at higher operating velocities and friction losses. The pressure loss in the riser at higher velocities however is mainly smaller. A higher pressure drop in the riser means a larger riser inventory.

Higher total flows also mean that the primary/secondary air distribution has a greater influence on the pressure profile hence flow regime/solids distribution in the reactor. There seems to be a trend between higher primary air percentage and higher pressure in the overall system. This statement is supported by the results given in figure 7.5, 7.6 and 7.7. The results in figure 7.8 however actually indicate that 70 % primary air gives the highest pressure. Also in figure 7.5 an odd result occurs, at a total flow of 2000 Nl/min and 25 % primary air. By further investigation it seemed clear that it was forgotten to adjust the fan so that the exit pressure should be zero. So these values should be displaced to the left hence following the trend described above.

The following four figures, figure 7.5 – 7.8, give the pressure profiles as a function of total flow and primary/secondary air distribution and total solid inventory.

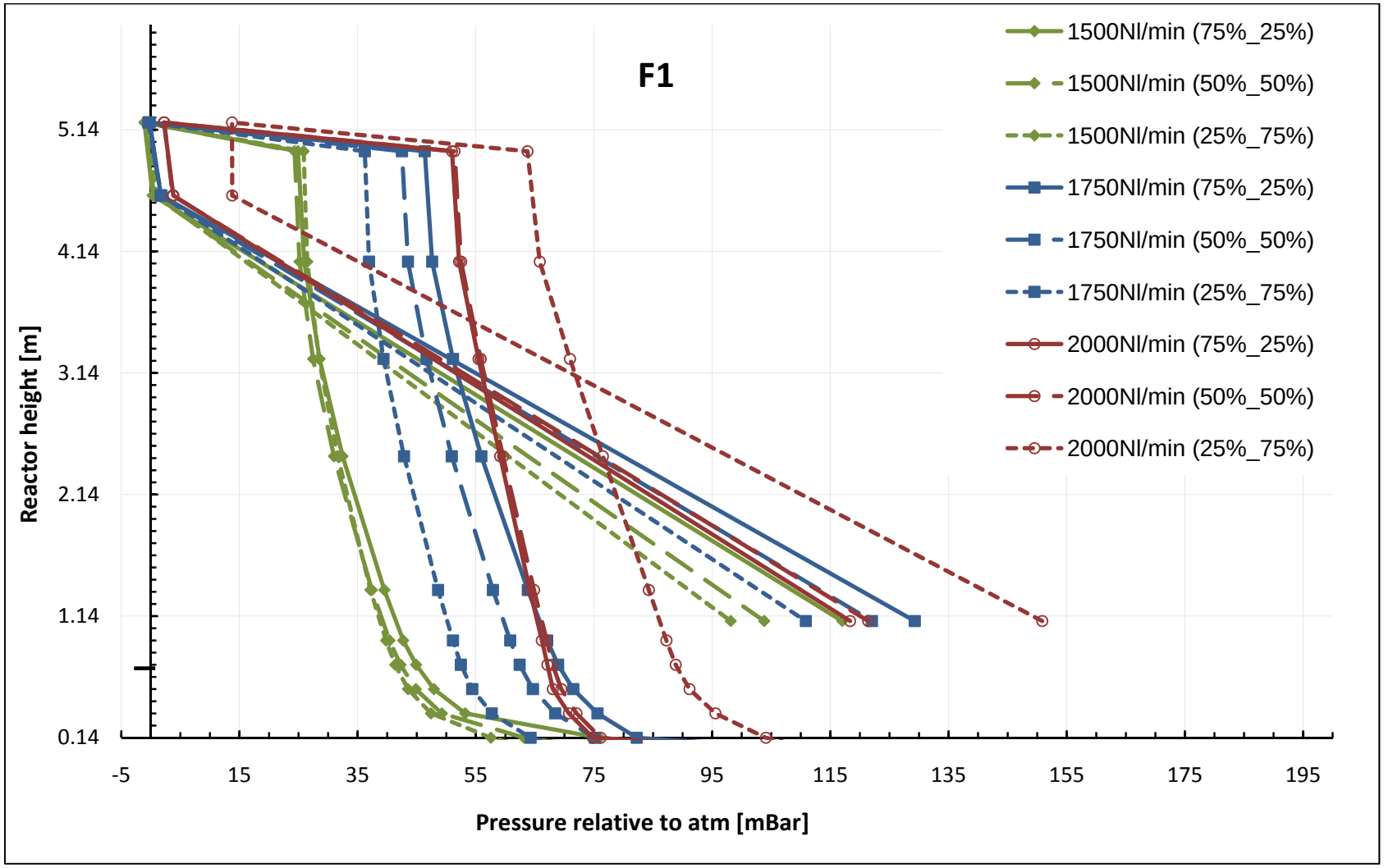

Figure 7.5 - *Pressure profiles for the FR with a total solid inventory of 35 kg, at different total flows and primary and secondary air distributions*

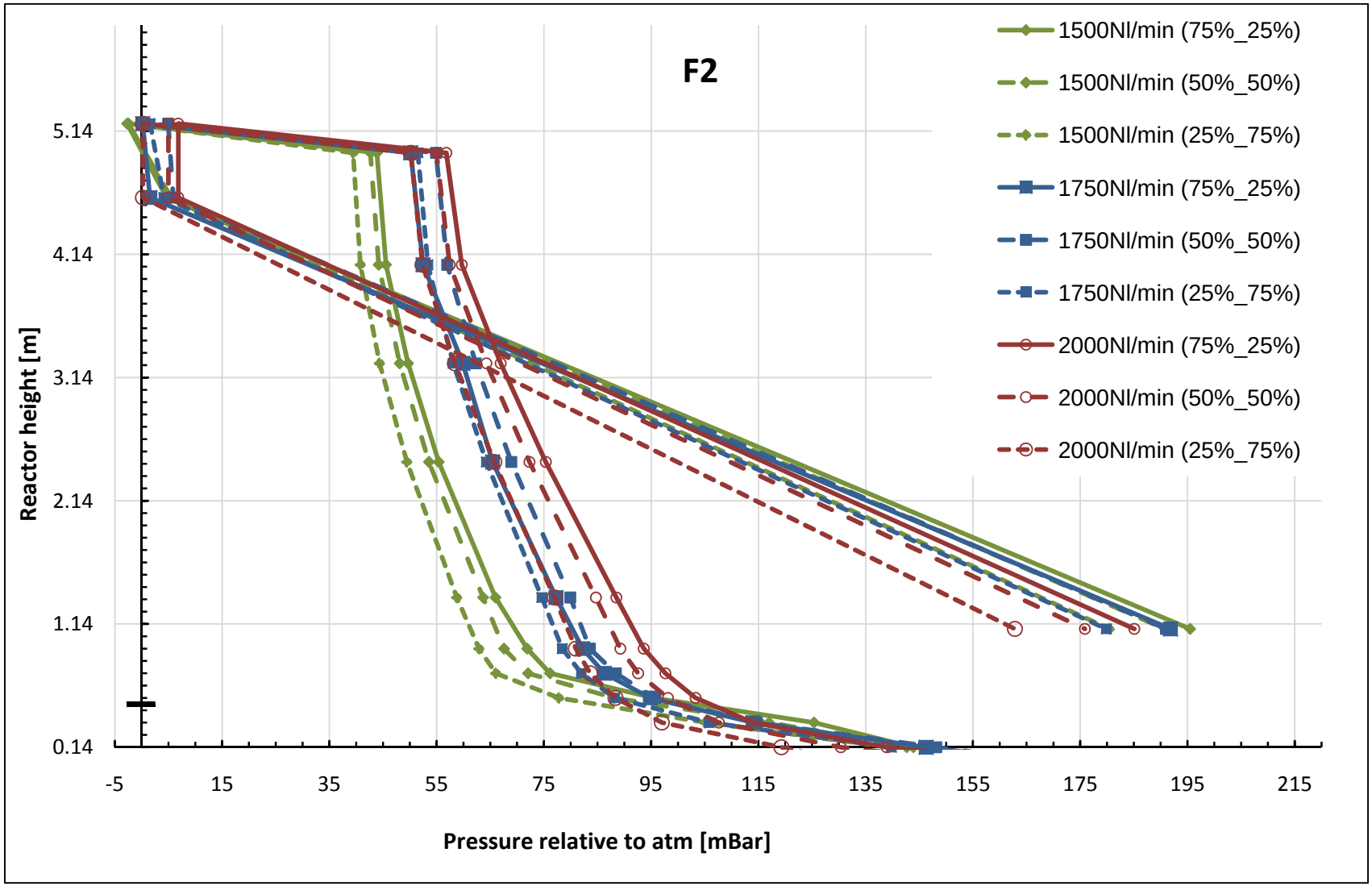

Figure 7.6 - *Pressure profiles for the FR with a total solid inventory of 50 kg, at different total flows and primary and secondary air distributions.*

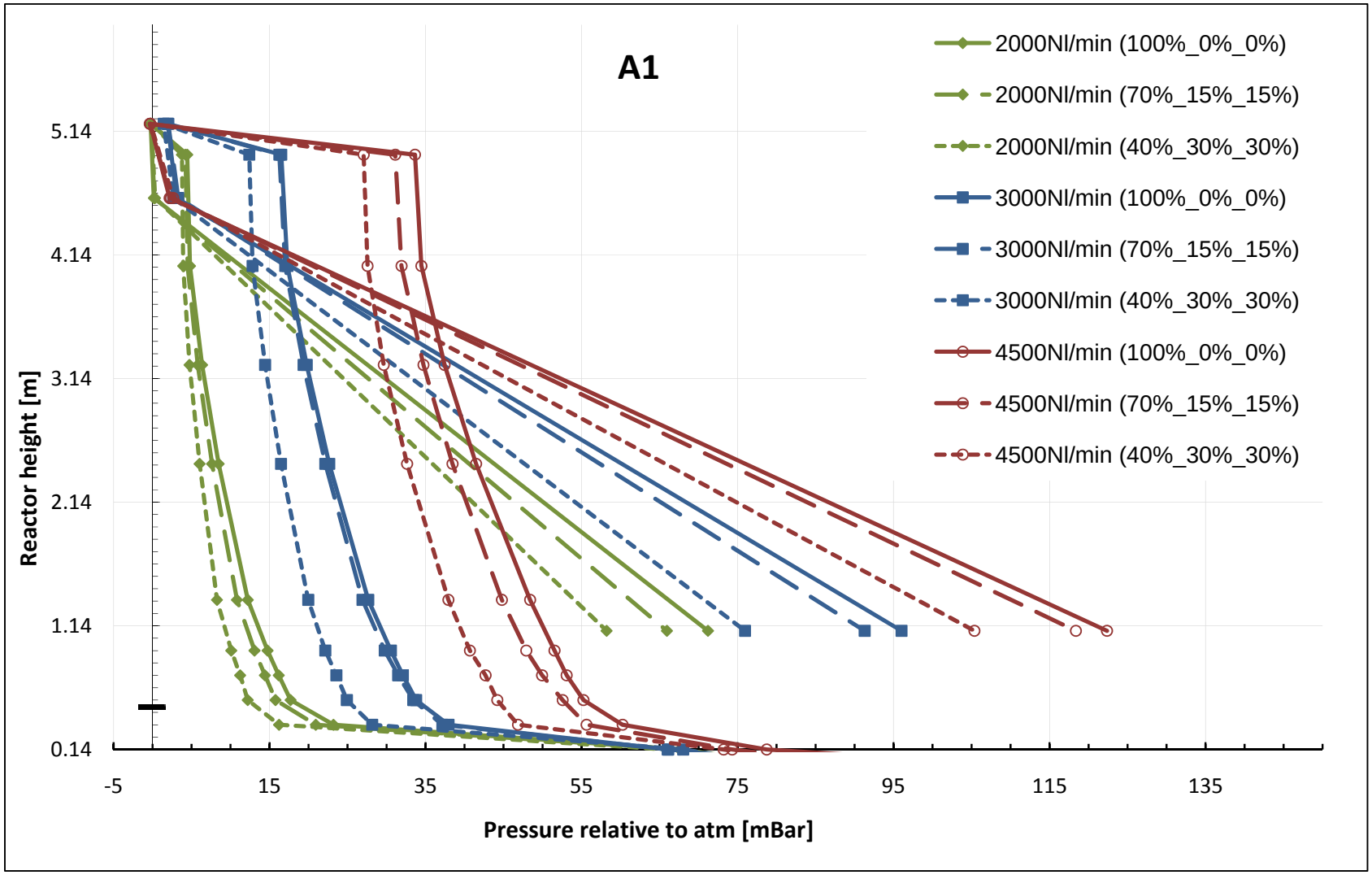

Figure 7.7 - *Pressure profiles for the AR with a total solid inventory of 35 kg, at different total flows and primary and secondary air distributions*

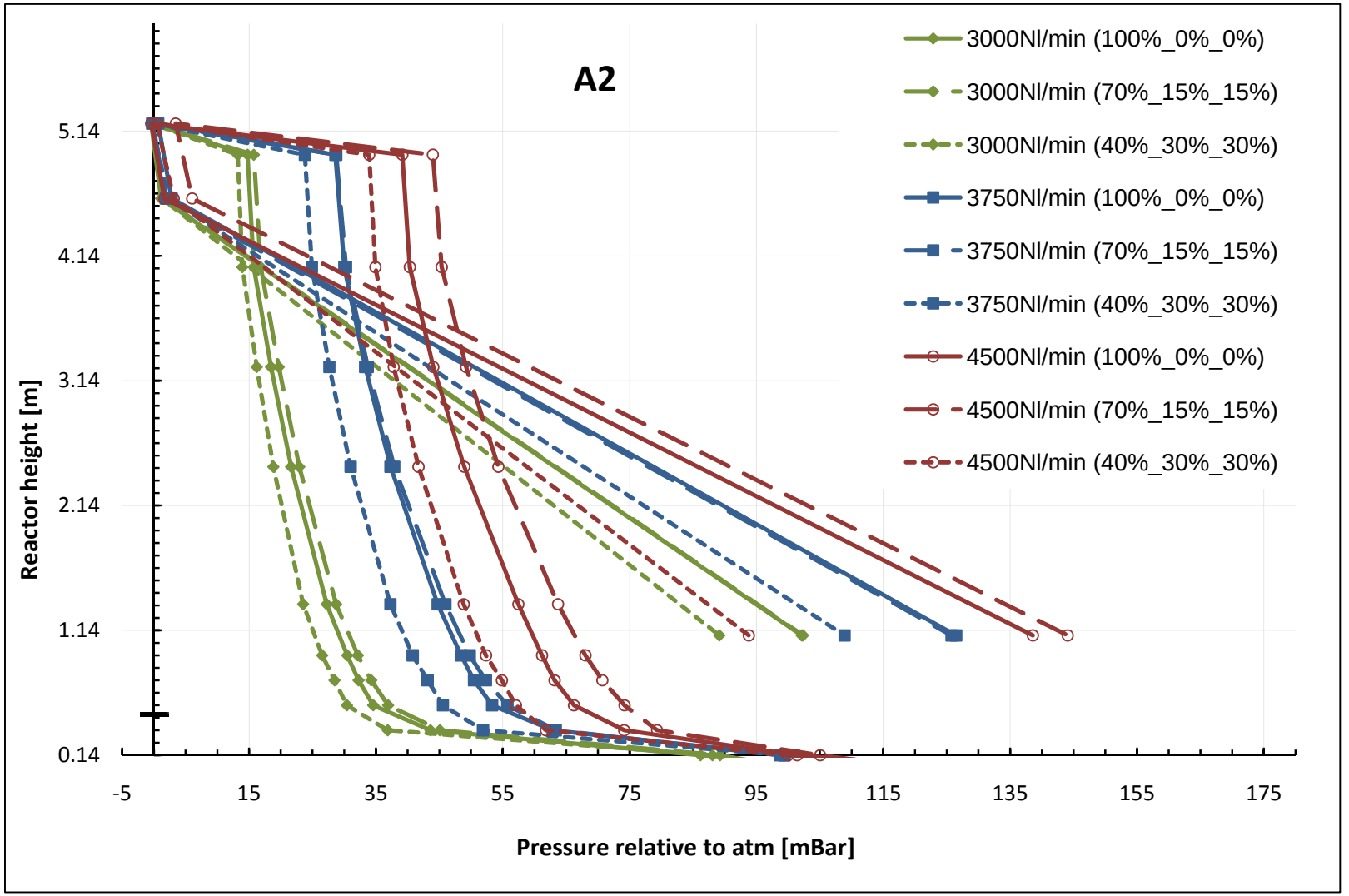

Figure 7.8 - *Pressure profiles for the AR with a total solid inventory of 45 kg, at different total flows and primary and secondary air distributions*

The results were also plotted as a function of the total solid inventory to easier see trends for how the solid inventory affects the pressure profiles. In figure 7.9 and 7.10 an example of the pressure profiles for AR and FR are given as a function of the solid inventory and primary/secondary air distribution. Plots for all of the single reactor experiments are given in appendix V.

Increasing the solid inventory changes the shape of the pressure profile to a more exponential shape and this is in congruence with theory presented in section 2.3.6. This trend can be seen in the figures and is most clear in figures 7.9 and 7.10.

Larger solid inventory also means in general higher pressures in the system. The pressure difference between the bottom and top of the reactor also increases which is expected from equation 24. The pressure drop in the cyclone separator becomes larger. The pressure in the loop seals increases with a larger total solid inventory.

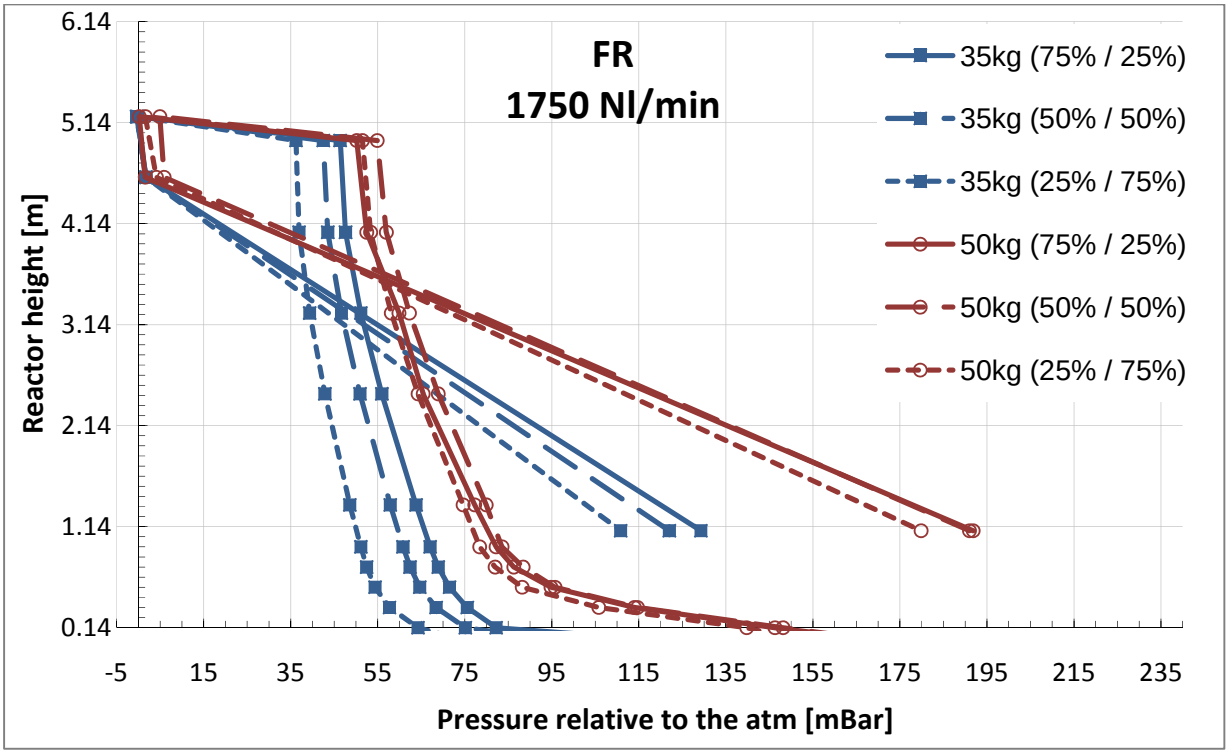

Figure 7.9 - *Pressure profiles for FR at a total flow of 1750Nl/min, at different total solid inventories, 35kg and 50kg, and different primary and secondary air distributions*

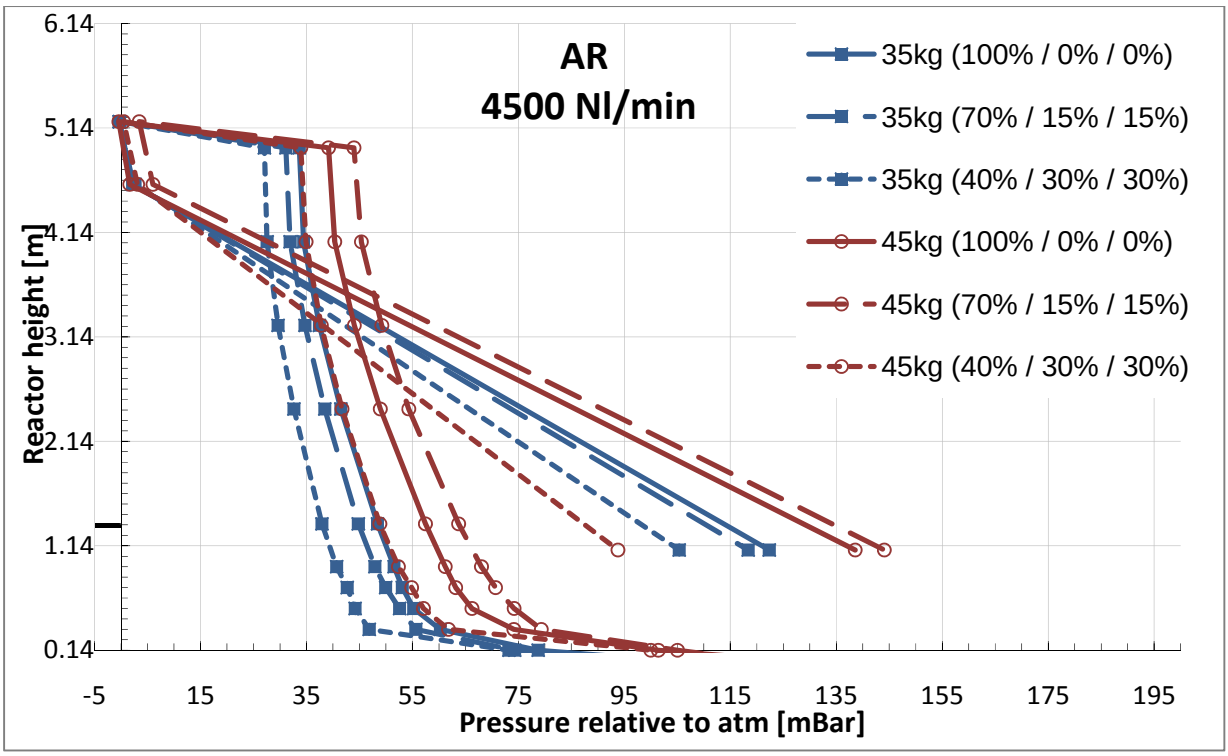

Figure 7.10 - *Pressure profiles for AR at a total flow of 4500Nl/min, at different total solid inventories, 35kg and 45kg, and different primary and secondary air distributions*

7.3.2 Mass flux for single reactors experiments

The results from mass flow measurements are here given in both flux and mass flows. The flux is considered an important characteristic of a CFB reactor because it is comparable to other reactors too. The mass flow is more a characteristic of a specific reactor.

In general there is a strong correlation between mass flux, total air flow and solid inventory. This makes sense since a larger solid inventory leads to a higher concentration of solids and the total air flow influences the velocities in the reactor, hence circulation rate. This trend is strongest in the results from the AR. It is also occurring in the results from the FR, but there are more odd points there. During experiments solids are lost to the filter box. The FR experiments were done first in the experimental campaign and no refilling was done during the whole length of an experiment for a certain total solid inventory. During the experiments in the AR however solids were systematically refilled each time the total flow was changed. This seems to be the best procedure and obviously has great effect on the results as they are presented in figure 7.11 and figure 7.12.

In the FR the largest percentage primary air in the test matrix, 75%, gave the largest flux. It should be mentioned that 100% primary air was not tested in the FR. In the AR 100% primary air was tested, however 70% and not 100% gave the largest flux. According to (Tobias Pröll 2009) and (J. H. Kim 2000) the largest flux should be achieved with 100% primary air. Other factors may have influenced the experiment.

In figure 7.11 and figure 7.12 it seems as the air distribution increasingly influences the flux at higher operating velocities and therefore becomes more important. Increased solid inventory seems to have the opposite effect and decreases the importance of air distribution.

Loop seal operation affects the mass flow of solids flowing through the loop seal. It was therefore attempted to keep the operating conditions in the loop seal constant. Further detailed operating conditions are given in appendix IV.

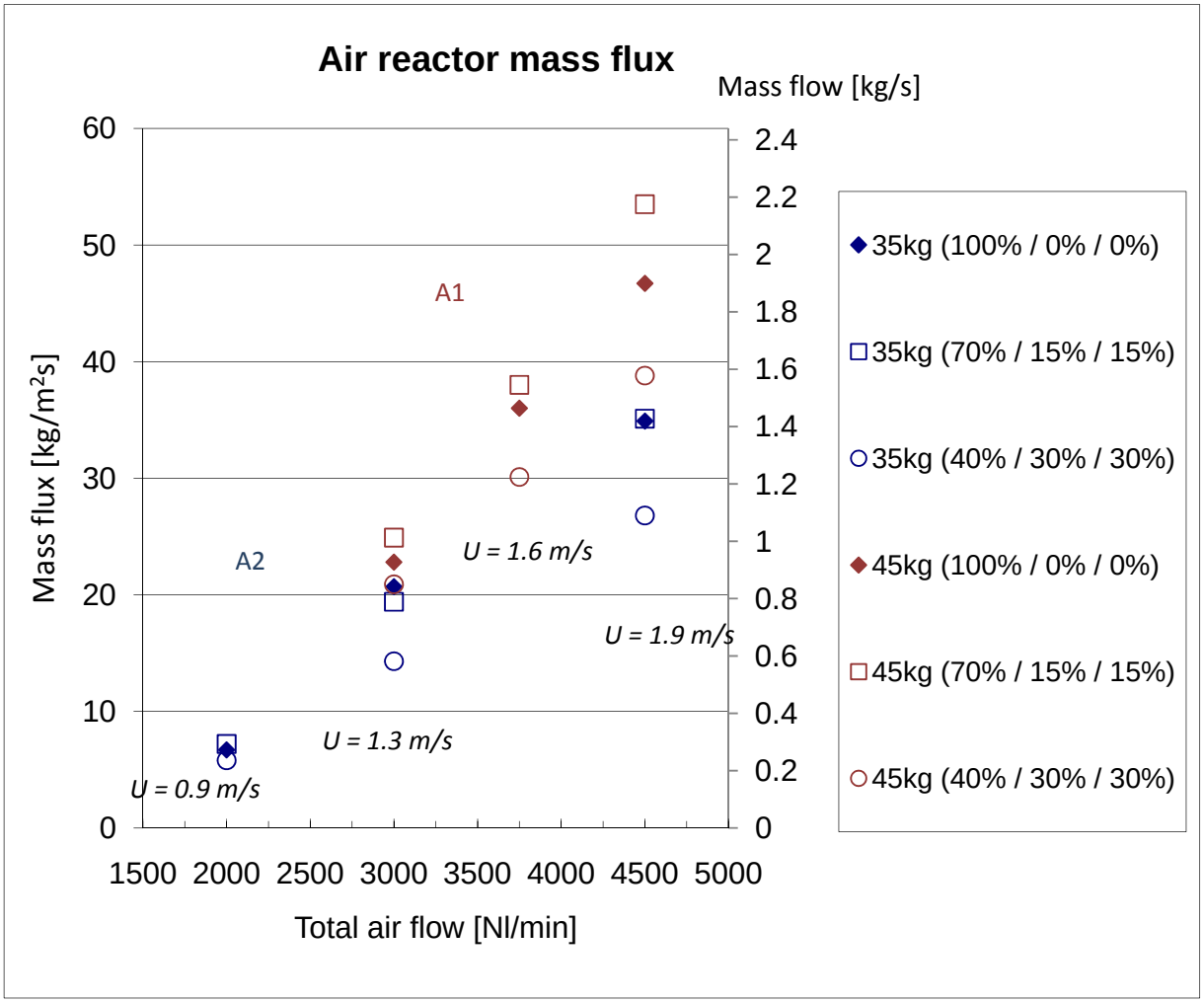

Figure 7.11 - *Mass flux of AR at different total flows, air distribution and mass inventories. The operating velocity U is also shown*

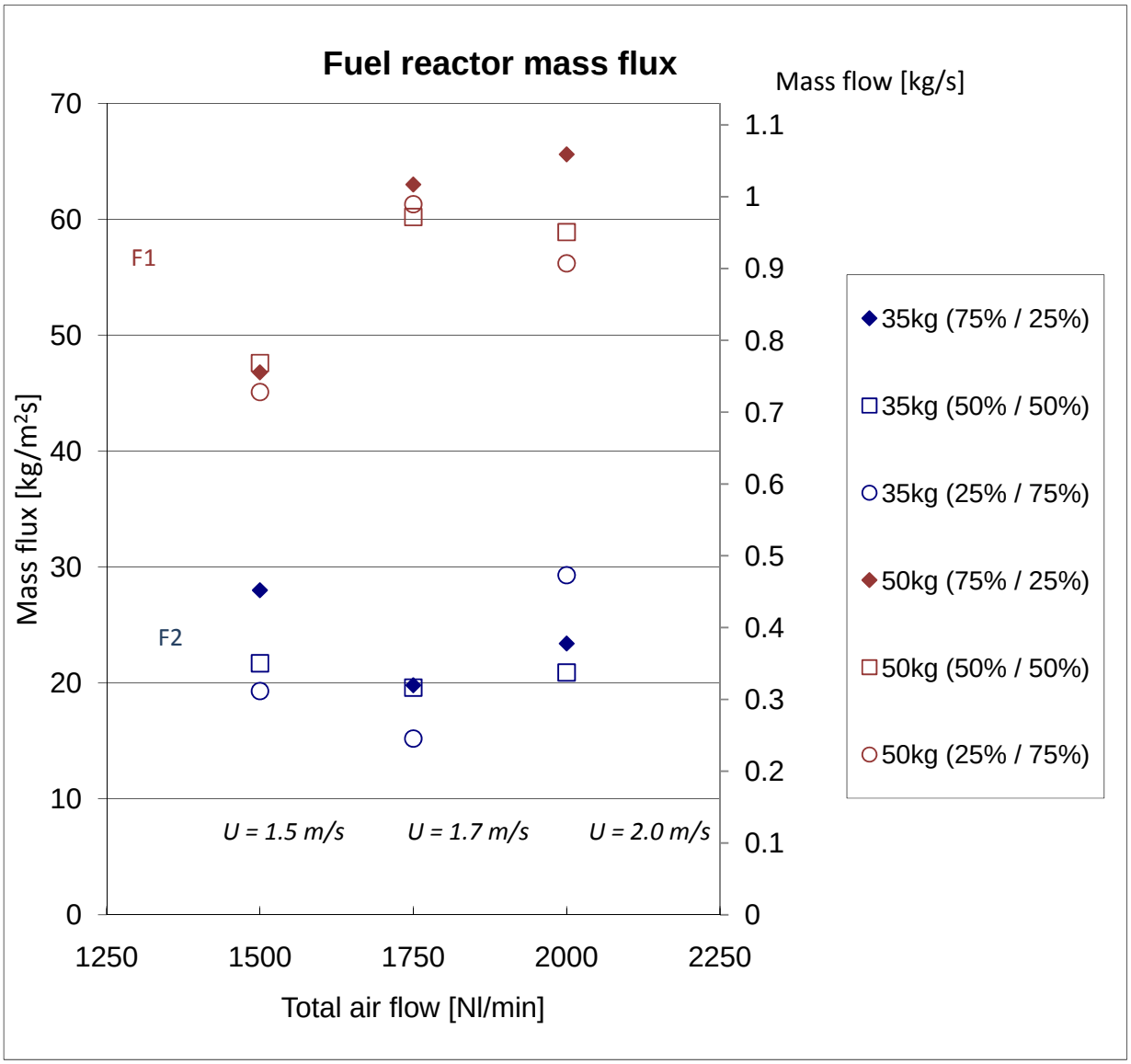

Figure 7.12 - *Mass flux of FR at different total flows, air distribution and mass inventories. The operating velocity U is also shown*

7.3.3 Coupled reactors

After mapping the operating area in the single reactor experiments, experiments with the two reactors coupled were performed. An overview of the experiments is given in figure 7.3.

One of the main challenges was to have a mass balance between the two reactors. Results from the single reactor experiments were used to know which operating conditions in the reactors that should be chosen to have a mass balance between the FR and AR. It was a challenging task to control the whole reactor system, risers and loop seals etc., at the same time. The system however turned out to be robust and a mass balance seems easy to achieve, at least if the approximate right operating conditions are given. When it comes to mass balance the reactor system seems to be self regulating to a certain degree. This may be explained like this: If a reactor have a larger solid flow out than in, the inventory in this reactor will decrease, hence decrease the solid flow out. The other reactor which receives more solids in than out will get an increased bed inventory. This leads to a larger solid flow out of the reactor and helps reestablish and increase the bed inventory in the first reactor. This process will after a certain time reach equilibrium, and equal solid flows will be exchanged between the two reactors.

To make sure the experimental results are from a steady-state condition, a criterion was made. This is further explained in chapter 5.

The idea behind the divided loop seal is to send one solid flow back to the reactor, internal part of the loop seal, and a second solid flow to the other reactor, the external part of the loop seal. The divided loop seal turned out to be difficult to operate. It is probably possible, but to make the already difficult to operate CFM easier to operate the loop seals where changed temporary. During the coupled reactors experiment presented here, C1, C2 and C3, the internal sections of the divided loop seals where blocked and isolated. This was done to avoid a pressure short circuit as explained in section 7.8.4. The external part of the loop seal, which only transports solids to the other reactor, was used.

7.3.3.1 Mass exchange between reactors through loop seals only

The experiments C1 and C2 were done with mass exchange only through the loop seals. The lifter was blocked. The experiments are shown and operating conditions are shown in figure 7.3 and further operating conditions given in appendix IV. Experiment C1 achieved a mass exchange of 0.7 kg/s between FR and AR using only loop seals. Experiment C2 achieved 1 kg/s.

The pressure profiles of the experiments are given in figure 7.13. It is obvious from the pressure profile that the pressure is higher in the FR than the AR. This is because there is a larger solid inventory in the fuel reactor than in the air reactor. By increasing the solid flow,

going from experiment C1 to C2, the pressure in general is increasing similar to the single reactor experiments.

An important point is the pressure difference between the return leg in the reactor and the loop seal which supplies the reactor with solids from the other reactor. A good overview of the whole reactor system is given in figure 3.1. The height of the return leg in the risers is marked in the y-axis, at 0.3m, in all pressure profiles given in this report. It is essential to ensure a solid flow from the loop seal to the riser, and maintain a pressure seal, that the pressure is higher in the loop seal than in the reactor where the return leg enters. This is explained in section 2.4.6. In figure 7.13 the pressure differences is marked by arrows for experiment C2. Both return legs transports 1kg/s and have the same operating conditions in the loop seal and should therefore have equal pressure difference.

The pressure out of the cyclones should be the same since they are connected to the same fan and has the same length and dimensions between the cyclone exit and the fan. In figure 7.13 it is clear that this is not the case. An investigation of this revealed that there had been some clogging in the FR pipe to the fan, probably due to abnormal operation of the rig. In addition plugging of the pressure transducer tubes resulted in some misleading pressure measurements.

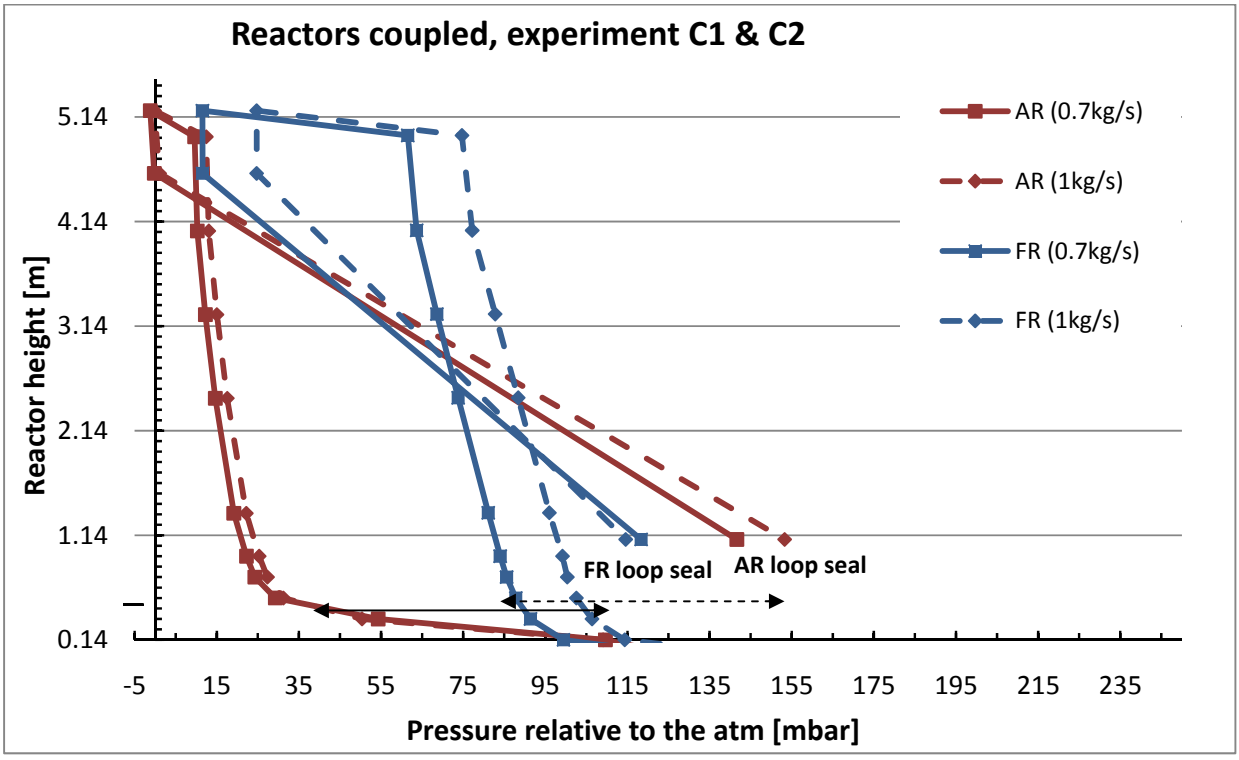

Figure 7.13 - *Pressure profiles of experiments C1 (0.7 kg/s) and C2 (1 kg/s)*

There is a much higher pressure drop in the FR cyclone separator than in the AR cyclone separator. They both process the same solid flow. However, the dimensions of the FR cyclone are smaller than the AR cyclone. This means that the FR cyclone process a larger gas flow compared to the dimensions, hence it has a larger pressure drop.

7.3.3.2 Mass exchange between reactors through loop seals and lifter

A third experiment was done with the reactors coupled, experiment C3. An overview and operating conditions are given in figure 7.3. 3800 Nl/min of air were injected in the AR and 2200 Nl/min in the FR. This means superficial operating velocities of 1.6 m/s and 2.2 m/s, respectively. The air injections in the lifter were set to max capacity of 240 Nl/min in the primary nozzle and 200 Nl/min in the secondary nozzle. Further and more detailed operating conditions are given in appendix IV.

The difference between the experiments C1 & C2, and C3 is that the latter one also utilizes a lifter. A lifter is an additional transporter of solids. It is illustrated in figure 3.1 and transports solids from the bottom of the FR and to the AR. The lifter is further explained in section 2.4.7.

A total mass exchange of 1.4kg/s was achieved by also using the lifter. 1.4 kg/s from the AR through AR loop seal, 1.0 kg/s from the FR through the FR loop seal and 0.4 kg/s from FR to AR through the lifter. The lifter was successfully tested.

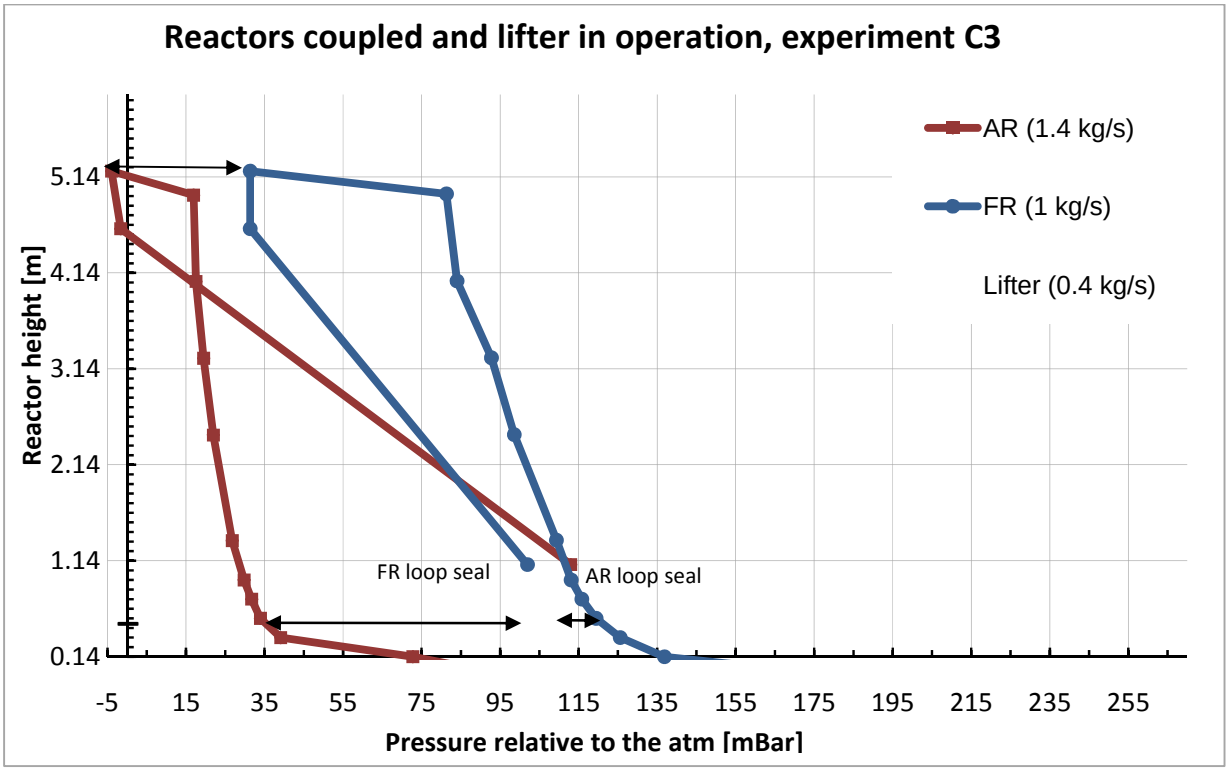

Figure 7.14 – *Experiment C3, reactors coupled and lifter in operation*

Figure 7.14 shows a pressure increase from the AR loop seal to the return leg in the FR. This is actually opposite of what it should be and indicate that there is not a pressure seal in the loop seal as it should be under normal operation. A gas flow will then go up the return leg in the FR, through the loop seal and to the cyclone. However, this may also be a pressure measurement error. As mentioned in section 7.3.3.1 the pressures out from the cyclone should be the same. Hence there seems to be some sort of pressure measurement error. Never the less, these results indicate that the transport of solids through the AR loop seal seems to be a bottleneck in the system. They also indicate that experiment C3 is close to the highest achievable global solid circulation rate. The pressure profiles indicate that the proper flow regimes were achieved for the reactors.

A fourth experiment was executed to achieve a global solid circulation rate of 2 kg/s. It did not succeed. Solids accumulated in the AR loop seal. The FR loop seal have a smaller solid flow because of the additional help of the lifter. The AR loop seal therefore has to transport the largest solid flow and seems to be the limiting factor. Operating conditions in the AR loop seal was adjusted, but it was not sufficient to ensure a larger solid flow. After the experimental campaign was finished a new operation and design of the loop seal was introduced. This is explained in section 2.4.6. This may help to debottleneck the AR loop seal. Another alternative may be to partially close the valve of the exhaust pipe for the AR. This will lead to a higher pressure in the AR and displace the AR pressure profile to the right in figure 7.14, hopefully increasing the pressure drop between AR loop seal and the return leg in the FR.

7.4 Cyclone efficiencies

The cyclone separator performed well, it had collection efficiencies >99%. This efficiency definition is given by equation 31. It seemed to have reduced performance when the pressure transducer tubes near the cyclone were flushed, during load changes on the rig and start-up. During stable operation the cyclone separators performed very well.

7.5 Uncertainty analysis

When doing experiments it is vital to be aware of potential error sources and their significance on the experimental results. This is important to be able to know if the results are reasonable and if it is possible to draw reasonable conclusions from the results. An uncertainty analysis has been performed to investigate if the experimental results were reasonable. Figure 7.15 shows the pressure measurements from selected pressure transducer during an experiment. The three flux measurements during the experiment are easy to see on the graph and are identified as the three dips in all of the pressure measurements. The system seems to be stable and recover quickly and to approximately the same pressure levels as before a flux measurement. In table 7.1 the average, standard deviation and the standard deviation percentage of the average of the pressure measurements are given. Pressure measurements during flux measurements are filtered out from the statistics. Statistics for all of the pressure measurements in the experiments are given in appendix VI. The trend for all

the pressure measurements is that they have a tolerable uncertainty. The standard deviation percentage of the average for P11 and P12 in the AR, and the corresponding P24 and P25 in the FR, are quite high. This can be explained by the nature of these measurements. P11/P12 and P24/P25 measure quite small pressure values in the system. This means that small fluctuations in pressure affect them relatively much.

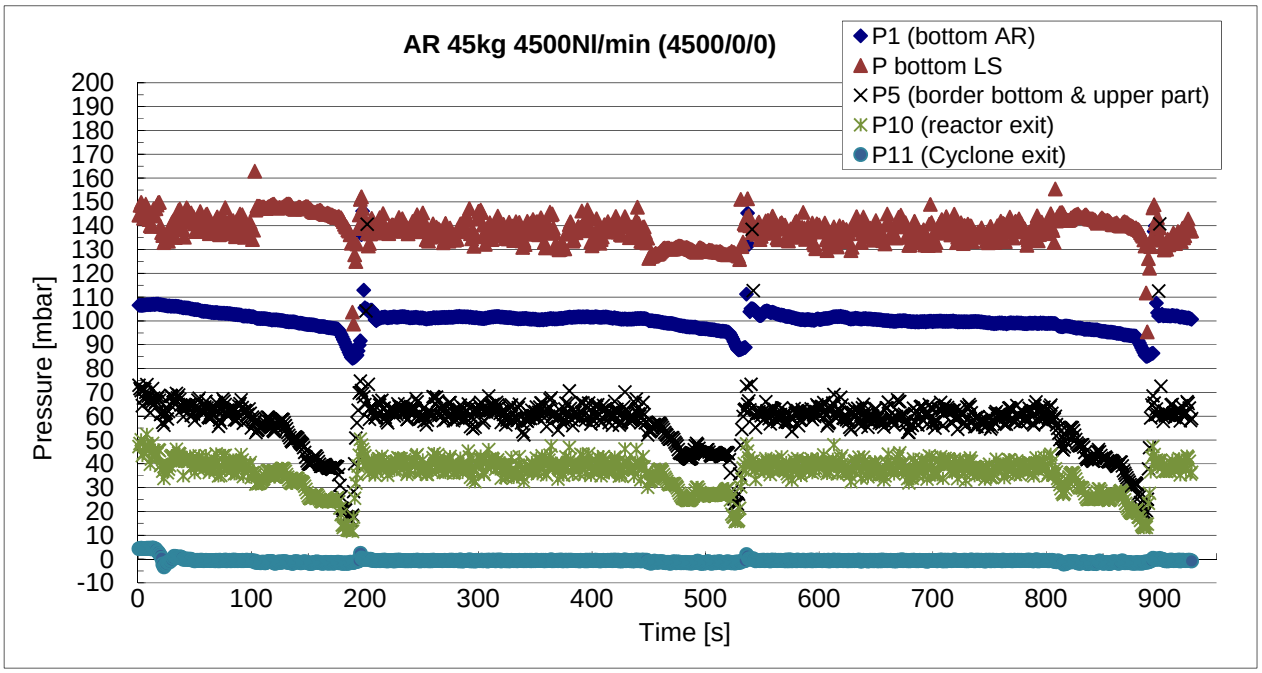

Figure 7.15 - *Pressure measurements from some selected pressure transducers during an experiment*

Pressures in [mBar]	P1	P2	P3	P4	P5	P6	P7	P8	P9	P10	P11	P12	P28*
Average	86.19	43.60	34.58	32.27	30.49	27.24	21.63	18.46	15.75	14.77	-0.43	1.12	146.63
STDEV	1.35	0.99	1.71	1.72	1.71	1.67	1.56	1.46	1.30	1.17	0.53	0.56	10.32
STDEV% of average	1.57	2.27	4.94	5.32	5.60	6.12	7.22	7.89	8.23	7.93	-124.77	50.39	7.04

** is explained in appendix VI*

Table 5.1 – *Pressure measurement statistics from the same experiment as in figure 7.15*

The steady-state criterion defined in chapter 5 uses P10 in the air reactor and P23 in the fuel reactor. In table 7.1 P10 has an acceptable standard deviation. The system also looks stable

from figure 7.15. Statistics like this were made for all of the experiments during the experimental campaign to ensure the quality of the experiments.

Several potential error sources in the experiments are discussed in this section:

- The experiments start with a certain total solid inventory. Even though the cyclones have a high efficiency some solids are lost during an experiment. This is because large gas/solid flows are treated during a time consuming experiment. This means that a significant amount of solids may be lost during an experiment.
- Even though the tubes connected to the pressure transducers were connected to a flushing system, clogging of the tubes is a potential error source.
- Measurement of the flux was done by eye and is explained in section 7.8.3. A fixed meter was installed to reduce uncertainty. However, measurement by eye is always related to uncertainty and may be somehow subjective. For the single reactor experiments three flux measurements were executed per operational mode. Data are given in appendix VII. For the coupled experiments only one flux measurement were done per operational mode due to the complex operation.
- The particles filled into to the CFM have a certain PSD. However the cyclone separates most efficient the coarsest particles, hence the finest leaves and enters the filter box. This means that the coarsest particles are left in the rig and the mean size particle actually is different from the mean size particle of the particles filled into the CFM. This influences the hydrodynamic behavior of the reactors.

7.6 Conclusions experimental campaign

An experimental campaign has been executed to investigate the hydrodynamics and design of the Cold Flow Model. This is an important step toward verifying the current design of the 150 kW_{th} CLC reactor system to be built on a later stage. The Cold Flow Model has been commissioned and is in general functioning satisfactory. The reactor system consists of two reactors exchanging solids in a loop. The operating area of the single reactors was mapped. On the basis of this mapping several experiments with coupled reactors were executed. A mass balance was achieved. In general a minimum of plugging in the pipes were observed during the experimental campaign.

Single reactor experiments were done to map the operating area of the reactors. The objectives for these experiments were achieved:

- The targets of solid circulation rates up to 2 kg/s in the AR and 1 kg/s in the FR were fulfilled.
- The proper flow regimes, hence good gas solid contact, were achieved for all of the experiments.

Coupled reactor experiments were performed. Two experiments were done with only mass exchange through loop seals, and one experiment which utilized a lifter. These experiments were more complex than the single reactor experiments. Several of the objectives for the coupled reactor experiments were achieved:

- The divided loop seal turned out to be difficult to operate. Probably possible to operate, but the internal part of the loop seals were sealed for the coupled reactor experiments.
- The cyclone showed collection efficiencies at approximately 99%.
- The targets of a global circulation rate with mass exchange only through loop seals of 1 kg/s were achieved. The reactors had the proper flow regimes.
- In experiment C3 the lifter was utilized successfully and was able to transport 0.4 kg/s. The aim was 1 kg/s. The result meant a global circulation rate of 1.4 kg/s. It did not however seem as the lifter was the bottleneck so it is unsure if it manages a transport of 1kg/s at the right operating conditions.
- A fourth experiment trying to achieve the target of a global solid circulation rate of 2 kg/s failed. The bottleneck in the system seems to be the transport of solids through the AR loop seal. Solids accumulate and build up in the downcomer.

7.7 Further work experimental campaign

The experimental campaign performed mapped the operating area of the reactors and was very useful. However the following further work is proposed done on the CFM:

- Additional single reactor experiments should be done. Only two mass inventories were tested for AR and FR. Several inventories should be investigated to confirm trends discovered in the experimental campaign and map a more extensive operating area.
- Testing of the divided loop seal, and mapping of the operating area.
- The particles filled into to the CFM have a certain PSD. However the cyclone separates best the coarsest particles, hence the finest leaves and enters the filter box. This means that the coarsest particles are left in the rig and the mean size particle actually is different than the mean size particle of the particles filled into the CFM. Samples of the particles in the rig and in the filter box should be evaluated to further understand the hydrodynamic behavior of the rig and the performance of the cyclone separator, the grade efficiency T(x).
- Optimize loop seal design and air use. In the hot rig air will not be used in the loop seals, but steam. Efficient use of the steam is therefore important. Purging air was experimented with and seems very promising. Since the AR loop seal seemed to be the bottleneck for achieving a global circulation rate of 2 kg/s, an optimized loop seal may lead to achieving that target.
- Run a coupled reactors experiment to achieve the target of achieving 1kg/s through the lifter. This is probably closely related to de-bottlenecking the AR loop seal and optimization of the loop seals. Hence the optimization of the loop seals/de-bottlenecking has to be done first.
- Execute additional coupled reactors experiments to further understand how the air injections and units in the CFM influence the operating conditions.
- Optimize the air use in the Cold Flow Model. In the hot rig air will be the fluidizing medium in the AR. In the loop seal it will be steam and in the FR it will comprise of the fuel, methane, and additional steam to ensure the proper flow regime. Efficient use of the steam, the air used in the CFM FR, is vital to achieve an economic feasible system. It should also be mentioned that the use of the fluidizing medium and flow regimes are connected to certain residence times and gas solids contact efficiencies which depends on the kinetics of the material chosen for the hot rig. When it comes to kinetics the FR, the reduction, seems to be the limiting factor. The residence times can also be improved by building the FR higher.
- Further investigate the behavior of the lifter

- Stop the rig instantaneously during an experiment. Then the amount of solids in the riser can be measured and compared with the active inventory estimation and the initial inventory.
- Calculate residence times with equation 13 for the experiments performed. The residence times are a vital and important result. This data is essential when different oxygen carriers are to be investigated.

7.8 Commissioning, preparation for the campaign

Before the campaign could start a commissioning for the campaign had to be performed. Some experiments were done to check that the data made sense. Needless to say, several issues had to be investigated and dealt with before the campaign could start, and some were dealt with during the campaign. This is also shown in the Gantt diagram in appendix II. Some of the most important ones are mentioned in this section.

7.8.1 Flushing system affected measurements when in closed mode

In order to avoid clogging and then wrong pressure measurements, the tubes to the pressure transducer were flushed. The magnetic valve flushing system was however not completely airtight when it was in a closed mode. The leakage from the flushing system went into the tubes to the pressure transducers and affected the pressure measurements. To avoid this, a valve further upstream the flushing system had to be closed when flushing was not performed.

7.8.2 Automatic flux measurement

It was attempted to introduce an automatic flux measurement with no need for visual measuring. This was done by closing a flap valve, fluidize the particles and measure the pressure drop across the bed of particles that accumulated on top of the flap valve. However this measurement technique requires different amounts of air to fluidize the solids on top of the flap valve. The amount of required fluidization air is a function of the amount of particles collected. This flux measurement solution turned to be a bit more advanced and time consuming to install than originally intended. Since a presentation was to be held at the 1st International Conference on Chemical Looping at 17-19 March 2010, it was decided to not use more effort on the automatic flux measurement and do a manually one instead.

7.8.3 Manual flux measurement

The manual flux measurement works in a simple way. A flap valve was installed in the downcomers. By closing the flap valve and measure the height of the column of particles accumulating during a certain time interval, the mass flow and flux can be calculated. Since the flap valve is not entirely air tight the air supply in the corresponding loop seal was shut down to avoid fluidization of the accumulated particles. The density of a bulk amount was measured and this is the bulk density in appendix III which is used in the mass flow and flux calculations. Closing of the flap valve, time measurement and air supply was done automatic by LabView. Reading of the particle column's height had to be read by eye. A fixed meter was introduced to reduce measurement uncertainty.

Figure 7.16 - *Manual flux measurement in downcomer*

7.8.4 Isolating the reactors during operation of a single reactor

Some single reactor experiments with the FR are excluded from this report. This is because particles in the divided loop seal were lost to the other reactor not in use, the AR. There was also a flow loss from the FR reactor and up in to the AR loop seal, up the downcomer and out of the AR exit. This affected the experimental results. They were therefore rejected and are not included in this report. The reactors were after this isolated when running single reactor experiments.

7.8.5 Cyclone separator

The cyclone and most of the rig is made of polycarbonate. The cyclone wall is especially exposed for erosion by the particles. The cyclone wall had to be reinforced with a metal plate. Otherwise the cyclone separator performed well and had collection efficiencies >99%.

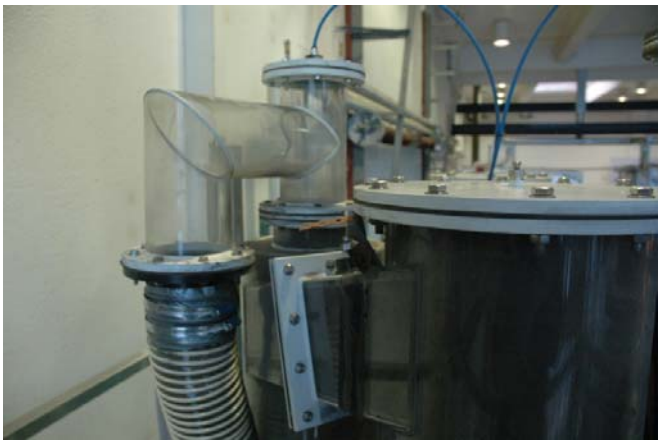

Figure 7.17 - *Top of riser and cyclone separator*

7.8.6 Pressure short circuit when running both reactors simultaneously

During the first run of both reactors simultaneously a pressure short circuit occurred. The loop seal usually works as a pressure seal between the return leg in the riser and the downcomer/cyclone. Running the loop seal almost empty of particles or using to much fluidization air can cause this pressure seal to cease. This pressure short circuit lead to a loss of 34,5 kg of solids out of the cyclone in a very short time.

The problem was solved sealing the internal return leg of both reactors. The divided loop seal could then not be tested since it was only possible to use the external recycle chambers and not the internal ones since they were sealed.

7.8.7 Plugging in downcomer after flux measurement

After a flux measurement which includes closing the flap valve and accumulate particles, the particles usually fall down and into the loop seal. However because of interparticle forces the particles sometimes did not fall down when the flap valve was opened, but stayed in the downcomer forming a plug growing larger and larger. Thus the whole experiment had to be aborted and the rig had to be shut down.

8. Simulation of experiments in the fluidization software ERGUN

ERGUN is a commercial software which is used to simulate CFBs. The experiments done in the experimental campaign have been simulated in ERGUN. The simulation program is made for CFBs that operate at high temperatures and were in the first place probably not intended for simulations of cold flow models. It is however possible to simulate a cold flow model in the program. ERGUN has several simulation possibilities. The flow structure in the risers was simulated and the results were compared to the single reactor experimental results. Three different models for modeling risers are available in ERGUN, Horio, Berruti and Wirth. Horio and Berruti's models are of most interest for the simulations done. Hence they are presented in the two following sections.

8.1 Horio's model

Horio's model is a pressure balance model for the entire loop of a circulating fluidized bed system. The gas flow between the riser and downcomer is also taken into account. The model is based on the principles of clustering suspension and core-annulus flow in the riser. The riser is axially divided into a lower dense region and an upper dilute region. In the lower dense region a constant solid fraction is assumed, and the effects of particle acceleration, particle friction and gas friction on the pressure drop is neglected. In the upper dilute region the axial solid fraction profile is assumed to decrease exponentially from the dense region height to the riser exit. A correlation for the decay factor of the voidage profile was developed for the model. The decay factor has an accuracy of ±30% accuracy. Exit effects in the riser are neglected.

Horio's model is further described in (Hongwei Lei 1998) and (Masayuki Horio 1997).

8.2 Berruti's model

The objective of the Berruti model is to be predictive, user-friendly and to be able to describe key parameters in a mixed flow of solids and gas. The key parameters include: Radial and axial voidage, solids velocity, solids mass flux profiles, core gas velocity and core radius. The concepts core gas velocity and core radius is related to the core-annulus model described in section 2.3.7. The input parameters for the model are the solids flux, superficial gas velocity, riser geometry and physical properties of gas and solids.

The model assumes the CFB riser to be axially composed of two regions: An acceleration zone at the riser base, where solids re-injected from the standpipe are accelerated to a constant upward velocity, and a fully developed flow region which extends from the end of the acceleration zone to the riser exit. Exit effects which may be caused by geometry of the riser exit is not included in the model.

The model postulates a core-annulus type of flow structure. Radial gas flow is allowed from the core to the annulus, equal to that from the annulus to the core. It should be noted that a

bed of constant suspension density is not assumed at the base of the riser and the suspension density profile is considered to decrease monotonically from the riser entrance. Hence the model is limited to describe axial flow structure of the turbulent and fast fluidization flow regime, and is not directly applicable for describing axial profiles in flow regimes where a dense bed exits at the base of the riser.

Berruti's model is further described in (Pugsley and Berruti 1996) and (Berruti and Kalogerakis 1989).

8.3 Simulation input data

The experiments performed in the campaign had three variables: total solid inventory, total flow and primary/secondary air distribution. The simulation option used in ERGUN, "Flow Structure", is not able to simulate the different primary/secondary air distributions performed in the experimental campaign. Hence a distribution was chosen for AR, 100% primary air, and FR 75% primary air and 25% secondary air. All the experiments with this air distribution have been simulated in ERGUN. The input data for the simulation is shown in table 8.1.

Input data		
Parameter	**Value**	**Unit**
Gas density	1.20	[kg/m^3]
Particle density	7000	[kg/m^3]
Viscosity	1.78E-05	[Ns/m^2]
Mean particle size	34.5	[µm]
Cross-sectional area , AR / FR	0.042 / 0.018	[m^2]
Bed height	5.0	[m]
Voidage at minimum fluidization, ϵ_{mf}	0.48	-
Variables:		
Operating velocity, U	0.9 – 2.0	[m/s]
Mass flow, Ws	0.36 – 1.96	[kg/s]

Table 8.1 - *Simulation input data*

The input data were acquired from different sources. (Wikipedia 6.04.2010) gives the gas (air) density and viscosity at 20°C and 1 atm. The particle density was acquired from the particle data sheet. The mean particle size was measured in the particle lab at NTNU. The minimum

fluidization voidage, ϵ_{mf}, was estimated to be 0.48. Detailed calculations of the voidage can be found in appendix X.

As seen in table 8.1 the simulation input data has two variables: Operating velocity U and mass flow Ws. The operating velocity can be calculated from the total flow in the experiment performed.

The operating velocity, also known as the superficial gas velocity U, was calculated with the following equation:

$$U \cong q\ \mathrm{Nl/min} \times \frac{1\ \mathrm{m^3}}{1000\ \mathrm{dm^3}} \times \frac{1\ \mathrm{min}}{60\ \mathrm{s}} \times \frac{1}{A\ \mathrm{m^2}} \times \frac{293\ \mathrm{K}}{273\ \mathrm{K}} \tag{39}$$

Where q is the flow in Nl/min given from LabView and A the cross sectional area of the riser. The last term in the equation is a temperature correction. It is assumed that the air flow has a temperature of 293 K. No pressure correction was done.

It should be noted that the riser inventory unfortunately is not the second variable. This would be practical for a future experimental campaign. Instead ERGUN requires the mass flow, which was measured in experiment.

The relation between the experiment data; solid inventory and total flow, and the simulation input data is given in appendix IX.

8.4 Simulation output data

The models have several output parameters. The most important ones in this context are the pressure as a function of the height in the riser, and the voidage also as a function of the height. An estimation of the inventory can therefore be made with equation 40, (Hongwei Lei 1998).

$$W_R = \rho_p \times A \int_0^{h_R} (1 - \epsilon(z))\, dz \tag{40}$$

Where $\epsilon(z)$ is the voidage as a function of the height of the reactor, z

The estimated riser inventory in the models can then be compared with the active inventory in the experiments. The active inventory is in this report defined as a mathematical estimation

of the solid inventory in the riser during an experiment. This estimation is done with equation 24. This is used instead of the initial inventory in the riser before the experiment starts. Initial inventories are given in appendix IV. The reason for this is that the solid distribution in the reactor system changes during operation and hopefully the active inventory gives a better estimation of the actual inventory in the riser during operation.

8.5 Results and discussion

The flow structure in the riser for all the single reactor experiments were simulated in ERGUN. The experimental data and the data from the models were compared. Horio and Berruti are two different models and are applicable to different flow regimes. An overview of earlier successfully tested operating conditions for the Berruti model are given by (Pugsley and Berruti 1996). A similar overview was not found for the Horio model.

Applicability of the Berruti model		
Parameter	**Range of operating conditions tested before**	**Operating conditions in experiments and simulations**
Mean particle size	50 – 350 µm	34.5 µm
Particle density	1400 – 2600 kg/m^3	7000 kg/m^3
Riser diameter	0.05 – 1 m	
Riser length	3 – 35 m	5 m
Operating velocity, U	Typically greater than 2 m/s	0.9 – 2.0 m/s
Solids mass flux	0 – 1000 kg/m^{2}s	5.8 – 65.6 kg/m^{2}s

Table 8.2 - *The Berruti model has earlier been tested under different operating conditions*

Several parameters are outside of the range of what has been tested successfully before for the Berruti model. The mean particle size 34.5 µm is smaller than tested before, which is 50 µm. The particle density 7000 kg/m3 is 2.7 times larger than the largest particle density tested before. Operating velocities is smaller. The other parameters seem to be in range. So, the particles are smaller, heavier and the experiments were done at smaller operating velocities than tested. Never the less the Berruti model seemed to fit quite good in some of the experiments.

ERGUN simulates the pressure drop in the riser. Any ambient pressure in the system is not considered. To compare the simulation results with the experiments, the simulated pressure drop has been added to the pressure at the top of the riser in the respective experiment.

In general the experiments performed with both AR and FR, Horio's model did not seem to have reasonable fit. This applies both to pressure profiles and estimated riser inventory. Horio's model seems to have a better fit with increased inventory/high pressure levels in the riser. Since equation 39 is not pressure corrected, a "high" pressure imply to a certain extent lower operating velocities than stated and a flow regime closer to bubbling fluidization where Horio's model probably is more appropriate. This also explains why the AR experiments are a worse fit with respect to Horio's model than the FR experiments. Examples of these trends are shown in figures 8.1 - 8.3. It should be mentioned that there are some uncertainty related to the active inventory from the experiments.

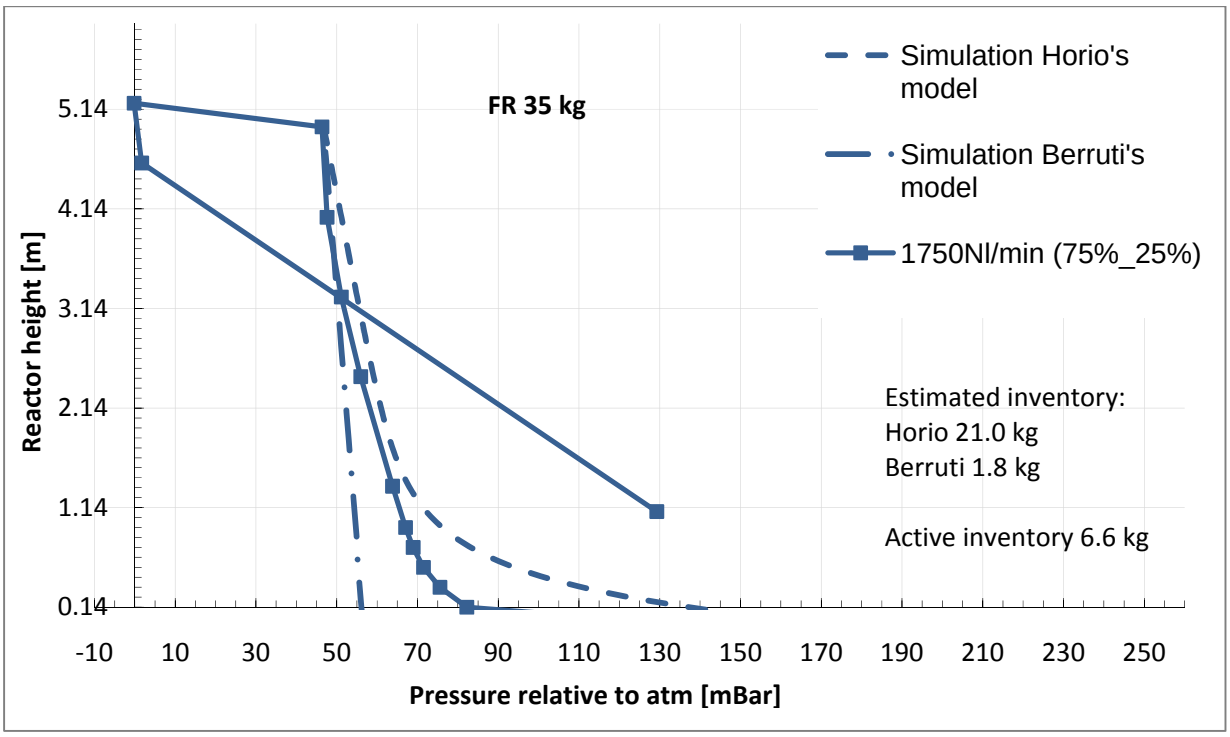

Figure 8.1 – *Experimental results compared with the simulation results for FR 35kg at 1750 Nl/min*

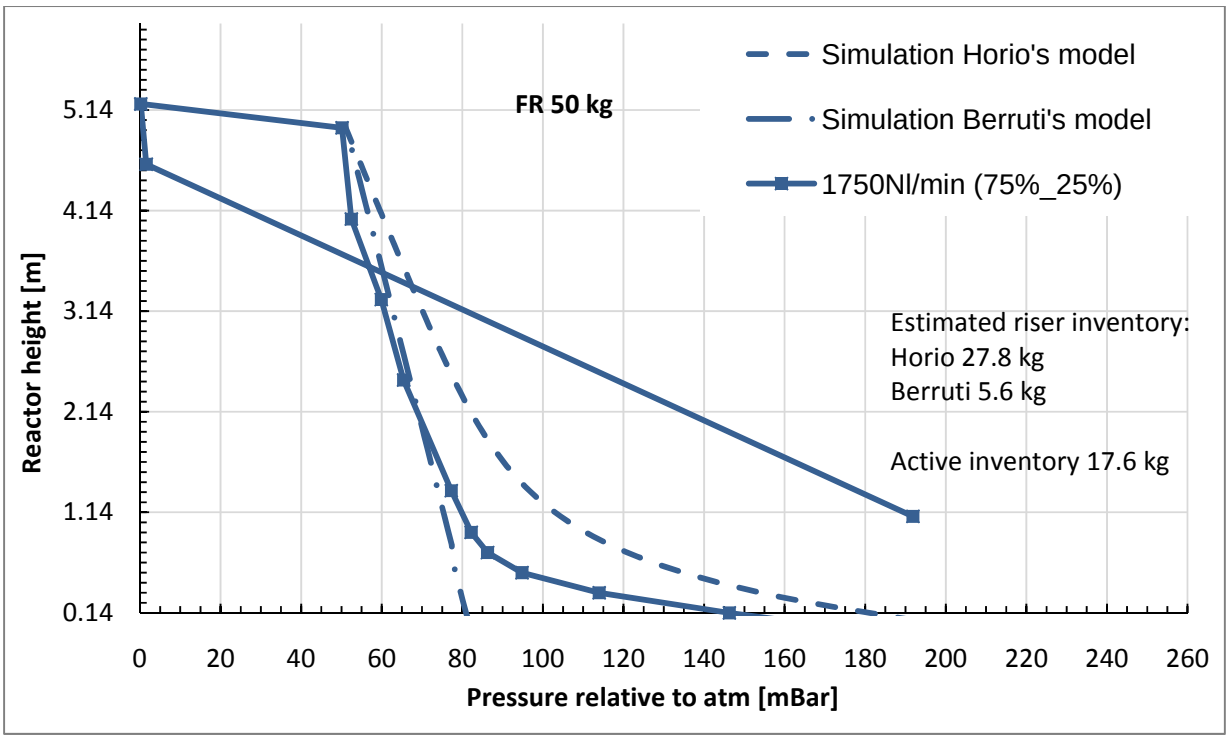

Figure 8.2 - *Experimental results compared with the simulation results for FR 50kg at 1750 Nl/min*

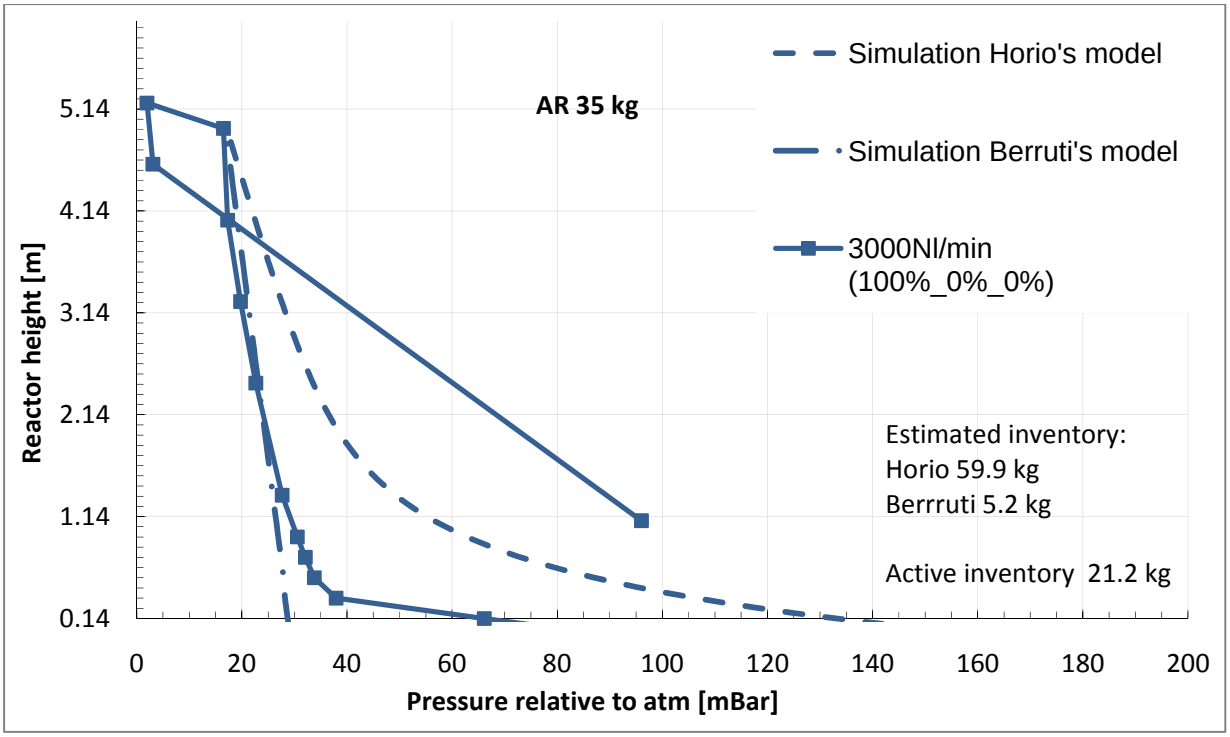

Figure 8.3 - *Example of the reasonable coherency between experiment and Berruti's model in the upper part of the AR*

In general the Berruti model seem to be a good fit both for the FR and AR experiments done, though only to model the upper part of the risers. By the upper part it is in this report meant the region of the riser over the dense bed in the bottom. This can be seen in the pressure profile as the break in the curve.

As explained in section 8.1-8.2 Berruti works well for flow regimes with no or a insignificant dense bed in the bottom of the riser, while Horio is made for flow regimes with a dense bed in the bottom. This seems to be the main cause of the varying suitability of the models. Berruti suits good for turbulent and fast fluidization but comes short when the flow regime is getting close to bubbling fluidization. Figure 8.4 shows the operating area of the experiments.

All of the simulations results are given in appendix XI.

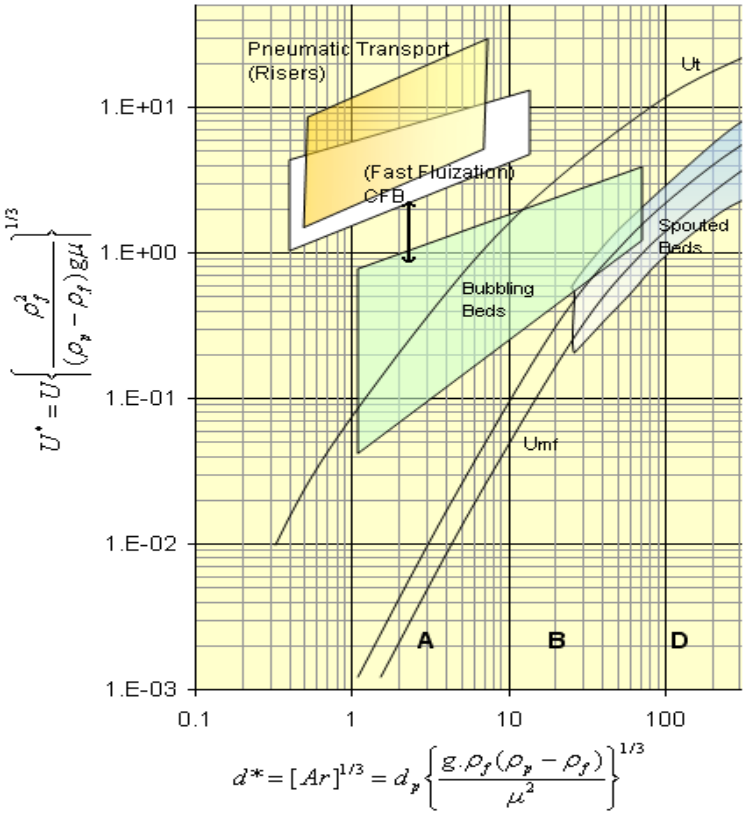

Figure 8.4 - *Grace diagram showing the range of flow regimes in the experiments. The operating velocities are not pressure corrected*

8.6 Uncertainties

The experimental data involves some level of uncertainty. So does the mathematical models in ERGUN. The mathematical models are not perfect. Even though they apply the same fundamental principles they are developed differently and take into consideration or emphasize different factors. There is also some uncertainty related to the input data given in table 8.1. The mean particle size is given, but the actual particle size distribution is not taken into consideration. The estimation of the sphericity also adds to the general uncertainty.

In the simulations of the flow structure it was not possible to take into consideration the primary/secondary air distribution. The experiments in AR with 100% primary air were therefore chosen to minimize that effect. Experiments with 100 % primary air were not done in the FR and therefore the closest air distribution was used in the simulation, 75 % primary air and 25 % secondary air. The air distribution issue adds uncertainty to the coherence between the experimental results and the simulations.

The simulation input data requires the diameter of the reactor. From the bottom of the reactor and up to 1m the diameter gets larger. The increased diameter is not large in size. The diameter used in the simulations is the diameter of the reactor after 1m, which is the diameter of the rest of the reactor. The simulation models seemed to be sensitive of the area, hence the diameter. However the relevant diameter changes are probably too small to have a major affect on the simulations.

The estimated active inventory has several error sources. The cross-sectional areas of the reactors are not constant but a function of the height the first meter. The next four meters the area is constant. The areas used in the estimations are the area above the cones in the lower part of the reactors. The estimation would be more correct if an integration of equation 24 was done along the height with area as a function of the height. Some of the pressure drop in the riser is also related to acceleration of the solids and a frictional pressure drop in the riser. However, the pressure drop due to solids acceleration and friction are not considered significant at low circulation rates according to (Bi and Zhu 1993).

Given that Horio and Berruti gave very different results it is clear that the simulation models may also be a essential error source. These mathematical models are based upon different reactor designs and are more applicable in certain flow regimes than others.

8.7 Conclusion simulations

The general incongruence between the ERGUN simulations and the experiments shows that Horio and Berruti's model should not be used for a detailed investigation of the flow structure in the CFM risers. At least not for the operating conditions tested. However, with certain reservations, a preliminary investigation of the risers with Berruti's model in ERGUN may be reasonable.

- Berruti's model is a reasonable tool for modeling the upper part of the pressure profile in the AR and FR at the operating conditions tested. The operating conditions tested in the AR are total solid inventories of 35 and 45 kg, and superficial gas velocities from 0.9-1.9 m/s. The operating conditions tested in the FR are total solid inventories of 35 and 50 kg, and superficial gas velocities from 1.5 - 2.0 m/s.
- Horio's model was not a good match for the experiments done with the AR or FR.
- Horio's model seems to be a better match at flow regimes closer to bubbling fluidization and with more internal recirculation.

8.8 Further work

Further work in this area is proposed and are given here:

- Calculate the average deviation the simulation results have from the lab experiments data. It would then be possible to give a more quantitatively analysis of the applicability of ERGUN for modeling the CFM. The one given in this chapter, chapter 8, is qualitatively.
- As mentioned in section 7.5, there is uncertainty related to the actual bed inventory. The lab experiments should be performed a second time and shut down instantaneously and the amount of solids in the riser should be measured. This accurate riser inventory should be compared with the active inventory estimated by equation 24 and the simulation models.
- Perform more lab experiments and map a larger operating area and investigate where the mathematical models may fit.
- Investigate the applicability of other mathematical models are better fitted for modeling the behavior of the CFM.
- Make a specific mathematical model for simulation of the CFM.

9. Conclusion

An experimental campaign has been executed to investigate the hydrodynamics and design of the Cold Flow Model. This is an important step toward verifying the current design of the 150 kW_{th} CLC reactor system to be built on a later stage. The Cold Flow Model has been commissioned and is in general functioning satisfactory. The reactor system consists of two reactors exchanging solids in a loop. The operating area of the single reactors was mapped. On the basis of this mapping several experiments with coupled reactors were executed. A mass balance was achieved. In general a minimum of plugging in the pipes were observed during the experimental campaign.

Single reactor experiments were done to map the operating area of the reactors. The objectives for these experiments were achieved:

- The targets of solid circulation rates up to 2 kg/s in the AR and 1 kg/s in the FR were fulfilled.
- The proper flow regimes, hence good gas solid contact, were achieved for all of the experiments.

Coupled reactor experiments were performed. Two experiments were done with only mass exchange through loop seals, and one experiment which utilized a lifter. These experiments were more complex than the single reactor experiments. Several of the objectives for the coupled reactor experiments were achieved:

- The divided loop seal turned out to be difficult to operate. Probably possible to operate, but the internal part of the loop seals were sealed for the coupled reactor experiments.
- The cyclone showed collection efficiencies at approximately 99 %.
- The targets of a global circulation rate with mass exchange only through loop seals of 1 kg/s were achieved. The reactors had the proper flow regimes.
- In experiment C3 the lifter was utilized successfully and was able to transport 0.4 kg/s. The aim was 1 kg/s. The result meant a global circulation rate of 1.4 kg/s. It did not however seem as the lifter was the bottleneck so it is unsure if it manages a transport of 1kg/s at the right operating conditions.
- A fourth experiment trying to achieve the target of a global solid circulation rate of 2 kg/s failed. The bottleneck in the system seems to be the transport of solids through the AR loop seal. Solids accumulate and build up in the downcomer.

The general incongruence between the ERGUN simulations and the experiments shows that Horio and Berruti's model should not be used for a detailed investigation of the flow structure in the CFM risers. At least not for the operating conditions tested. However, with certain reservations, a preliminary investigation of the risers with Berruti's model in ERGUN may be reasonable.

- Berruti's model is a reasonable tool for modeling the upper part of the pressure profile in the AR and FR at the operating conditions tested. The operating conditions tested in the AR are total solid inventories of 35 and 45 kg, and superficial gas velocities from 0.9-1.9 m/s. The operating conditions tested in the FR are total solid inventories of 35 and 50 kg, and superficial gas velocities from 1.5-2.0 m/s.
- Horio's model was not a good match for the experiments done with the AR or FR.
- Horio's model seems to be a better match at flow regimes closer to bubbling fluidization and with more internal recirculation.

References

AT&P.Journal (2010). FCX-AII, Differential Pressure Transducer

Basu, P. (2006). Combustion and Gasification in Fluidized Beds.

Berruti, F. and N. Kalogerakis (1989). "Modelling the internal flow structure of circulating fluidized beds." The Canadian Journal of Chemical Engineering **67**(6): 1010-1014.

Bi, H. and J. Zhu (1993). "Static instability analysis of circulating fluidized beds and concept of high-density risers." AIChE Journal **39**(8): 1272-1280.

Bolland, O. (2009). "Lecture in the course: TEP03 CO2 capture in power plants, NTNU ".

Brooks.Instruments (2008). Installation and Operation Manual - Brooks® Mass Flow Meter Model 5863.

Daizo Kunii, O. L. (1991). Fluidization Engineering.

Eckhoff, R. K. (1994). Dust explosion hazards in the ferro-alloys industry. 52nd Electric Furnace Conference, Nashv., TN, USA.

ENCAPCO2 (2009). "ENCAP - WP1.2 Deliverable D1.2.6 Power systems evaluation and benchmarking - Public version."

H. T. Bi, J. R. G. (1995). "Flow regime diagrams for gas-solid fluidization and upward transport." International Journal of Multiphase Flow **21**(No.6): 1229-1236.

Hongwei Lei, M. H. (1998). "A comprehensive Pressure Balance Model of Circulating Fluidized Beds." Journal of Chemical Engineering of Japan **31**(No.1): 83-94.

Hossain, M. M. and H. I. de Lasa (2008). "Chemical-looping combustion (CLC) for inherent CO2 separations--a review." Chemical Engineering Science **63**(18): 4433-4451.

IEA, I. E. A. (2009). "World Energy Outlook 2009, Part 1." 75.

IPCC (2007). "Fourth Assessment Report "The Physical Science Basis"." IPCC

J. H. Kim, K. S. (2000). "Analysis and modelling of solid flow in a closed loop circulating fluidized bed with secondary air injection." Powder Technology **111**: 179-184.

J.R Grace, A. A. A., T.M Knowlton (1997). Circulating Fluidized Beds. London, Blackie Academic and Professional.

Krammer, G. (2008a). Particle Technology - Fundamentals. Compendium for course TEP 4212: Environmental and Cleaning Technologies. Trondheim, Department of Energy and Process Engineering, NTNU.

Krammer, G. (2008b). Particle Separation Technologies. Compendium for course TEP4212: Environmental and Cleaning Technologies. Trondheim, Department of Energy and Process Engineering, NTNU.

Krohmer, B. (2006). "Operating Experience with Measures for Improvement of Cyclone Removal Efficiency." VGB Powertech **12**: 77-81.

M. Bysveen, J. B., Ø. Langørgen, I. Saanum, M. Seljeskog, J-X Morin, A. Bischi (2009). Design of a 150 kW Chemical Looping Combustion reactor ready for pressurization. The 5th Trondheim Conference on CO2 Capture, Transport and Storage, Trondheim Norway.

Masayuki Horio, M. I. (1997). "Prediction of cluster size in circulating fluidized beds." Journal of Chemical Engineering of Japan **30**(No.4): 691-697.

P. Kolbitsch, T. P., J. Bolhar-Nordenkampf, Hermann Hofbauer (2009). "Design of a Chemical Looping Combustor using a Dual Circulating Fluidized Bed Reactor System." Chem. Eng technol. **32**(No.3): 398-403.

Pugsley, T. S. and F. Berruti (1996). "A predictive hydrodynamic model for circulating fluidized bed risers." Powder Technology **89**(1): 57-69.

Rubel, A., K. Liu, et al. (2009). "Oxygen carriers for chemical looping combustion of solid fuels." Fuel **88**(5): 876-884.

T. Abbasi, S. A. A. (2006). "Dust explosions-Cases, causes, consequences, and control." Journal of Hazardous Materials **140**: 7-44.

Tobias Pröll, K. R., Philipp Kolbitsch, Johannes BolhàrNordenkampf, hermann Hofbauer (2009). "Cold Flow Model Study on a dual Circulating Fluidized Bed System for Chemical Looping Processes " Chem. Eng technol. **32**(No.3): 418-424.

Wikipedia (6.04.2010). "Density of air." from http://en.wikipedia.org/wiki/Density_of_air.

Appendices

Appendix I LabView control system layout

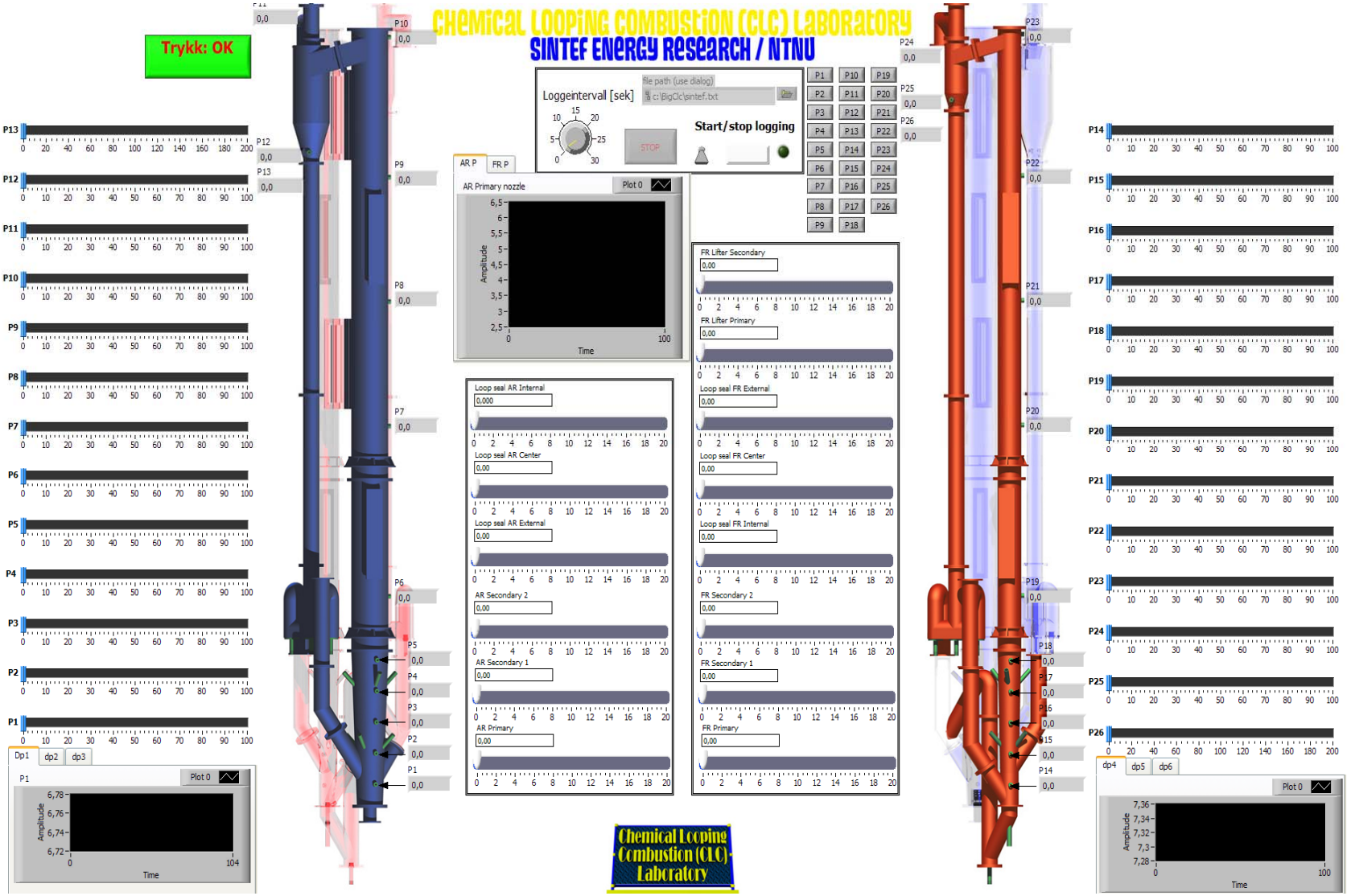

Appendix II Gantt diagram

ID	Task Name	Start	Finish	Duration
1	Commissioning	18.01.2010	23.02.2010	27d
2	Experimental campaign	12.02.2010	02.03.2010	13d
3	Interpret results from exp.campaign	15.02.2010	26.03.2010	30d
4	Eastern vacation	24.03.2010	06.04.2010	10d
5	Simulations in ERGUN	06.04.2010	30.04.2010	19d
6	Writing of report	01.03.2010	22.06.2010	82d
7	Deadline Master Thesis	22.06.2010	22.06.2010	1d

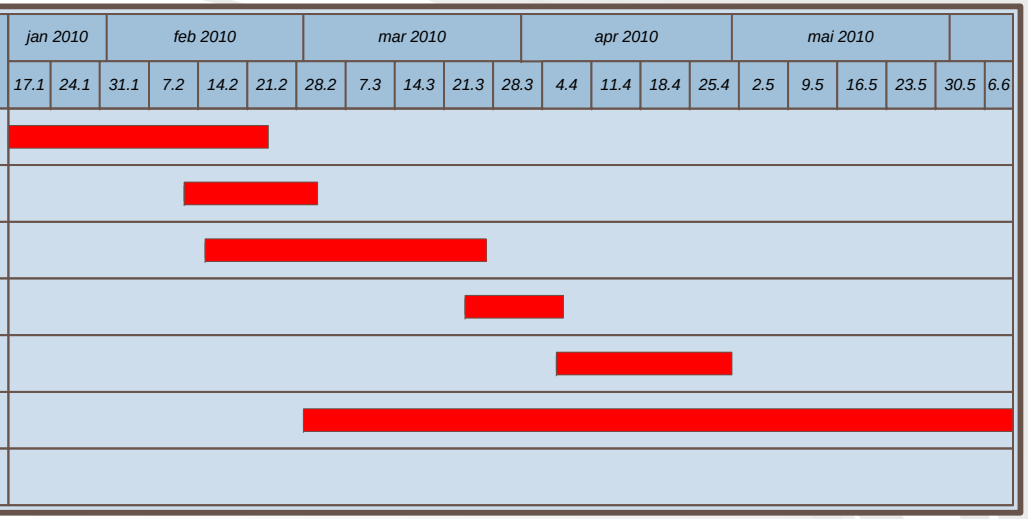

Appendix III Cold Flow Model data

CFM Design Parameters

Parameter	Value	Unit
Air Reactor height	5.00	[m]
Air Reactor diameter	0.23	[m]
Fuel Reactor height	5.00	[m]
Fuel Reactor diameter	0.15	[m]
Particle density	6969,8	[kg·m^{-3}]
Bulk particle density	3900	[kg·m^{-3}]
Particle diameter	34.5	[µm]
Pressure range	0-100	[mbar]
Volume flow range, Air Reactor	2000-5000	Nl/min
Volume flow range, Fuel Reactor		Nl/min

Appendix IV Additional operating conditions for experiments

Single reactor experiments, FR:

Experiment F1, 35kg	
FR loop seal internal	180 Nl/min
FR loop seal center	70 Nl/min
FR loop seal external	-
Bed inventory in riser before start up	20 kg
Loop seal filled to predefined level	15 kg
Total solid inventory	**35 kg**

Experiment F2, 50 kg	
FR loop seal internal	199 Nl/min
FR loop seal center	140 Nl/min
FR loop seal external	-
Bed inventory in riser before start up	35 kg
Loop seal filled to defined level	15 kg
Total solid inventory	**50 kg**

Single reactor experiments, AR:

Experiment A1, 35 kg	
AR loop seal internal	180 Nl/min
AR loop seal center	100 Nl/min
AR loop seal external	-
Bed inventory in riser before start up	20 kg
Loop seal filled to defined level	15 kg
Total solid inventory	**35 kg**

Experiment A2, 45 kg	
AR loop seal internal	180 Nl/min
AR loop seal center	140 Nl/min
AR loop seal external	-
Bed inventory in riser before start up	30 kg
Loop seals filled to defined level	15 kg
Total solid inventory	**45 kg**

Coupled reactors

Experiment C1	
AR total flow	1000 / 1000 Nl/min
FR total flow	2100 / 450 /450 Nl/min
AR loop seal internal	-
AR loop seal center	100 Nl/min
AR loop seal external	100 Nl/min
FR loop seal internal	-
FR loop seal center	100 Nl/min
FR loop seal external	100 Nl/min
Bed inventory in AR riser before start up	30 kg
Bed inventory in FR riser before start up	35 kg
Loop seals filled to defined level	2x15 kg
Lifter	Filled but not used in experiment
Total solid inventory	**= 95 kg**

Experiment C2	
AR total flow	1100 / 1100 Nl/min
FR total flow	2100 / 450 /450 Nl/min
AR loop seal internal	-
AR loop seal center	100 Nl/min
AR loop seal external	160 Nl/min
FR loop seal internal	-
FR loop seal center	100 Nl/min
FR loop seal external	100 Nl/min
Bed inventory in AR riser before start up	33 kg
Bed inventory in FR riser before start up	35 kg
Loop seals filled to defined level	2x15 kg
Lifter	Filled but not used in experiment
Total solid inventory	**= 95 kg**

Experiment C3	
AR total flow	1100 / 1100 Nl/min
FR total flow	2600 / 600 /600 Nl/min
AR loop seal internal	-
AR loop seal center	199 Nl/min
AR loop seal external	199 Nl/min
FR loop seal internal	-
FR loop seal center	100 Nl/min
FR loop seal external	100 Nl/min
Lifter primary	239 Nl/min
Lifter secondary	199 Nl/min
Bed inventory in AR riser before start up	33 kg
Bed inventory in FR riser before start up	35 kg
Loop seals filled to defined level	2x15 kg
Lifter	25.6 kg
Total solid inventory	= 123.5 kg ≈ **124kg**

Appendix V Pressure profiles as a function of the solid inventory

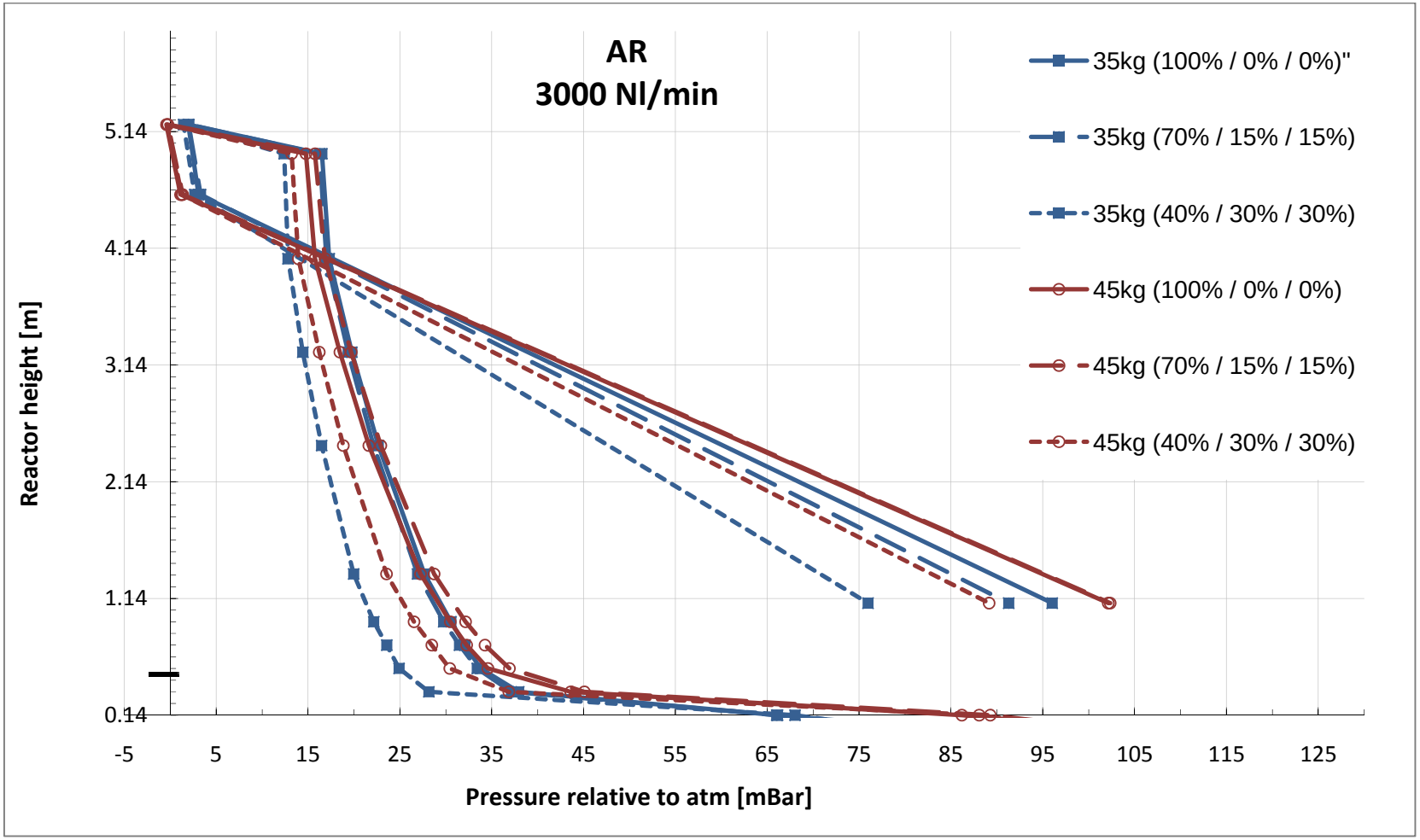

Pressure profiles for AR at a total flow of 3000Nl/min, at different total solid inventories, 35kg and 45kg, and different primary and secondary air distributions

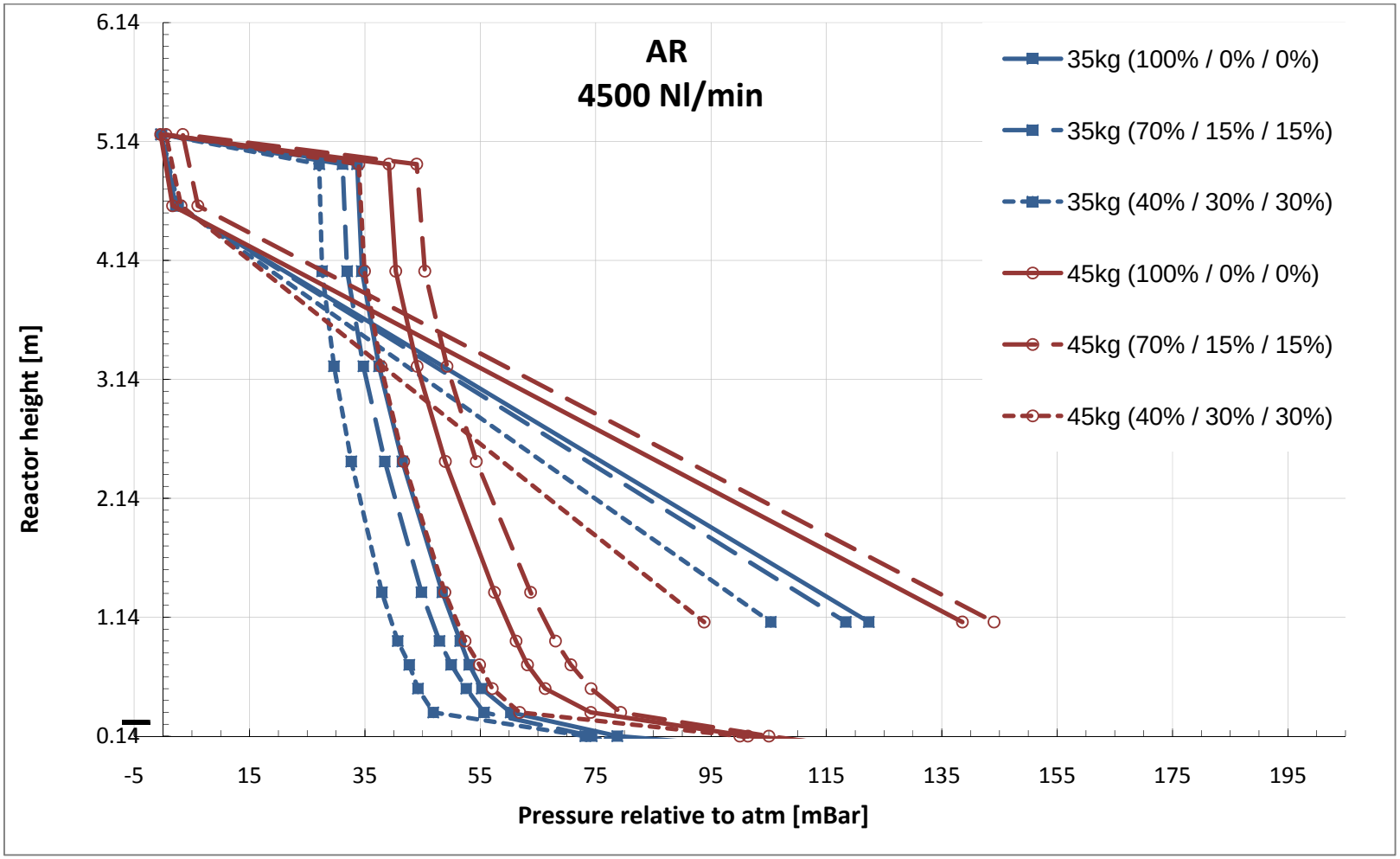

Pressure profiles for AR at a total flow of 4500Nl/min, at different total solid inventories, 35kg and 45kg, and different primary and secondary air distributions

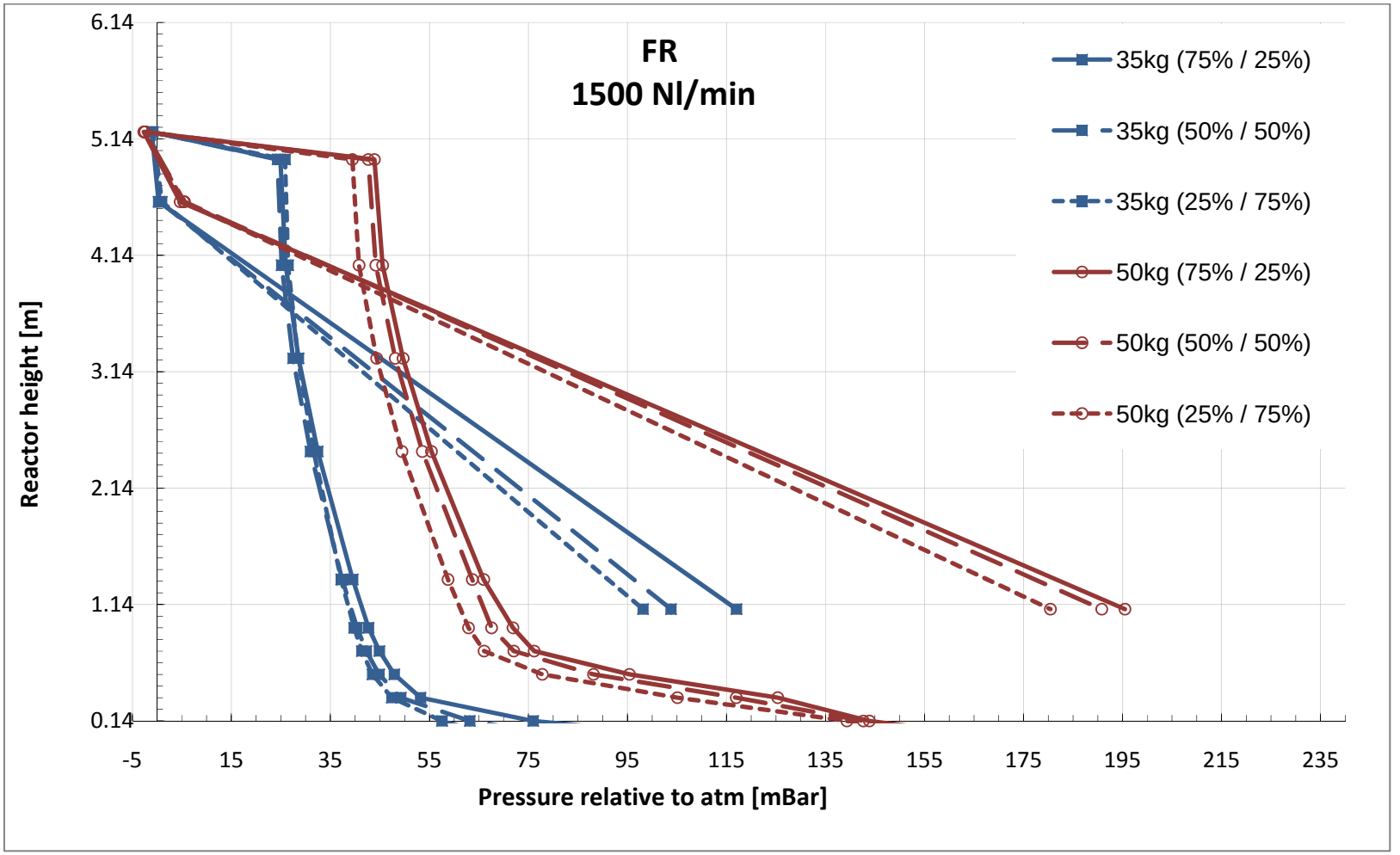

Pressure profiles for FR at a total flow of 1500Nl/min, at different total solid inventories, 35kg and 50kg, and different primary and secondary air distributions

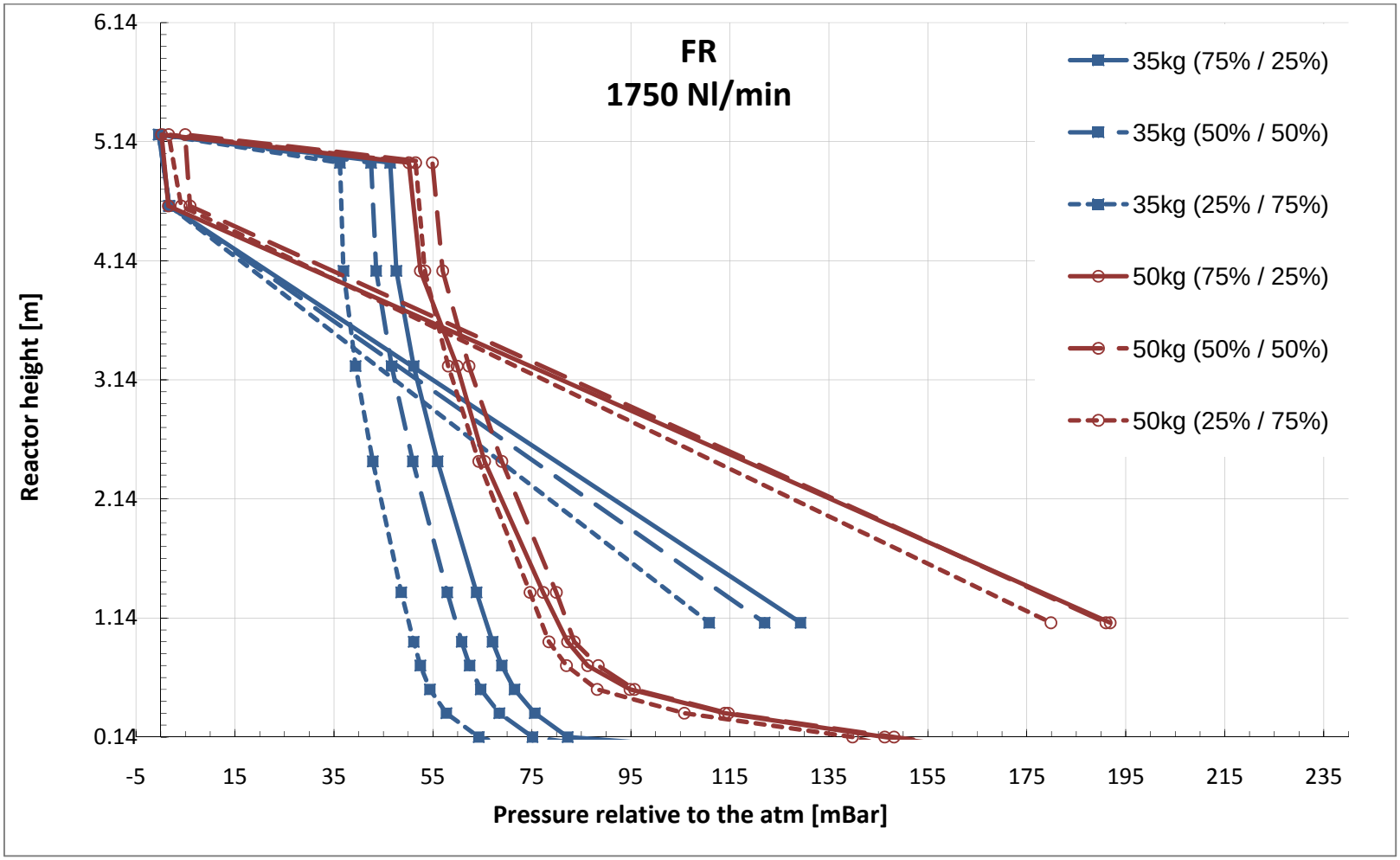

Pressure profiles for FR at a total flow of 1750Nl/min, at different total solid inventories, 35kg and 50kg, and different primary and secondary air distributions

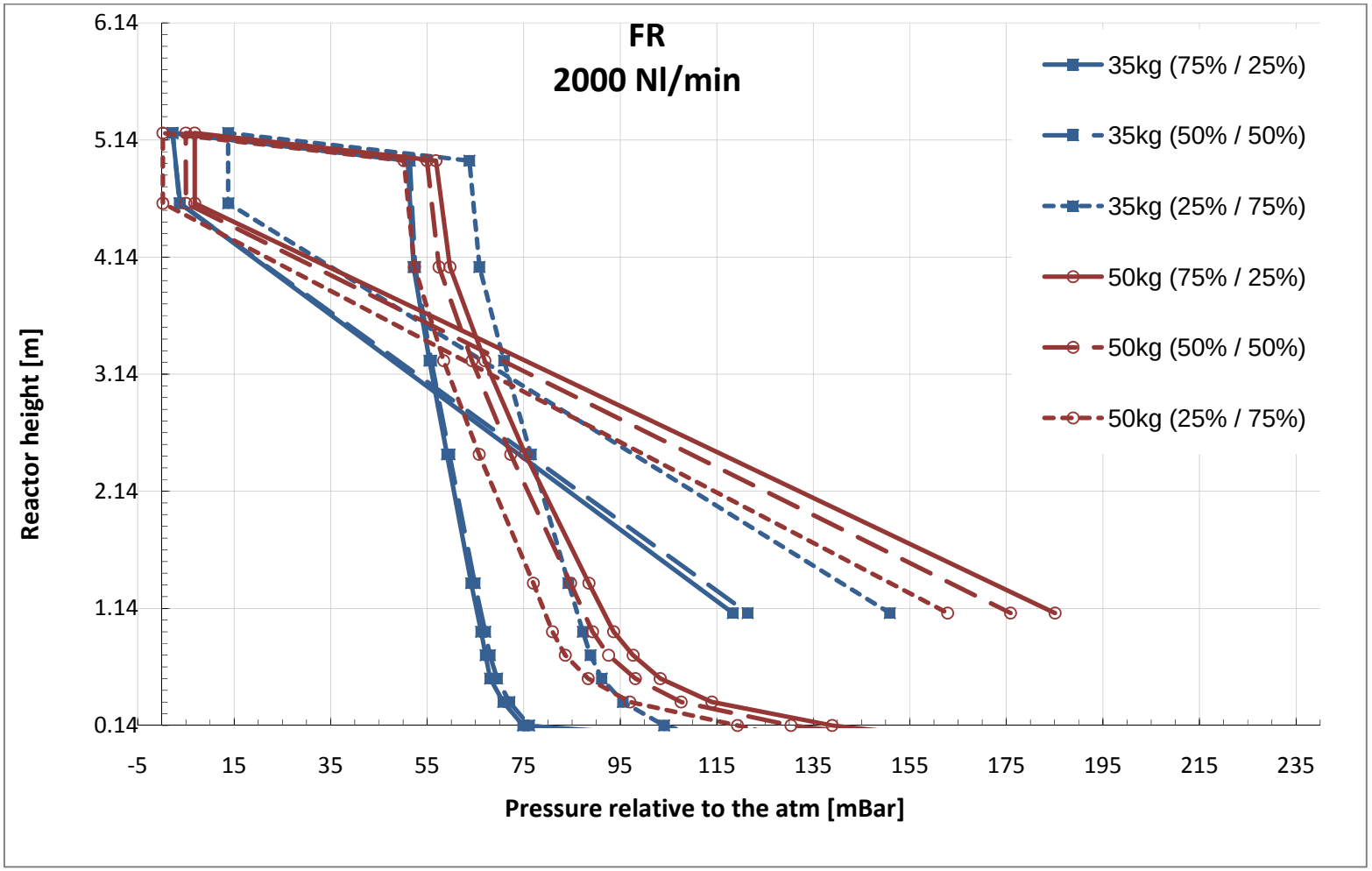

Pressure profiles for FR at a total flow of 2000Nl/min, at different total solid inventories, 35kg and 50kg, and different primary and secondary air distributions

Appendix VI Uncertainty analysis of experimental results: Pressure measurements

The statistics given in this appendix does not include the dips in pressure due to flux measurements as shown in figure 7.15. These data are filtered out.

* = P28 and P31 are the pressure measurements before the nozzles that distributes the center air flow in FR and AR loop seals. These values do not correspond with the values given in the pressure profiles in chapter 7. This is due to that in chapter 7 the actual pressure in the loop seal is given. The pressure before the nozzle is measured by P28 and/or P31. Then this pressure is subtracted with the pressure drop in the nozzle giving the actual pressure in the loop seal. The pressure drop is given by an investigation of the nozzle with the pressure drop as a function of the flow.

A1

AR 35kg

2000 Nl/min

Primary/secondary air distribution: 100% / 0% / 0%

Pressures in [mBar]	P1	P2	P3	P4	P5	P6	P7	P8	P9	P10	P11	P12	P28*
AVERAGE	67.61	23.20	17.70	16.18	14.75	12.22	8.47	6.36	4.80	4.46	-0.23	0.17	95.21
STDEV	1.23	0.72	0.97	0.87	0.82	0.73	0.55	0.44	0.30	0.25	0.05	0.05	1.81
STD%ofAVER	1.82	3.11	5.49	5.40	5.56	5.98	6.51	6.94	6.26	5.67	-22.67	29.74	1.90

Primary/secondary air distribution: 70% / 15% / 15%

Pressures in [mBar]	P1	P2	P3	P4	P5	P6	P7	P8	P9	P10	P11	P12	P28*
AVERAGE	67.64	20.94	15.77	14.41	13.08	10.82	7.63	5.80	4.50	4.23	-0.19	0.24	89.87
STDEV	1.19	0.42	0.61	0.55	0.53	0.50	0.40	0.34	0.26	0.24	0.07	0.08	2.47
STDEV% of AVER	1.76	2.01	3.88	3.82	4.04	4.58	5.27	5.83	5.87	5.78	-36.38	32.74	2.75

Primary/secondary air distribution: 40% / 30% / 30%

	P1	P2	P3	P4	P5	P6	P7	P8	P9	P10	P11	P12	P28*
AVERAGE	65.87	16.22	12.21	11.24	10.10	8.27	6.04	4.74	3.94	3.77	-0.17	0.33	82.17
STDEV	1.31	0.37	0.49	0.43	0.40	0.36	0.30	0.25	0.21	0.21	0.08	0.10	2.35
STDEV% of AVER	1.99	2.28	4.00	3.86	3.99	4.41	4.92	5.32	5.40	5.48	-43.24	30.73	2.86

3000 Nl/min

Primary/secondary air distribution: 100% / 0% / 0%

	P1	P2	P3	P4	P5	P6	P7	P8	P9	P10	P11	P12	P28*
AVERAGE	66.12	37.95	33.79	32.08	30.56	27.67	22.66	19.76	17.30	16.51	1.95	3.08	117.47
STDEV	1.00	1.05	1.68	1.67	1.65	1.59	1.46	1.34	1.16	1.03	0.21	0.23	3.05
STDEV% of AVER	1.51	2.77	4.96	5.21	5.40	5.74	6.45	6.79	6.71	6.25	10.69	7.50	2.60

Primary/secondary air distribution: 70% / 15% / 15%

	P1	P2	P3	P4	P5	P6	P7	P8	P9	P10	P11	P12	P28*
AVERAGE	66.04	37.15	33.43	31.50	29.77	26.91	22.14	19.36	17.01	16.27	2.01	3.30	115.17
STDEV	1.05	0.91	1.45	1.43	1.43	1.40	1.30	1.20	1.04	0.93	0.07	0.10	3.75
STDEV% of AVER	1.59	2.46	4.34	4.55	4.79	5.18	5.86	6.18	6.11	5.71	3.39	3.08	3.26

Primary/secondary air distribution: 40% / 30% / 30%

	P1	P2	P3	P4	P5	P6	P7	P8	P9	P10	P11	P12	P28*
AVERAGE	68.03	28.16	24.92	23.57	22.15	19.97	16.48	14.43	12.83	12.41	1.44	2.66	99.96
STDEV	1.93	0.75	1.05	1.01	1.73	3.47	2.51	0.79	0.68	0.62	0.08	0.15	3.26
STDEV% of AVER	2.83	2.68	4.20	4.27	7.83	17.38	15.24	5.49	5.28	5.02	5.27	5.62	3.26

4500 Nl/min

Primary/secondary air distribution: 100% / 0% / 0%

	P1	P2	P3	P4	P5	P6	P7	P8	P9	P10	P11	P12	P28*
AVERAGE	78.74	60.27	55.24	53.09	51.53	48.41	41.49	37.44	34.47	33.65	-0.30	2.18	146.33
STDEV	1.50	2.15	2.93	3.16	4.19	4.71	3.65	2.73	2.62	2.50	0.12	0.20	3.62
STDEV% of AVER	1.90	3.57	5.30	5.95	8.13	9.73	8.81	7.29	7.59	7.43	-39.92	9.35	2.47

Primary/secondary air distribution: 70% / 15% / 15%

	P1	P2	P3	P4	P5	P6	P7	P8	P9	P10	P11	P12	P28*
AVERAGE	75.43	58.95	55.45	53.10	51.03	47.70	40.87	37.00	34.14	33.32	-0.21	2.47	143.63
STDEV	1.43	2.72	3.08	3.21	3.18	3.16	3.06	2.98	2.85	2.70	0.13	0.25	3.91
STDEV% of AVER	1.90	4.62	5.56	6.05	6.24	6.62	7.50	8.06	8.35	8.12	-65.44	10.22	2.72

Primary/secondary air distribution: 40% / 30% / 30%

	P1	P2	P3	P4	P5	P6	P7	P8	P9	P10	P11	P12	P28*
AVERAGE	73.21	46.85	44.20	42.69	40.69	37.94	32.63	29.64	27.57	27.07	-0.27	2.66	129.35
STDEV	2.08	1.41	2.08	2.05	2.03	2.02	1.97	1.91	1.82	1.75	0.10	0.16	3.14
STDEV% of AVER	2.84	3.01	4.70	4.80	4.99	5.33	6.02	6.45	6.59	6.45	-38.76	5.84	2.43

A2

AR 45kg

3000 Nl/min

Primary/secondary air distribution: 100% / 0% / 0%

	P1	P2	P3	P4	P5	P6	P7	P8	P9	P10	P11	P12	P28*
AVERAGE	86.19	43.60	34.58	32.27	30.49	27.24	21.63	18.46	15.75	14.77	-0.43	1.12	146.63
STDEV	1.35	0.99	1.71	1.72	1.71	1.67	1.56	1.46	1.30	1.17	0.53	0.56	10.32
STDEV% of AVER	1.57	2.27	4.94	5.32	5.60	6.12	7.22	7.89	8.23	7.93	-124.77	50.39	7.04

Primary/secondary air distribution: 70% / 15% / 15%

	P1	P2	P3	P4	P5	P6	P7	P8	P9	P10	P11	P12	P28*
AVERAGE	89.28	45.09	36.93	34.27	32.15	28.72	22.92	19.70	16.85	15.76	-0.26	1.34	151.82
STDEV	2.05	1.02	1.54	1.53	1.51	1.48	1.38	1.29	1.15	1.01	0.08	0.10	4.03
STDEV% of AVER	2.30	2.25	4.18	4.45	4.69	5.14	6.04	6.57	6.82	6.44	-29.53	7.74	2.65

Primary/secondary air distribution: 40% / 30% / 30%

	P1	P2	P3	P4	P5	P6	P7	P8	P9	P10	P11	P12	P28*
AVERAGE	88.08	36.86	30.43	28.48	26.54	23.54	18.84	16.22	13.95	13.21	-0.30	1.23	138.81
STDEV	1.54	0.73	1.14	1.12	1.10	1.08	1.05	1.00	0.88	0.79	0.06	0.09	2.73
STDEV% of AVER	1.75	1.98	3.73	3.93	4.15	4.60	5.57	6.16	6.32	5.95	-19.97	7.51	1.97

3750 Nl/min

Primary/secondary air distribution: 100% / 0% / 0%

	P1	P2	P3	P4	P5	P6	P7	P8	P9	P10	P11	P12	P28*
AVERAGE	99.44	62.86	53.34	50.48	48.44	44.73	37.30	33.32	30.02	28.60	0.67	2.78	175.58
STDEV	3.57	3.81	4.66	4.80	4.69	4.79	4.85	4.82	3.45	2.43	1.01	0.95	5.17
STDEV% of AVER	3.59	6.06	8.74	9.51	9.67	10.71	13.01	14.47	11.51	8.48	151.01	34.00	2.94

Primary/secondary air distribution: 70% / 15% / 15%

	P1	P2	P3	P4	P5	P6	P7	P8	P9	P10	P11	P12	P28*
AVERAGE	98.68	63.37	55.73	52.35	49.79	45.96	37.89	33.71	30.28	28.75	-0.20	1.87	164.38
STDEV	0.83	1.15	2.60	2.59	2.59	2.74	2.50	2.40	2.21	2.00	0.10	0.40	11.83
STDEV% of AVER	0.84	1.82	4.67	4.95	5.20	5.95	6.60	7.13	7.30	6.97	-51.82	21.35	7.19

Primary/secondary air distribution: 40% / 30% / 30%

	P1	P2	P3	P4	P5	P6	P7	P8	P9	P10	P11	P12	P28*
AVERAGE	99.40	51.89	45.56	43.15	40.80	37.28	31.01	27.66	24.90	23.81	-0.29	2.24	158.42
STDEV	1.75	1.00	1.83	1.80	1.80	1.80	1.74	1.70	1.58	1.45	0.08	0.14	3.66
STDEV% of AVER	1.76	1.93	4.02	4.17	4.42	4.82	5.62	6.15	6.34	6.09	-27.16	6.06	2.31

4500 Nl/min

Primary/secondary air distribution: 100% / 0% / 0%

	P1	P2	P3	P4	P5	P6	P7	P8	P9	P10	P11	P12	P28*
AVERAGE	101.41	74.15	66.24	63.17	61.19	57.46	48.94	44.05	40.34	39.16	-0.42	1.66	188.09
STDEV	1.94	1.97	3.36	3.48	3.46	3.42	3.38	3.32	3.23	3.08	0.92	0.91	4.44
STDEV% of AVER	1.92	2.65	5.07	5.51	5.66	5.95	6.90	7.54	8.01	7.87	-219.00	55.04	2.36

Primary/secondary air distribution: 70% / 15% / 15%

	P1	P2	P3	P4	P5	P6	P7	P8	P9	P10	P11	P12	P28*
AVERAGE	105.03	79.33	74.20	70.70	68.03	63.72	54.31	49.22	45.37	43.97	3.43	6.03	193.74
STDEV	10.29	5.90	5.95	6.44	5.90	5.19	4.02	3.98	3.90	3.75	2.47	2.46	4.21
STDEV% of AVER	9.79	7.44	8.02	9.10	8.67	8.15	7.41	8.09	8.59	8.53	72.10	40.80	2.17

Primary/secondary air distribution: 40% / 30% / 30%

	P1	P2	P3	P4	P5	P6	P7	P8	P9	P10	P11	P12	P28*
AVERAGE	99.99	61.81	57.07	54.86	52.36	48.84	41.71	37.79	34.92	33.93	0.50	3.12	210.88
STDEV	4.11	2.55	3.21	3.18	3.14	3.10	3.04	3.03	2.98	2.98	3.43	7.28	8.80
STDEV% of AVER	4.11	4.13	5.62	5.80	5.99	6.34	7.30	8.02	8.55	8.78	692.92	233.07	4.17

F1

FR 35kg

1500 Nl/min

Primary/secondary air distribution: 75% / 25%

	P14	P15	P16	P17	P18	P19	P20	P21	P22	P23	P24	P25	P31*
AVERAGE	75.96	53.20	47.91	44.89	42.71	39.53	32.44	28.56	25.96	24.89	-1.08	0.31	127.40
STDEV	4.24	1.61	1.45	1.44	1.42	1.42	1.35	1.29	1.24	1.16	0.05	0.10	4.55
STDEV% of AVER	5.58	3.03	3.02	3.21	3.32	3.58	4.15	4.50	4.76	4.64	-5.01	33.51	3.57

Primary/secondary air distribution: 50% / 50%

	P14	P15	P16	P17	P18	P19	P20	P21	P22	P23	P24	P25	P31*
AVERAGE	63.17	49.24	44.84	42.26	40.39	37.40	30.98	27.45	25.16	24.31	-1.01	0.54	114.18
STDEV	1.11	1.31	1.33	1.32	1.30	1.30	1.19	1.15	1.11	1.06	0.05	0.08	2.14
STDEV% of AVER	1.76	2.67	2.97	3.12	3.23	3.47	3.84	4.17	4.40	4.35	-5.09	15.72	1.88

Primary/secondary air distribution: 25% / 75%

	P14	P15	P16	P17	P18	P19	P20	P21	P22	P23	P24	P25	P31*
AVERAGE	57.55	47.40	43.51	41.35	39.81	37.16	31.63	28.45	26.46	25.84	-0.83	0.95	108.55
STDEV	0.88	1.53	1.66	1.67	1.66	1.64	1.52	1.46	1.40	1.35	0.05	0.06	2.11
STDEV% of AVER	1.54	3.22	3.82	4.03	4.17	4.42	4.82	5.13	5.27	5.21	-5.87	6.74	1.94

1750 Nl/min

Primary/secondary air distribution: 75% / 25%

	P14	P15	P16	P17	P18	P19	P20	P21	P22	P23	P24	P25	P31*
AVERAGE	82.23	75.58	71.49	68.92	67.06	63.81	55.94	51.12	47.61	46.36	-0.17	1.71	139.70
STDEV	1.49	2.45	2.21	2.61	2.63	2.68	2.59	2.51	2.46	2.41	0.54	0.30	2.16
STDEV% of AVER	1.81	3.24	3.09	3.78	3.92	4.19	4.64	4.90	5.18	5.20	-314.70	17.41	1.54

Primary/secondary air distribution: 50% / 50%

	P14	P15	P16	P17	P18	P19	P20	P21	P22	P23	P24	P25	P31*
AVERAGE	75.13	68.42	64.66	62.42	60.81	57.89	50.93	46.65	43.53	42.49	-0.40	1.70	132.45
STDEV	1.42	2.43	2.27	2.50	2.50	2.51	2.42	2.33	2.27	2.22	0.08	0.15	2.28
STDEV% of AVER	1.89	3.56	3.52	4.01	4.11	4.34	4.74	5.00	5.22	5.21	-19.49	8.76	1.72

Primary/secondary air distribution: 25% / 75%

	P14	P15	P16	P17	P18	P19	P20	P21	P22	P23	P24	P25	P31*
AVERAGE	64.27	57.71	54.39	52.46	51.13	48.60	42.85	39.36	36.93	36.21	-0.41	1.77	121.28
STDEV	1.26	1.95	2.02	2.04	2.05	2.09	2.03	1.94	1.89	1.86	0.06	0.10	2.87
STDEV% of AVER	1.96	3.38	3.72	3.90	4.01	4.29	4.73	4.94	5.12	5.13	-14.11	5.71	2.36

2000 Nl/min

Primary/secondary air distribution: 75% / 25%

	P14	P15	P16	P17	P18	P19	P20	P21	P22	P23	P24	P25	P31*
AVERAGE	74.84	70.74	68.03	67.12	66.17	64.12	59.12	55.46	52.17	50.96	2.23	3.81	128.78
STDEV	6.46	6.23	6.29	5.89	6.17	6.28	6.33	6.74	6.22	4.56	3.68	3.17	4.34
STDEV% of AVER	8.63	8.81	9.25	8.77	9.33	9.80	10.71	12.16	11.92	8.96	165.23	83.30	3.37

Primary/secondary air distribution: 50% / 50%

	P14	P15	P16	P17	P18	P19	P20	P21	P22	P23	P24	P25	P31*
AVERAGE	76.12	72.04	69.47	67.99	67.01	64.85	59.61	55.82	52.50	51.38	2.26	3.69	131.85
STDEV	3.15	3.36	3.26	3.32	3.32	3.30	3.20	3.12	3.04	2.96	2.08	1.35	3.74
STDEV % of AVER	4.13	4.67	4.69	4.88	4.95	5.09	5.37	5.60	5.78	5.76	91.93	36.55	2.84

Primary/secondary air distribution: 25% / 75%

	P14	P15	P16	P17	P18	P19	P20	P21	P22	P23	P24	P25	P31*
AVERAGE	95.34	90.95	88.63	87.06	84.09	76.33	70.77	65.67	63.60	13.75	13.76	149.31	161.22
STDEV	5.23	5.16	5.52	5.47	5.38	5.07	4.88	4.69	4.58	3.67	3.64	7.90	4.18
STDEV % of AVER	5.48	5.68	6.22	6.29	6.40	6.65	6.89	7.13	7.20	26.71	26.46	5.29	2.60

F2

FR 50kg

1500 Nl/min

Primary/secondary air distribution: 75% / 25%

	P14	P15	P16	P17	P18	P19	P20	P21	P22	P23	P24	P25	P31*
AVERAGE	143.87	125.36	95.40	76.16	71.88	65.97	55.40	49.68	45.56	43.87	-2.70	4.65	242.76
STDEV	2.71	1.73	1.99	2.34	2.75	3.03	2.93	2.73	2.76	2.71	0.96	1.08	4.49
STDEV % of AVER	1.88	1.38	2.09	3.08	3.82	4.60	5.29	5.50	6.05	6.17	-35.72	23.33	1.85

Primary/secondary air distribution: 50% / 50%

	P14	P15	P16	P17	P18	P19	P20	P21	P22	P23	P24	P25	P31*
AVERAGE	142.65	116.98	88.14	72.05	67.55	63.66	53.56	48.10	44.19	42.65	-2.46	5.53	238.19
STDEV	2.30	1.50	1.43	2.59	3.17	2.77	2.56	2.46	2.38	2.30	0.29	0.18	4.04
STDEV % of AVER	1.61	1.28	1.63	3.60	4.70	4.35	4.78	5.12	5.39	5.40	-11.62	3.34	1.70

Primary/secondary air distribution: 25% / 75%

	P14	P15	P16	P17	P18	P19	P20	P21	P22	P23	P24	P25	P31*
AVERAGE	139.32	105.10	77.80	66.05	62.90	58.77	49.45	44.35	40.78	39.43	-2.55	5.36	227.69
STDEV	2.04	1.31	1.40	2.61	2.39	2.58	2.44	2.32	2.24	2.18	0.08	0.17	5.33
STDEV % of AVER	1.46	1.25	1.80	3.95	3.80	4.39	4.94	5.24	5.50	5.53	-3.30	3.15	2.34

1750 Nl/min

Primary/secondary air distribution: 75% / 25%

	P14	P15	P16	P17	P18	P19	P20	P21	P22	P23	P24	P25	P31*
AVERAGE	146.28	113.99	94.82	86.26	82.21	77.28	65.43	59.88	52.47	50.16	0.19	1.56	239.10
STDEV	3.71	4.01	3.63	4.13	4.20	4.61	4.42	3.29	4.29	4.26	4.21	3.76	6.62
STDEV % of AVER	2.54	3.52	3.83	4.79	5.10	5.96	6.76	5.49	8.17	8.49	2240.97	241.47	2.77

Primary/secondary air distribution: 50% / 50%

	P14	P15	P16	P17	P18	P19	P20	P21	P22	P23	P24	P25	P31*
AVERAGE	148.17	114.71	95.73	88.41	83.56	79.93	68.92	62.28	56.98	54.90	4.94	5.91	238.39
STDEV	1.53	1.87	2.19	3.26	4.22	4.40	5.39	4.89	3.81	3.76	3.72	2.75	3.86
STDEV % of AVER	1.03	1.63	2.29	3.69	5.05	5.50	7.83	7.85	6.68	6.85	75.38	46.46	1.62

Primary/secondary air distribution: 25% / 75%

	P14	P15	P16	P17	P18	P19	P20	P21	P22	P23	P24	P25	P31*
AVERAGE	139.80	105.81	88.19	81.98	78.44	74.62	64.27	58.10	53.36	51.50	1.59	4.14	227.39
STDEV	1.39	1.57	2.24	3.39	3.70	3.62	3.46	3.38	3.37	3.31	3.19	1.40	3.34
STDEV % of AVER	0.99	1.49	2.54	4.14	4.72	4.86	5.39	5.81	6.31	6.44	200.44	33.95	1.47

2000 Nl/min

Primary/secondary air distribution: 75% / 25%

	P14	P15	P16	P17	P18	P19	P20	P21	P22	P23	P24	P25	P31*
AVERAGE	138.90	113.97	103.29	97.66	93.62	88.51	75.36	66.93	59.69	56.81	6.82	6.83	232.36
STDEV	1.64	2.47	2.90	3.88	4.40	4.68	4.56	4.55	4.49	4.41	4.41	4.41	5.17
STDEV % of AVER	1.18	2.17	2.81	3.97	4.69	5.29	6.05	6.79	7.53	7.77	64.64	64.59	2.23

Primary/secondary air distribution: 50% / 50%

	P14	P15	P16	P17	P18	P19	P20	P21	P22	P23	P24	P25	P31*
AVERAGE	107.35	97.87	92.33	89.02	84.48	72.12	64.11	57.30	54.83	5.09	5.10	239.37	223.23
STDEV	6.05	5.70	6.08	6.45	6.51	6.74	6.16	5.23	5.21	5.55	5.55	12.94	4.23
STDEV % of AVER	5.64	5.83	6.59	7.25	7.71	9.34	9.60	9.13	9.50	109.12	108.97	5.41	1.90

Primary/secondary air distribution: 25% / 75%

	P14	P15	P16	P17	P18	P19	P20	P21	P22	P23	P24	P25	P31*
AVERAGE	119.28	96.99	88.35	83.61	80.95	76.99	65.76	58.40	52.35	50.18	0.22	0.23	209.77
STDEV	3.71	5.65	6.81	7.06	8.05	8.17	7.29	6.12	5.31	5.27	5.19	5.15	6.72
STDEV % of AVER	3.11	5.82	7.71	8.45	9.95	10.61	11.08	10.47	10.15	10.50	2398.29	2218.05	3.20

C1

AR 3000 Nl/min

	P1	P2	P3	P4	P5	P6	P7	P8	P9	P10	P11	P12	P28*
AVERAGE	109.63	54.31	29.26	24.30	22.24	19.15	14.66	12.22	10.25	9.63	-1.20	-0.21	165.66
STDEV	0.62	1.34	0.55	1.05	1.12	1.05	0.93	0.84	0.69	0.63	0.10	0.11	3.37
STDEV % of AVER	0.57	2.47	1.87	4.31	5.04	5.49	6.35	6.86	6.77	6.49	-8.36	-55.76	2.04

FR 2000 Nl/min

	P14	P15	P16	P17	P18	P19	P20	P21	P22	P23	P24	P25	P31*
AVERAGE	99.41	91.40	87.82	85.56	84.01	81.10	73.80	68.59	63.67	61.51	11.53	11.53	141.59
STDEV	3.44	4.22	4.19	4.19	4.19	4.16	3.98	3.89	3.82	3.69	3.69	3.68	4.31
STDEV % of AVER	3.46	4.61	4.77	4.90	4.98	5.12	5.39	5.67	6.01	6.00	32.00	31.91	3.05

C2

AR 3000 Nl/min

	P1	P2	P3	P4	P5	P6	P7	P8	P9	P10	P11	P12	P28*
AVERAGE	109.06	50.36	31.22	27.33	25.32	22.18	17.55	15.02	13.05	12.43	-0.18	1.06	177.29
STDEV	1.85	1.34	0.86	1.33	1.39	1.33	1.22	1.10	0.94	0.86	0.11	0.15	3.75
STDEV % of AVER	1.70	2.67	2.75	4.87	5.50	6.02	6.93	7.35	7.18	6.89	-61.49	14.52	2.11

FR 2000 Nl/min

	P14	P15	P16	P17	P18	P19	P20	P21	P22	P23	P24	P25	P31*
AVERAGE	114.34	106.37	102.56	100.35	99.18	95.99	88.40	82.80	77.20	74.71	24.72	24.72	137.83
STDEV	4.66	4.64	4.62	4.64	4.91	4.63	4.48	4.37	4.27	4.13	4.13	4.13	4.04
STDEV % of AVER	4.08	4.37	4.51	4.62	4.96	4.82	5.06	5.27	5.53	5.52	16.69	16.68	2.93

C3

AR

	P1	P2	P3	P4	P5	P6	P7	P8	P9	P10	P11	P12	P28*
AVERAGE	72.80	39.12	33.96	31.71	29.81	26.79	21.98	19.50	17.55	16.92	-3.96	-1.63	216.92
STDEV	1.01	0.97	1.66	1.83	1.83	1.80	1.73	1.64	1.50	1.40	0.15	0.15	1.40
STDEV % of AVER	1.39	2.49	4.89	5.77	6.14	6.71	7.87	8.43	8.56	8.26	-3.82	-8.96	0.64

FR

	P14	P15	P16	P17	P18	P19	P20	P21	P22	P23	P24	P25	P31*
AVERAGE	136.86	125.59	119.44	115.81	113.09	109.35	98.60	92.79	84.03	81.33	31.34	31.35	200.61
STDEV	1.29	2.26	0.88	4.94	4.66	4.92	4.91	6.49	4.75	4.73	4.73	4.73	2.25
STDEV % of AVER	0.94	1.80	0.73	4.26	4.12	4.50	4.98	7.00	5.65	5.82	15.10	15.10	1.12

Appendix VII Uncertainty analysis of experimental results: Flux measurements

Data from flux measurements from the coupled reactor experiments are not given. This is due to that only one measurement of the flux were executed for each experiment. No average, standard deviation is therefore available.

The flux was measured three times for each single reactor experiment. Data are given below:

Single reactor experiments

A1

	AR								
Total solid Inventory	**35 kg**								
Total flow	**2000 Nl/min**			**3000 Nl/min**			**4500 Nl/min**		
Primary/secondary air distribution	**100%/ 0%/ 0%**	**70%/ 15%/ 15%**	**40%/ 30%/ 30%**	**100%/ 0%/ 0%**	**70%/ 15%/ 15%**	**40%/ 30%/ 30%**	**100%/ 0%/ 0%**	**70%/ 15%/ 15%**	**40%/ 30%/ 30%**
Average flux [kg/m^{2}s]	6.67	7.15	5.84	20.67	19.45	14.29	34.88	35.14	26.75
STDEV	0.55	0	0.21	2.02	0.38	0.60	0.45	2.76	2.73
STDEV% of Average	8.18	0	3.53	9.75	1.95	4.20	1.30	7.86	10.19

A2

	AR								
Total solid Inventory	**45 kg**								
Total flow	**3000 Nl/min**			**3750 Nl/min**			**4500 Nl/min**		
Primary/secondary air distribution	**100%/ 0%/ 0%**	**70%/ 15%/ 15%**	**40%/ 30%/ 30%**	**100%/ 0%/ 0%**	**70%/ 15%/ 15%**	**40%/ 30%/ 30%**	**100%/ 0%/ 0%**	**70%/ 15%/ 15%**	**40%/ 30%/ 30%**
Average flux [kg/m^{2}s]	22.81	24.91	20.89	36.49	38.02	30.16	46.68	34.09	38.81
STDEV	0.79	1.64	1.64	0.38	1.31	0.00	1.82	3.96	1.82
STDEV% of Average	3.45	6.57	7.85	1.04	3.45	0.00	3.89	11.62	4.68

F1

	FR								
Total solid Inventory	**35 kg**								
Total flow	**1500 Nl/min**			**1750 Nl/min**			**2000 Nl/min**		
Primary/secondary air distribution	**75%/ 25%**	**50%/ 50%**	**25%/ 75%**	**75%/ 25%**	**50%/ 50%**	**25%/ 75%**	**75%/ 25%**	**50%/ 50%**	**25%/ 75%**
Average flux [kg/m^{2}s]	28.01	21.74	19.33	19.86	19.59	15.20	23.41	20.88	29.27
STDEV	1.45	2.61	1.29	2.12	0.83	0.53	0.00	0.84	7.24
STDEV% of Average	5.17	12.01	6.66	10.65	4.22	3.46	0.00	4.01	24.74

F2

	FR								
Total solid Inventory	**50 kg**								
Total flow	**1500 Nl/min**			**1750 Nl/min**			**2000 Nl/min**		
Primary/secondary air distribution	**75%/ 25%**	**50%/ 50%**	**25%/ 75%**	**75%/ 25%**	**50%/ 50%**	**25%/ 75%**	**75%/ 25%**	**50%/ 50%**	**25%/ 75%**
Average flux [kg/m^{2}s]	46.83	47.66	45.16	63.00	60.21	61.32	65.56	58.87	56.19
STDEV	2.90	0.00	0.00	6.76	6.69	1.93	1.16	3.07	0.00
STDEV% of Average	6.19	0.00	0.00	10.73	11.11	3.15	1.77	5.21	0.00

Appendix VIII Technical data for the weight Mettler Toledo XS 32000L

Technical data	XS8001L	XS16001L	XS32001L	XS32001LDR	XS16000L	XS32000L
Stand alone weighing platform	–	X16001L	X32001L	–	–	X32000L
Maximum capacity	8100 g	16100 g	32100 g	32100 g	16100 g	32100 g
Maximum capacity, fine range	–	–	–	6400 g	–	–
Readability	0.1 g	0.1 g	0.1 g	1 g	1 g	1 g
Readability, fine range	–	–	–	0.1 g	–	–
Repeatability (sd)	80 mg	80 mg	80 mg	600 mg	600 mg	600 mg
Repeatability, fine range (sd)	–	–	–	100 mg	–	–
Linearity	200 mg	200 mg	300 mg	300 mg	600 mg	600 mg
Eccentric load deviation (test load)	0.3 g (5 kg)	0.3 g (5 kg)	0.3 g (10 kg)	1 g (10 kg)	1 g (5 kg)	1 g (10 kg)
Sensitivity offset	$8 \times 10^{-5} \cdot R_{nt}$	$5 \times 10^{-5} \cdot R_{nt}$	$3 \times 10^{-5} \cdot R_{nt}$	$3 \times 10^{-5} \cdot R_{nt}$	$8 \times 10^{-5} \cdot R_{nt}$	$6 \times 10^{-5} \cdot R_{nt}$
Sensitivity temperature drift[1]	$1.5 \times 10^{-5}/°C \cdot R_{nt}$	$1.5 \times 10^{-5}/°C \cdot R_{nt}$	$1 \times 10^{-5}/°C \cdot R_{nt}$	$1 \times 10^{-5}/°C \cdot R_{nt}$	$1.5 \times 10^{-5}/°C \cdot R_{nt}$	$1.5 \times 10^{-5}/°C \cdot R_{nt}$
Sensitivity stability[2]	$5 \times 10^{-5}/a \cdot R_{nt}$	$5 \times 10^{-5}/a \cdot R_{nt}$	$3 \times 10^{-5}/a \cdot R_{nt}$	$3 \times 10^{-5}/a \cdot R_{nt}$	$5 \times 10^{-5}/a \cdot R_{nt}$	$5 \times 10^{-5}/a \cdot R_{nt}$
Settling time	1.5 s	1.5 s	1.5 s	1.5 s	1.2 s	1.2 s
Interface update rate	23 /s	23 /s	23 /s	23 /s	23 /s	23 /s
Platform dimensions (WxDxH mm)	360x280x130					
Terminal dimensions (D mm)	124					
Weighing pan dimensions (WxD mm)	280x360					

R_{nt} = net weight sd = Standard deviation a = Year (annum)

Appendix IX Data and results from experimental campaign applied in ERGUN simulations

	AR						FR					
Total solid Inventory	**35 kg**			**45 kg**			**35 kg**			**50 kg**		
Total flow	**2000 Nl/min**	**3000 Nl/min**	**4500 Nl/min**	**3000 Nl/min**	**3750 Nl/min**	**4500 Nl/min**	**1500 Nl/min**	**1750 Nl/min**	**2000 Nl/min**	**1500 Nl/min**	**1750 Nl/min**	**2000 Nl/min**
Operating velocity, U	0.9 m/s	1.3 m/s	1.9 m/s	1.3 m/s	1.6 m/s	1.9 m/s	1.5 m/s	1.7 m/s	2 m/s	1.5 m/s	1.7 m/s	2 m/s
Mass flow	0.3 kg/s	0.82 kg/s	1.47 kg/s	0.96 kg/s	1.51 kg/s	1.96 kg/s	0.5 kg/s	0.36 kg/s	0.42 kg/s	0.84 kg/s	1.13 kg/s	1.18 kg/s

Appendix X Estimation of minimum fluidization voidage

The minimum fluidization voidage was estimated with the following relation from (Daizo Kunii 1991):

$$\frac{1.75}{\epsilon_{mf^3} \times \varphi_s} \times Re_{p,mf}^2 + \frac{150 \times (1-\epsilon_{mf})}{\epsilon_{mf^3} \times \varphi_s{}^2} \times Re_{p,mf} = \frac{d_p^3 \times \rho_g \times (\rho_s - \rho_g) \times g}{\mu^2} = Ar \quad \text{(A)}$$

There are however several unknowns. The Archimedes number should be calculated, $Re_{p,mf}$ and the U_{mf}. When these values have been calculated equation A only have one unknown, the minimum fluidization voidage. Sphericity, φ_s, is a difficult parameter to find. A qualified guess was done and it was set to 0.65. The Archimedes number is defined as:

$$\mathrm{Ar} = \frac{d_p^3 \times \rho_g \times (\rho_s - \rho_g) \times g}{\mu^2} = \frac{(34 \times 10^{-6})^3 \times 1.252 \times (7000 - 1.252) \times 9.81}{(1.82 \times 10^{-5})^2} = 10.19970 = 10.2 \quad \text{(B)}$$

A relation for the minimum fluidization Reynolds number for very fine particles are given in (Daizo Kunii 1991):

$$\mathrm{Re_{p,mf}} = [(33.7)^2 + 0.0408 \times Ar]^{0.5} - 33.7 = 0.00617 \quad \text{(C)}$$

The minimum fluidization Reynolds number is defined in equation D:

$$\mathrm{Re_{p,mf}} \equiv \frac{d_p \times U_{mf} \times \rho_g}{\mu} \quad \text{(D)}$$

The minimum fluidization velocity can then be calculated:

$$\mathrm{U_{mf}} \equiv \frac{\mathrm{Re_{p,mf}} \times \mu}{d_p \times \rho_g} = \frac{0.0061 \times 1.82 \times 10^{-5}}{34 \times 10^{-6} \times 1.252} = 0.00261 \quad \text{(E)}$$

Equation A now only has one unknown and ϵ_{mf} was calculated to be $0.48116 \cong 0.48$. For comparison the voidage of a packed bed is estimated and this voidage should be smaller than ϵ_{mf} :

$$\epsilon = 1 - \frac{\rho_s}{\rho_{s,bulk}} = 1 - \frac{3900\ kg/m^3}{6968\ kg/m^3} = 0.43 < 0.48 \quad \text{(F)}$$

0.48 seems to be a good estimation of the minimum fluidization voidage.

Appendix XI ERGUN simulation results

F1: FR, total solid inventory 35 kg

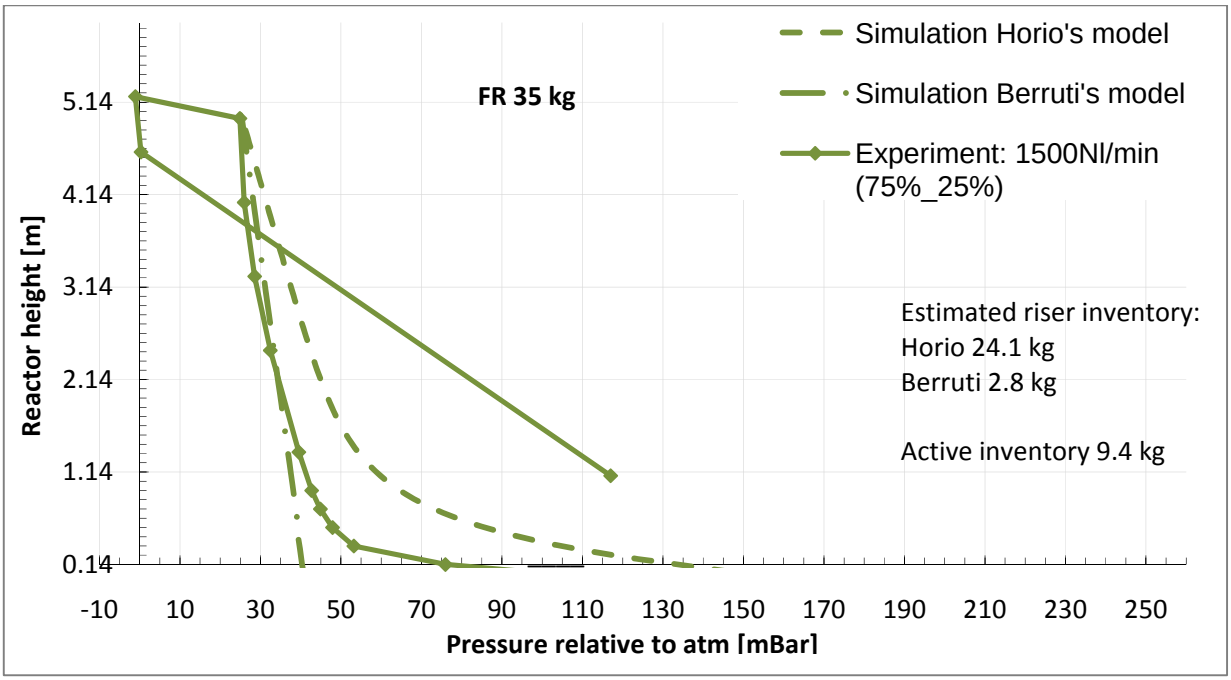

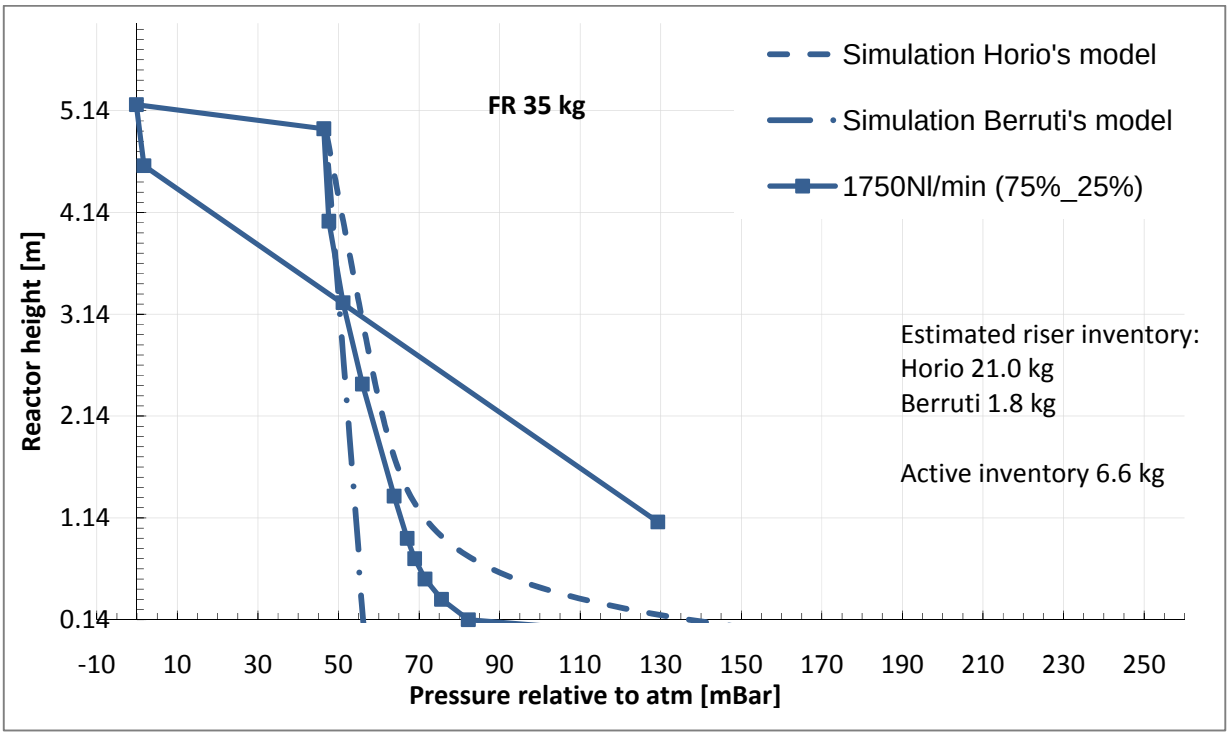

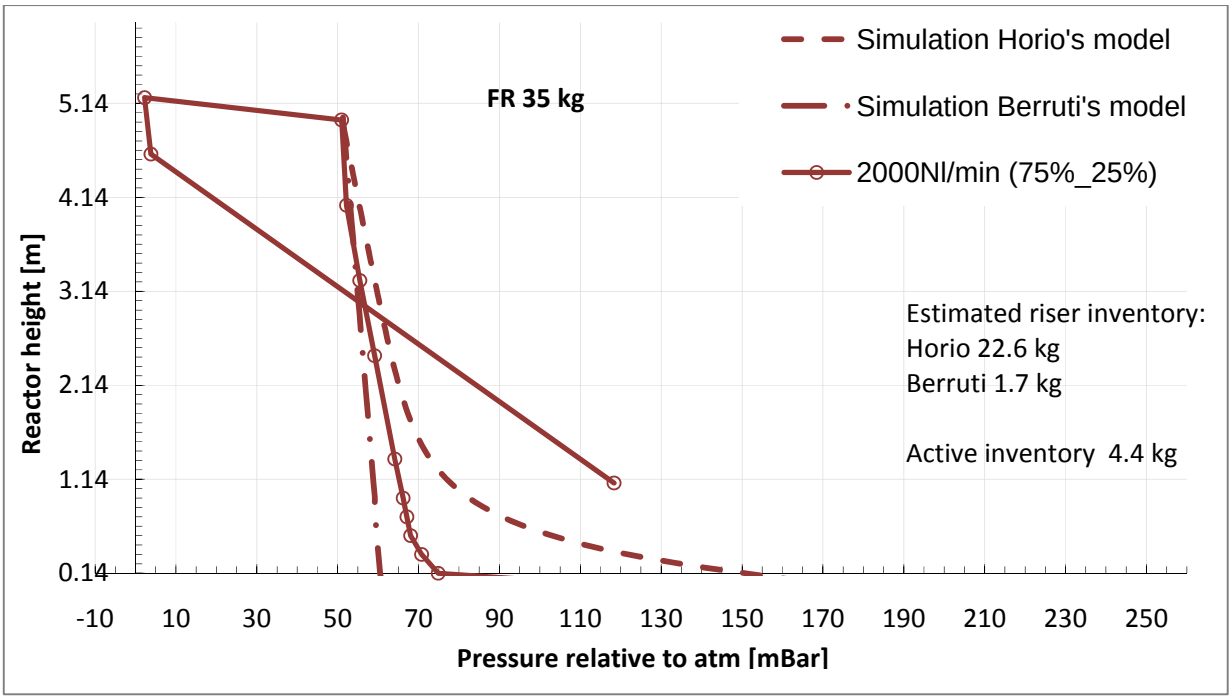

F2: FR, total solid inventory 50 kg

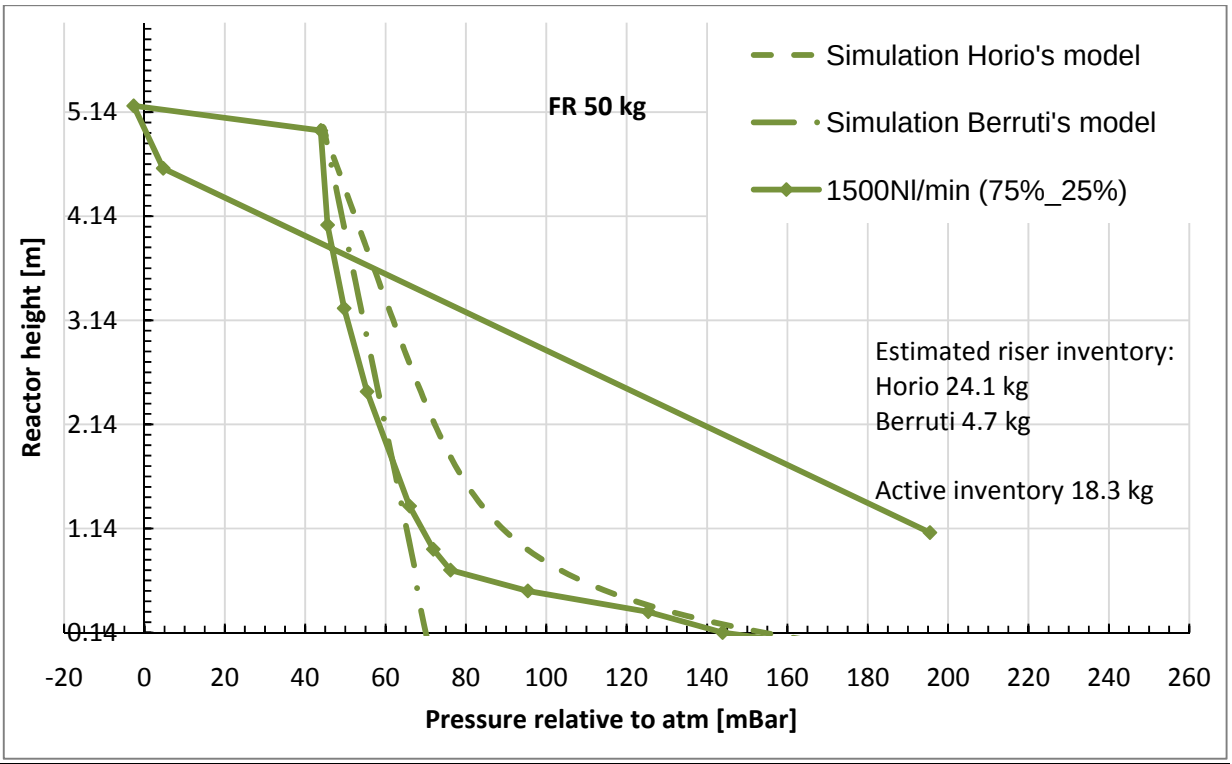

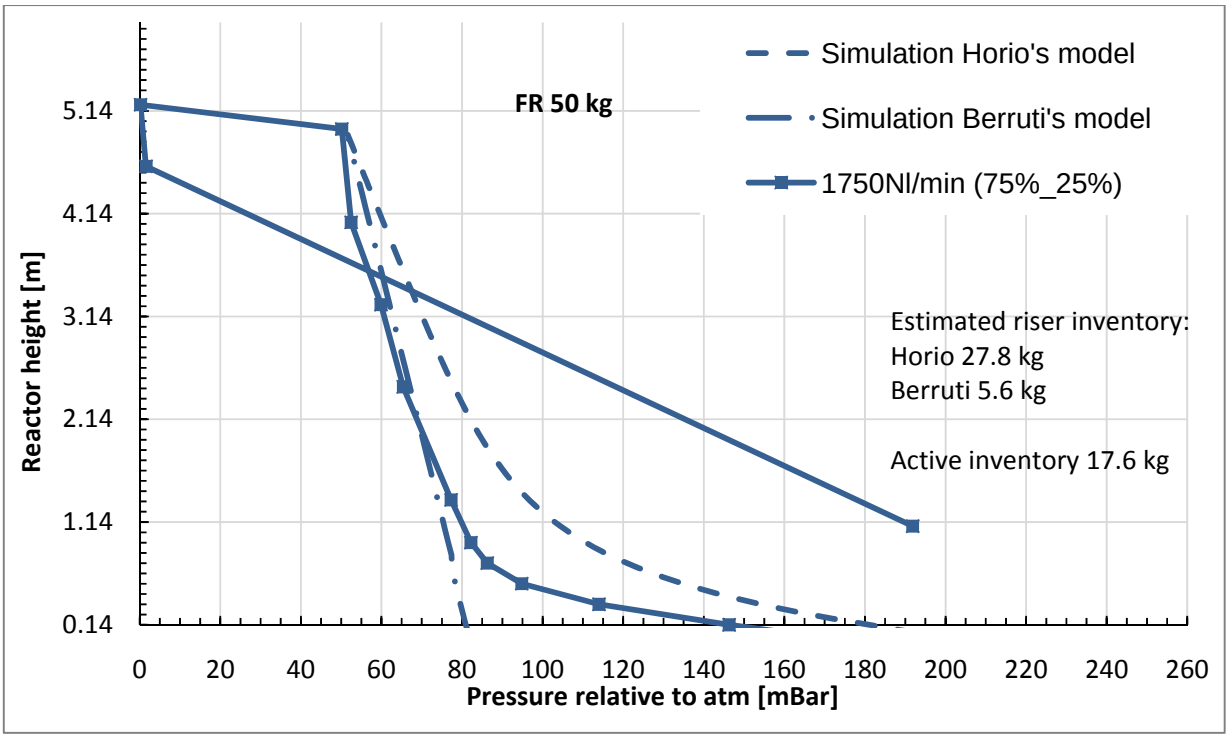
FR 50 kg
Simulation Horio's model
Simulation Berruti's model
1750Nl/min (75%_25%)
Estimated riser inventory:
Horio 27.8 kg
Berruti 5.6 kg
Active inventory 17.6 kg
Reactor height [m]
5.14
4.14
3.14
2.14
1.14
0.14
0
20
40
60
80
100
120
140
160
180
200
220
240
260
Pressure relative to atm [mBar]

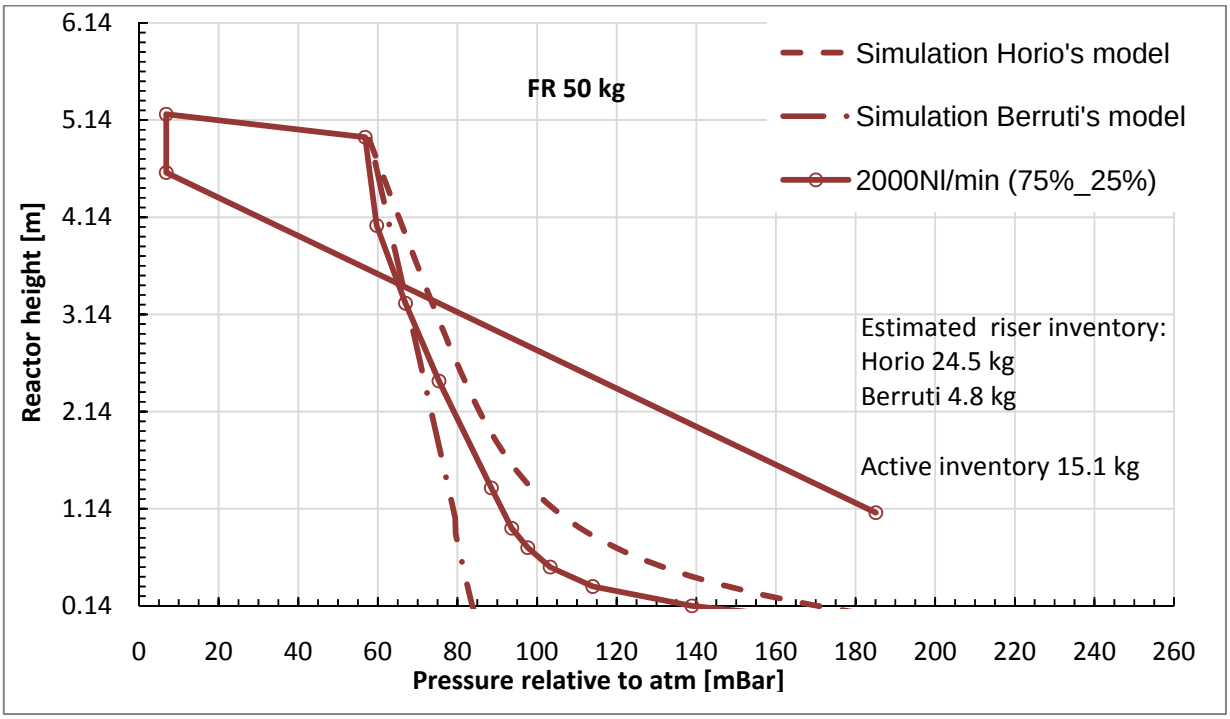
FR 50 kg
Simulation Horio's model
Simulation Berruti's model
2000Nl/min (75%_25%)
Estimated riser inventory:
Horio 24.5 kg
Berruti 4.8 kg
Active inventory 15.1 kg
Reactor height [m]
6.14
5.14
4.14
3.14
2.14
1.14
0.14
0
20
40
60
80
100
120
140
160
180
200
220
240
260
Pressure relative to atm [mBar]

A1: AR, total solid inventory 35 kg

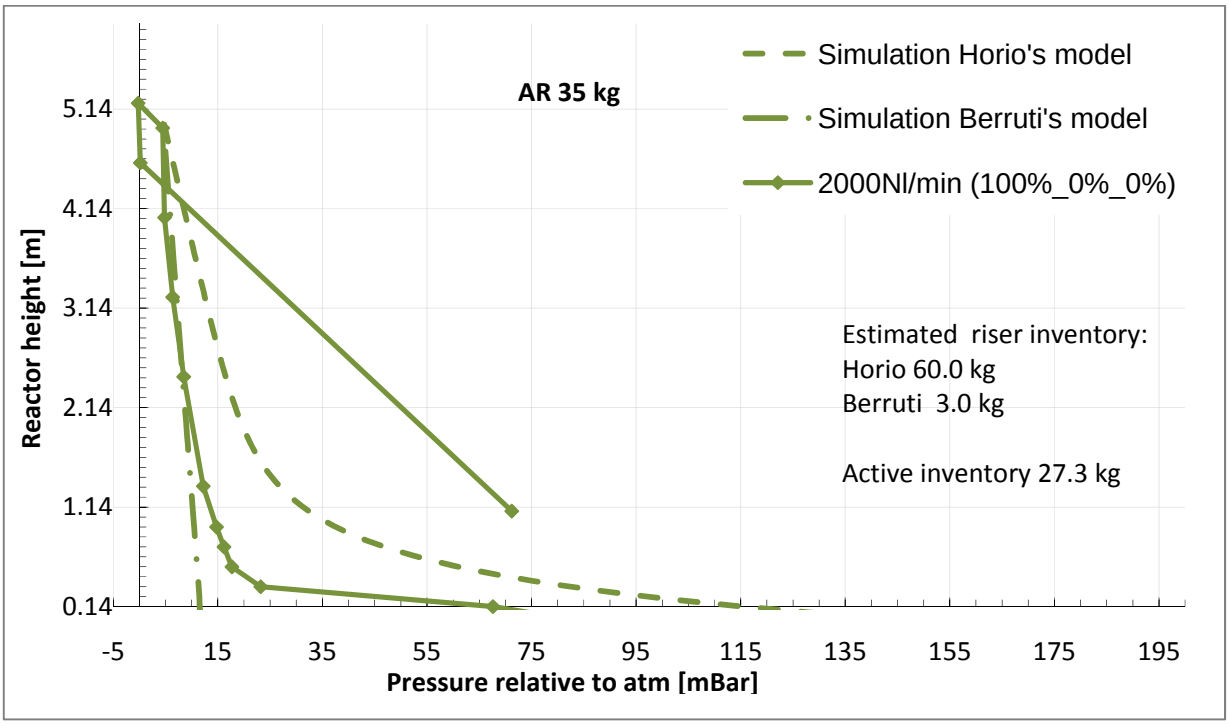

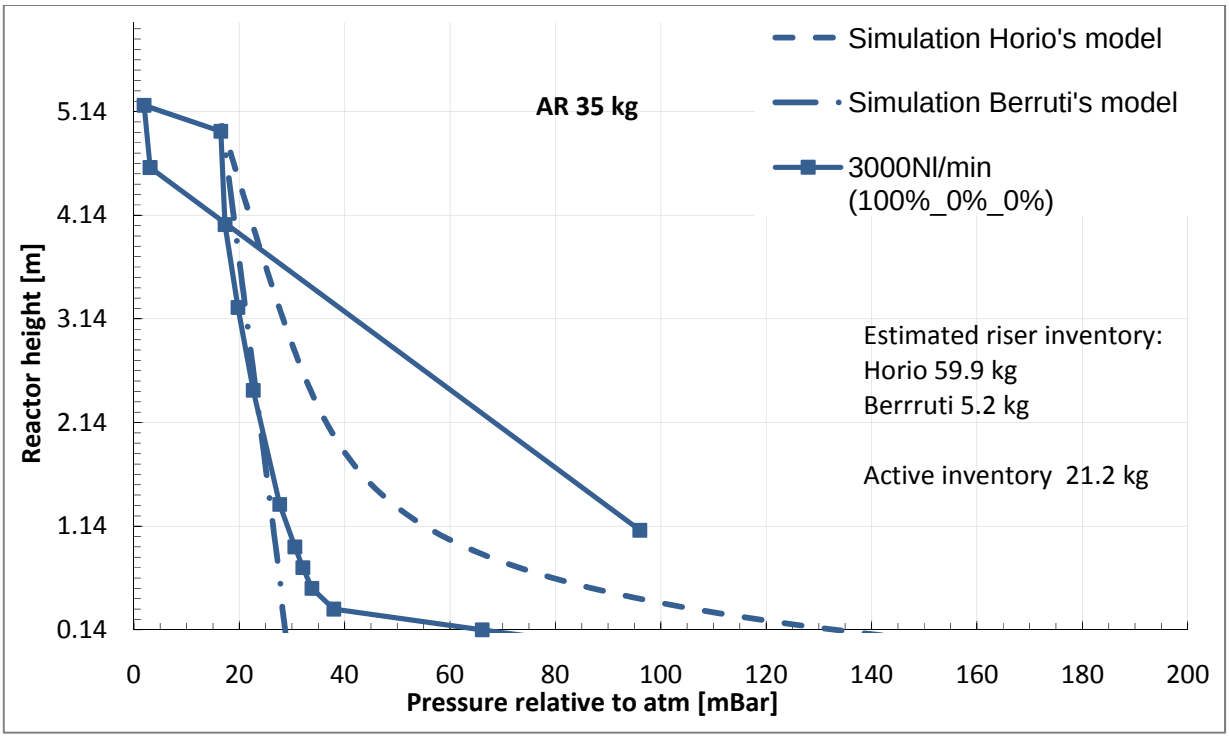

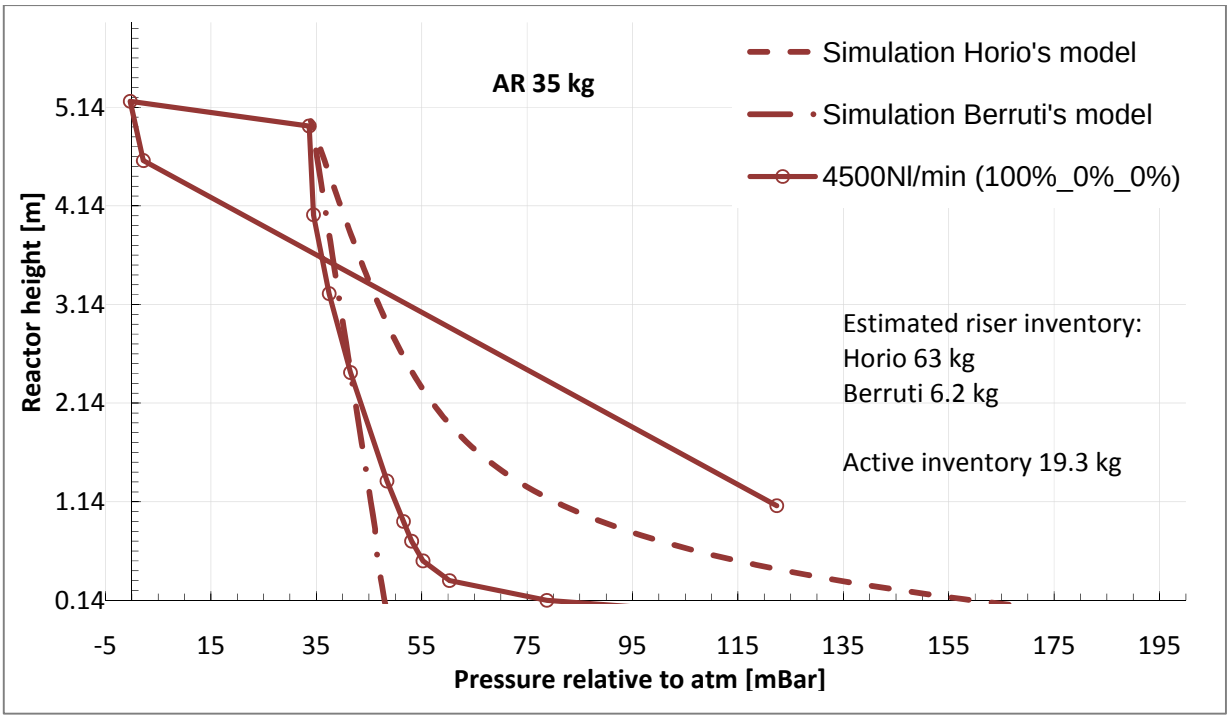

A2: AR, total solid inventory 45 kg

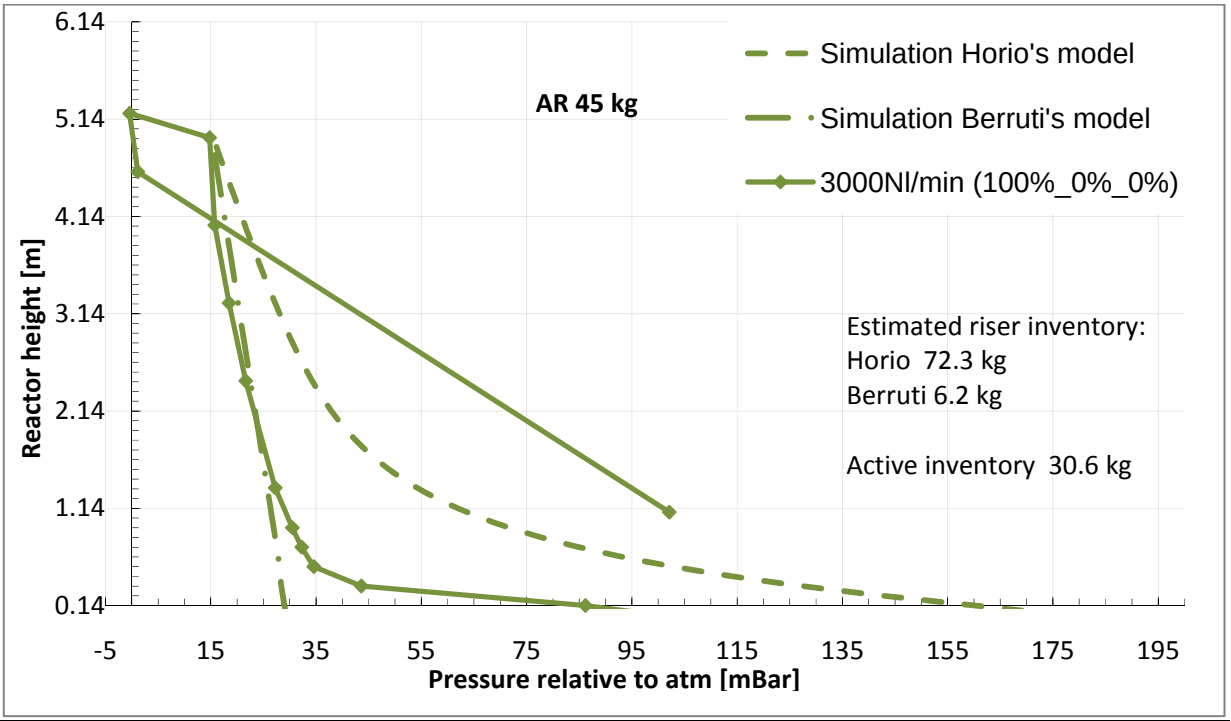

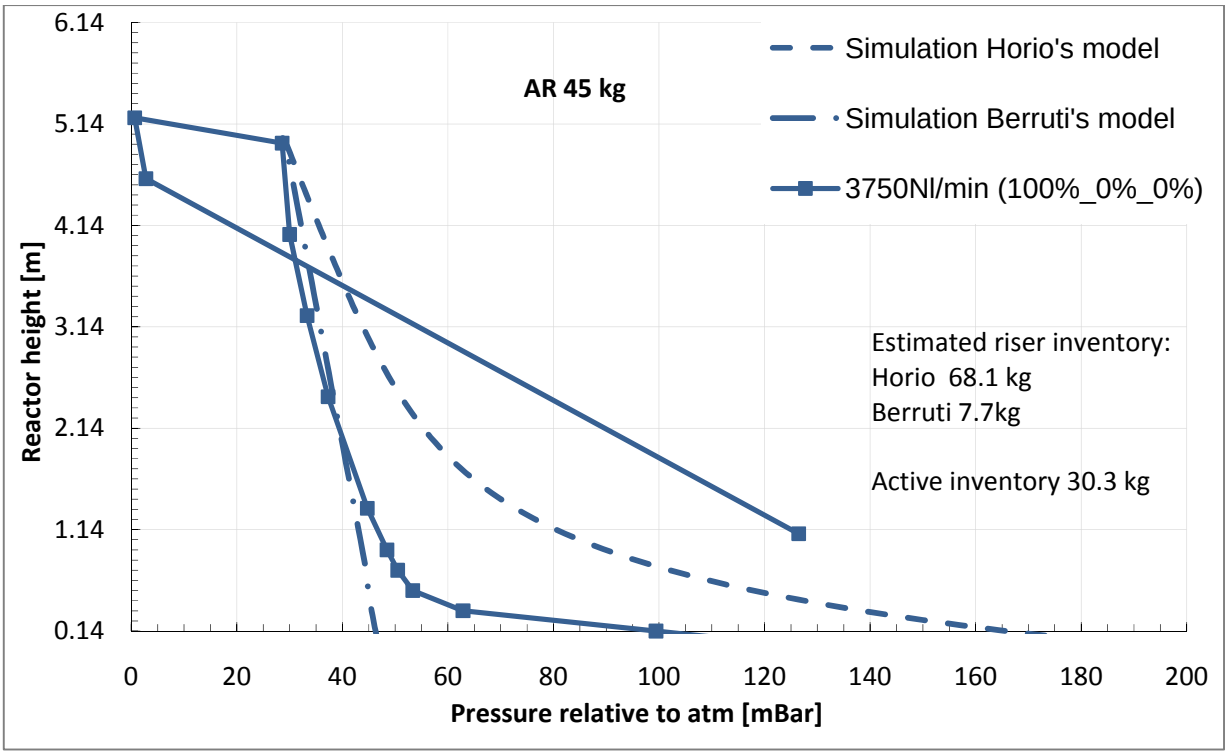
AR 45 kg
Simulation Horio's model
Simulation Berruti's model
3750Nl/min (100%_0%_0%)
Estimated riser inventory:
Horio 68.1 kg
Berruti 7.7kg
Active inventory 30.3 kg
Reactor height [m]
6.14
5.14
4.14
3.14
2.14
1.14
0.14
0
20
40
60
80
100
120
140
160
180
200
Pressure relative to atm [mBar]

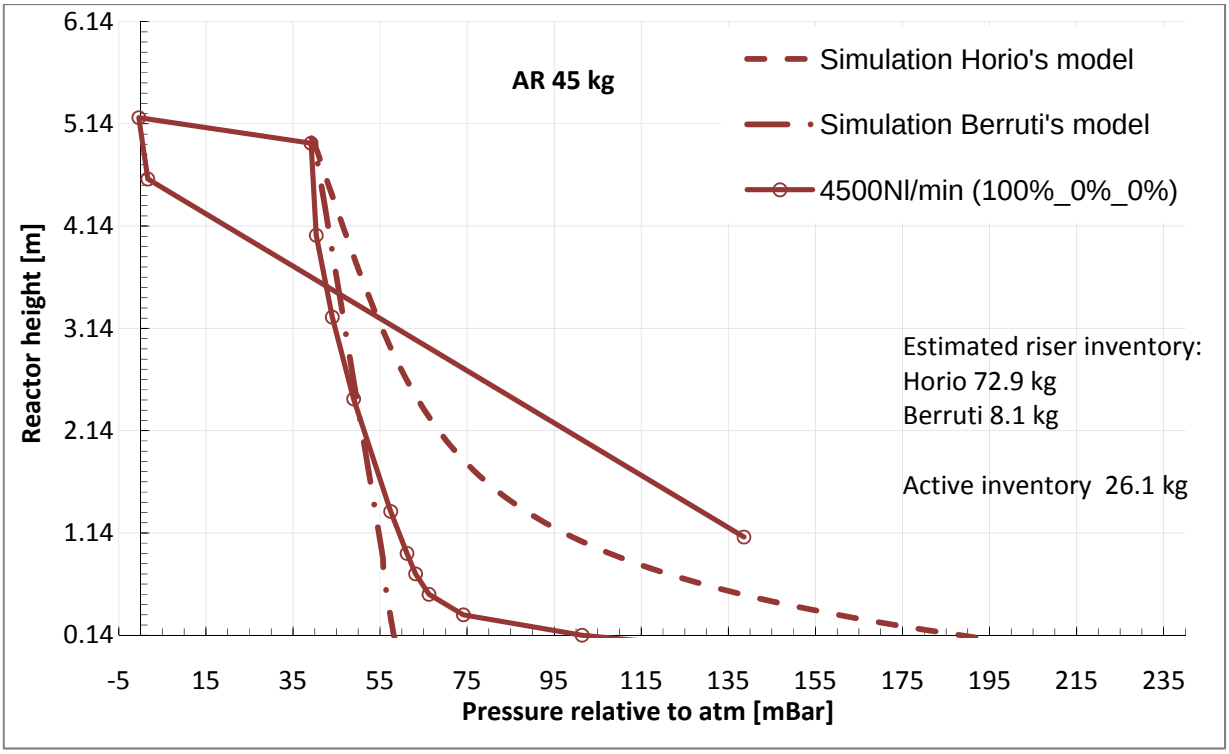
AR 45 kg
Simulation Horio's model
Simulation Berruti's model
4500Nl/min (100%_0%_0%)
Estimated riser inventory:
Horio 72.9 kg
Berruti 8.1 kg
Active inventory 26.1 kg
Reactor height [m]
6.14
5.14
4.14
3.14
2.14
1.14
0.14
-5
15
35
55
75
95
115
135
155
175
195
215
235
Pressure relative to atm [mBar]